UNIVERSITÀ DEGLI STUDI DI TRIESTE

XXVII CICLO DEL DOTTORATO DI RICERCA IN

SCIENZE DELL'INGEGNERIA - INDIRIZZO INGEGNERIA MECCANICA, NAVALE, DELL'ENERGIA E DELLA PRODUZIONE

STRUCTURE BORNE NOISE DUE TO MARINE DIESEL ENGINES: EXPERIMENTAL STUDY AND NUMERICAL SIMULATION FOR THE PREDICTION OF THE DYNAMIC BEHAVIOUR OF RESILIENT MOUNTS

Settore scientifico-disciplinare: ING-IND/02

DOTTORANDO
LORENZO MORO

COORDINATORE
PROF. DIEGO MICHELI

SUPERVISORE DI TESI
PROF. MARCO BIOT

ANNO ACCADEMICO 2013/2014

UNIVERSITÀ DEGLI STUDI DI TRIESTE

XXVII CYCLE OF PHILOSOPHY DOCTORATE IN

MECHANICAL ENGINEERING, NAVAL ARCHITECTURE, ENERGY AND PRODUCTION

STRUCTURE BORNE NOISE DUE TO MARINE DIESEL ENGINES: EXPERIMENTAL STUDY AND NUMERICAL SIMULATION FOR THE PREDICTION OF THE DYNAMIC BEHAVIOUR OF RESILIENT MOUNTS

Subject area: ING-IND/02

PHD CANDIDATE
LORENZO MORO

PHD PROGRAM COORDINATOR
PROF. DIEGO MICHELI

THESIS SUPERVISOR
PROF. MARCO BIOT

ACADEMIC YEAR 2013/2014

Table of Contents

LIST OF FIGURES V

NOMENCLATURE XI

RIASSUNTO 1

ABSTRACT 3

INTRODUCTION 5

General Background 9

THEORETICAL BACKGROUND 13

1. Transfer function 17
1.1. Mechanical Mobility and Mechanical Impedance Functions 18
1.2. Transmissibility Function 20
1.3. Mechanical Mobility and Impedance Matrices 21

2. Sub-structuring 23

3. Resilient mounts 27
3.1. Four-pole parameters theory 28
3.2. Four-pole parameters of passive resilient mounts 29
3.3. Calculation of the receiver velocity 32
3.4. Resilient mount characterization in the six degrees of freedom 33

4. Source power: characterization of a structure-borne noise source 37
4.1. Source power of a suspended machine 38

5. Multi-point connected sources 41
5.1. Source power of multi-point connected systems 42

6. Experimental characterization of resilient mounts 45
6.1. Direct Method 47
6.2. Indirect Method 49

7. Mechanical mobility of the diesel engine foundation 53

8. Simulation of rubber resilient mounts 57

9. Simulation of the dynamics of diesel engine foundations 61

METHODS 65

10. Testing of the test rig at the Ship Noise and Vibration Laboratory 67
10.1. Description of the test rig at the NVL Laboratory 67
10.2. Excitation system 70
10.3. Acquisition system 71

11. Prescription for test accuracy 73

12. Procedure for the test rig testing 75
12.1. Stinger rod 76
12.2. Excitation mass 78
12.3. Blocking mass 81
12.4. Soft Isolators 83
12.5. Centring of the moving system of the test rig 85

13. Experimental Tests for the measurement of the dynamic transfer stiffness of a resilient mount 87
13.1. Experimental tests for the measurement of the dynamic transfer stiffness in the normal direction 89
13.2. Experimental tests for the measurement of the dynamic transfer stiffness in the transversal direction 91

14. Simulation of the dynamic transfer stiffness of a resilient mount 93
14.1. Dynamic behaviour of rubber 93
14.2. Outline of the numerical procedure 94

15. Measurement of the mobility of the diesel engine foundations 97

16. Dynamic Simulation of the diesel engine foundation 99

RESULTS 103

17. Resilient mount under investigation 105
17.1. FE linear dynamic analysis of the cast iron components of the resilient mount 107

18. Outcomes of the experimental tests for the dynamic characterization of a resilient mount in the normal direction 111
18.1. Frequency range of the experimental tests 111
18.2. Test for linearity 112
18.3. Unwanted input vibration 114

19. Coupling between the top casting of the resilient mount and the excitation mass 117
19.1. The ODS based analysis 119
19.2. The FEM simulation of the moving system 120

20. Outcomes of the experimental tests for the dynamic characterization of a resilient mount in the transversal direction 123

21. Outcomes of the numerical simulations 125
21.1. Numerical Simulation of the compression test: identification of the main parameters of rubber material 125
21.2. Numerical simulation of the dynamic response of rubber 129

22. Simulation of the dynamics of the diesel engine foundation 133

23. Structure-borne noise prediction according to the single-point method 141

CONCLUSIONS AND FUTURE RESEARCH 149

BIBLIOGRAPHY..... 157

List of Figures

Figure 1- Structure-borne noise transmission paths, from the marine diesel engine towards the ship structures [2].....10
Figure 2 - Flow chart of the single-point approach; the green cells show the theoretical basics that have been applied in the thesis.....15
Figure 3 - Source-Isolator-Receiving structure system 27
Figure 4 - Four-pole parameters for the characterization of a lumped mechanical system.....28
Figure 5 - Resilient mounting in marine application 30
Figure 6 - Block diagram of unidirectional resilient mounting path.....31
Figure 7 - A view of an actual multi-point-connected system [19].....41
Figure 8 - Three block scheme of a source-isolator-receiver system 46
Figure 9 – Layout of a test rig for the direct measurement of dynamic transfer stiffness of a resilient mount.....48
Figure 10 – Layout of a test rig to carry out measurement according to the indirect method.....50
Figure 11 - Typical transmissibility curve of marine diesel engine resilient mountings.....52
Figure 12 - Typical example of a cell element, part of the diesel engine foundation.....55
Figure 13 – Measurement points of a diesel engine foundation designed for marine diesel engine. 55
Figure 14 – a) Qualitative trend of the shear modulus vs temperature graph. b) Qualitative trend of the loss factor vs temperature graph [18] 58
Figure 15 – a) Qualitative trend of the shear modulus vs frequency graph. b) Qualitative trend of the loss factor vs frequency graph [18] 59
Figure 16 -- Test rig facility at the NVL 68
Figure 17 - Moving system of the test rig 68
Figure 18 - Connection between the moving system and the shaker.....69

Figure 19 - Test rig layout for the laboratory experiments according to the indirect method. 70
Figure 20 – Different types of stinger rods: (from left to right) nylon rod, M8 steel rod, M12 steel rod, M20 steel rod 76
Figure 21 - Flanking transmission of vibration energy 77
Figure 22 - Steel sleeve designed to improve the connection between the stinger rod and the excitation mass 78
Figure 23 - FE model of an aluminium disk of the excitation mass 79
Figure 24 - First vibration mode shape (1026 Hz) 79
Figure 25 - Second vibration mode shape (1695 Hz) 79
Figure 26 - Third vibration mode shape (2243 Hz) 79
Figure 27 - FE model of the excitation mass made of three aluminum disks 80
Figure 28 - First vibration mode shape (2567 Hz) 80
Figure 29 - Second vibration mode shape (3926 Hz) 80
Figure 30 - Third vibration mode shape (4210 Hz) 80
Figure 31 - FE model of the blocking mass made of three steel disks 81
Figure 32 - First vibration mode shape (2567 Hz) 81
Figure 33 - Second vibration mode shape (3926 Hz) 81
Figure 34 - Third vibration mode shape (4210 Hz) 81
Figure 35 - Scheme of the experimental test for the measurement of the effective mass 82
Figure 36 - Experimental curve of the effective mass of the Blocking mass 83
Figure 37 – Steel springs used as soft isolators to decouple the moving system by the rigid frame of the test rig 84
Figure 38 - Rubber disks used as soft isolators 84
Figure 39 – Device for the centring and the alignment of the shaker table with the moving system of the test rig 85
Figure 40 – Scheme of the device for the alignment and centring between the shaker table and the moving system. 86
Figure 41 - FE model of a conical resilient mount for marine diesel engine 88
Figure 42 - Section of an FE model for marine diesel engine. The cast iron parts are blue and the rubber part of the resilient mount is white 88
Figure 43 - Resilient mount under test 90

Figure 44 - Plan of acceleration transducers on the moving system (E.M.: excitation mass, B.M.: blocking mass). 91
Figure 45 - Set up of the test rig to carry out the measurement of the dynamic transfer stiffness in the transversal direction 91
Figure 46 - Scheme of the experimental test for the measurement of the effective mass of the blocking mass in the transversal directions 92
Figure 47 - Flow chart of the iterative procedure for the simulation of the dynamic transfer stiffness of the resilient mount 96
Figure 48 - measurement points on a diesel engine foundation 97
Figure 49 - example of diesel engine foundation for marine diesel engines 97
Figure 50 - Passive resilient mount for marine diesel engine 105
Figure 51- Components of conical passive resilient mount for marine diesel engine 106
Figure 52 - Force-displacement curve of the resilient mount under investigation 107
Figure 53 - FE model of the resilient mount top casting 108
Figure 54 - First vibration mode shape (964 Hz) 108
Figure 55 - Second vibration mode shape (1677 Hz) 108
Figure 56 - Third vibration mode shape (1864 Hz) 108
Figure 57 - FE model of the resilient mount base casting 108
Figure 58 - First vibration mode shape (953 Hz) 108
Figure 59 - Second vibration mode shape (1381 Hz) 108
Figure 60 - Third vibration mode shape (1912 Hz) 108
Figure 61 - First mode shape of the base casting of the resilient mount, when it is bolted to a rigid foundation (5674 Hz) 109
Figure 62 - Vertical Transmissibility at different static loading 113
Figure 63 – Vertical Transmissibility curve at different dynamic loads (a_z levels) 113
Figure 64 - Vertical transmissibility curve at the design static load of 75 kN 114
Figure 65 - Accelerometers layout for the measurement of the acceleration levels of the excitation mass in *x* and *y* directions 114
Figure 66 - Acceleration levels of the excitation mass in *x*, *y* and *z* direction 115
Figure 67 - Accelerations measured on the exciting mass (resilient element fitted with the top flange) 118

Figure 68 - Mode shape of the bodies of the moving system at the resonance frequency of about 681 Hz (resilient element fitted with the top flange). 120
Figure 69 - Coupled mode shape of the exciting mass and the top casting (without flange) at the frequency of about 780 Hz. 122
Figure 70 - Accelerations on the excitation mass (transverse driving direction) 123
Figure 71 - Dynamic transmissibility of the resilient mount 124
Figure 72 - Section of the FE model of the resilient mount under test. Ring nut (brown), top casting (blue), rubber core (red), base casting (green).....125
Figure 73 - Force-displacement curve obtained by compression experiments (dashed curve) and by simulations (point-dashed and continuous curves) with different values of the C_{10} coefficient. The continuous curve has been achieved with the coefficient obtained at the end of the fitting procedure. 127
Figure 74 - Force-displacement curve obtained by compression experiments (dashed curve) and by simulations (point-dashed and continuous curves) with different values of the C_{20} coefficient. The continuous curve has been achieved with the coefficient obtained at the end of the fitting procedure. 127
Figure 75 - Force-displacement curve obtained by compression experiments (dashed curve) and by simulations (point-dashed and continuous curves) with different values of the C_{30} coefficient. The continuous curve has been achieved with the coefficient obtained at the end of the fitting procedure. 128
Figure 76 - Force-displacement curve obtained by compression experiments (dashed curve) and by simulations (continuous curves) carried out with the three different coefficients obtained once the numerical procedure has been completed. 128
Figure 77 - Section of the FE model of the resilient mount with the loads applied for the dynamic symulations. Ring nut (brown), top casting (blue), rubber core (red), base casting (green). 130
Figure 78 - Measured dynamic transfer stiffness k_{21}.....130
Figure 79 - Acceleration levels a_x a_y a_z measured during the experimental tests on the excitation mass: the acceleration levels a_z have been used as input acceleration in the numerical simulations.....131
Figure 80 - Measured (dashed curve) and simulated (continuous curve) dynamic transfer stiffness 131
Figure 81 - Half foundation (FE model level 0) 134

Figure 82 - Foundation & the whole hull double bottom extended over the engine room 134
Figure 83 – Normal mode shape at 311 Hz 136
Figure 84 – Normal mode shape at 313 Hz 136
Figure 85 – Normal mode shape at 645 Hz 136
Figure 86 – Normal mode shape at 664 Hz 136
Figure 87 – Normal mode shape at 680 Hz 136
Figure 88 – Normal mode shape at 704 Hz 136
Figure 89 – Normal mode shape at 776 Hz 136
Figure 90 – Normal mode shape at 820 Hz 136
Figure 91 - FRF in the vertical direction 137
Figure 92 - FRF of resilient mount in transversal direction 137
Figure 93 - Mobility curves, measurement point 3Y. 139
Figure 94 - LAC correlation indicator, measurement point 3Y, Level 1 FE model. 139
Figure 95 - Mobility curves, measurement point 3Z. 140
Figure 96 - LAC correlation indicator, measurement point 3Z, Level 1 FE model. 140
Figure 97 – Source velocity level 143
Figure 98 - Foundation mobility levels 144
Figure 99 - Resilient mount transmissibility levels 144
Figure 100 - Source velocity levels $L_{v,s}$, Resilient mount impedance levels L_{Z21}, Foundation mobility levels $L_{Y,r}$, Velocity levels of the foundation $L_{v,r}$.....145
Figure 101 - Comparison of the predicted levels with the measured levels of the structure-borne noise 145
Figure 102 - Receiver to source velociy ratio 146
Figure 103 - Procedure for the prediction of the structure-borne noise generated by resiliently mounted diesel engines, according to the single-point approach..153

Nomenclature

Roman Symbols

$a_i(\omega)$	Fourier transform of complex acceleration
$a_z(t)$	Acceleration in the *z* direction in time domain
A	Contact surface between the output flange of the isolator and the blocking mass
$A_{a,F}(\omega)$	Accelerance
$\mathbf{C}$	Damping matrix
C_f	Coupling function
C_{i0}	Yeoh coefficients
d	Static deflection of resilient mount
$D_{F,v}(\omega)$	Dynamic inertia
$\mathbf{D}_R$	Rigid body vector
E	Young modulus
E'	Storage modulus
E''	Loss modulus
f_e	Lowest internal resonance of the resilient mount
f_n	Natural frequency of a system
f_2	Lower limit of test frequency range
f_3	Upper frequency limit of test frequency range
$F(\omega)$	Fourier transform of input force
$F_b(\omega)$	Fourier transform of the blocked force

F_i	Generalized force vector
$F_r(\omega)$	Fourier transform of external force applied to the receiver
$F_{s,i}(\omega)$	Fourier transform of total internal force developed by the source
F_0	Input force
$\vec{F}(\omega)$	Column vector of forces
F_s	Static load applied to the resilient mount
$F_z(t)$	Force in the *z* direction in time domain
$h(\tau)$	Response of a dynamic linear system to a unit-amplitude impulsive input
$H(s)$	Laplace transformation of the impulse-response function of the linear system
$H(\omega)$	Frequency Response Function of the linear system
I_i	Stress invariant
$k_{ij}(\omega)$	Dynamic transfer stiffness
$k_{ii}(\omega)$	Dynamic driven-point stiffness
k_0	Low-frequency dynamic stiffness of resilient mount
$K_{F,v}(\omega)$	Dynamic stiffness
$\mathbf{K}(\omega)$	Dynamic stiffness matrix
L_{a1}	Acceleration level of the excitation mass
L_{a2}	Acceleration level of the blocking mass
L_T	Transmissibility level
$L_{v,r}$	Foundation velocity level
$L_{v,r(lim)}$	Maximum structure-borne noise levels
L_{vs}	Source velocity level

L_{Yr}	Foundation mobility level
L_{Z21}	Resilient mount mechanical impedance
m_{e1}	Inertia of the rubber core of a resilient mount
m_r	Inertia of the receiving structure
m_s	Inertia of the source
m_2	Inertia of blocking mass
$m_{2,eff}$	Effective mass of blocking mass
$\mathbf{M}$	Structural mass matrix
$\mathbf{M}_{\mathrm{A}}$	Fluid added mass matrix
$p(\omega)$	Fourier transform of output sound pressure
Q	Complex power transmitted by source
R_z	Constrain force in z direction
s	Laplace variable
S	Source descriptor
t	Transmission efficiency
$T_F(\omega)$	Force transmissibility
$T_v(\omega)$	Motion transmissibility
$u_i(\omega)$	Fourier transform of complex displacement
$v(\omega)$	Fourier transform of output velocity
$v_f(\omega)$	Fourier transform of the free velocity of the source
$v_r(\omega)$	Fourier transform of receiver velocity
$v_s(\omega)$	Fourier transform of source velocity
V_i	Generalized velocity vector
$\vec{V}(\omega)$	Column vector of velocities
W	Strain energy density function

$x(t)$	Generic input excitation
$x(\omega)$	Fourier transform of output displacement
$X(s)$	Laplace transformation of the generic input excitation
$X(\omega)$	Fourier transforms of the input excitation
$X_{v,F}(\omega)$	Compliance function
$y(t)$	Response of a dynamic linear system to a generic input excitation
$Y(s)$	Laplace transformation of the response of a dynamic linear system
$Y(\omega)$	Fourier transforms of the response of a linear system
$Y_{v,F}(\omega)$	Mobility function
$Y_r(\omega)$	Driving point mobility of the receiving structures
$Y_s(\omega)$	Driving point mobility of the source in its passive state
$\mathbf{Y}(\omega)$	Matrix of mobility functions
$Z_{F,v}(\omega)$	Impedance function
$Z_{ii}(\omega)$	Driving point mechanical impedance
$Z_{ij}(\omega)$	Transfer mechanical impedance
$Z_r(\omega)$	Driving point mechanical impedance of receiving structures
$\mathbf{Z}(\omega)$	Matrix of impedance functions

Greek symbols

$\alpha_{i,j}$	Four-pole parameter
ε^2	Effective mass vector
$\delta\zeta$	Damping ratio

λ	Wavelength of the excitation signal
μ	Initial shear modulus
Φ	Vector of eigenvectors ϕ

Abbreviations

DMA	Dynamic mechanical analysis
DOF	Degree of freedom
FEM	Finite Element Method
FRAC	Frequency Response Assurance Criterion
FRF	Frequency Response Function
LAC	Local Amplitude Criterion
MAC	Modal Assurance Criterion
MCR	Maximum Continuous Rating of diesel engine
MDOF	Multi Degree of Freedom
ODS	Operational Deflection Shape
SDOF	Single Degree of Freedom
STB	Starboard side

Riassunto

Gli alti livelli di comfort che sono richiesti oggigiorno a bordo di navi da crociera e mega-yachts, portano i progettisti a concentrare la loro attenzione sul problema del rumore strutturale. I motori diesel quattro tempi che sono installati a bordo nave come motori principali o diesel generatori, sono tra le principali sorgenti di rumore strutturale. Per questa ragione, al fine di ridurre l'energia vibrazionale generata da queste sorgenti e trasmessa, tramite le strutture nave, ai locali alloggio, i motori diesel sono sospesi mediante elementi resilienti. Tali elementi resilienti disaccoppiano la sorgente di rumore e vibrazioni (motore diesel) dal mezzo di propagazione (le strutture nave) e isolano dunque la sorgente dalle strutture riceventi. I livelli di rumore strutturale misurati alle fondazioni del motore diesel dipendono dai livelli di velocità misurati sulla sorgente (cioè ai piedi del motore diesel), dai livelli di impedenza meccanica degli elementi resilienti e dai livelli di mobilità meccanica delle fondazioni del motore diesel.

Il single-point approach è un approccio semplificato per la previsione dei livelli di rumore strutturale che trascura l'interazione tra elementi resilienti. Secondo tale teoria, al fine di ridurre il rumore strutturale trasmesso attraverso gli elementi resilienti alle strutture nave, si deve ridurre l'impedenza meccanica degli elementi resilienti così come la mobilità meccanica delle fondazioni del motore diesel. In altre parole, si devono aumentare la rigidezza dinamica degli elementi resilienti così come l'impedenza meccanica delle fondazioni del motore diesel. Ad oggi, l'impedenza meccanica degli elementi resilienti può essere ricavata solo mediante prove sperimentali in laboratorio, mentre la mobilità meccanica del motore diesel è solitamente misurata quando la nave è in costruzione. Dunque non vi è la possibilità di predire, in fase progettuale, il rumore strutturale dovuto ai motori diesel.

In questa tesi, viene presentata una procedura per la simulazione del rumore strutturale dovuto a motori diesel marini. La procedura si basa su test sperimentali

e simulazioni numeriche. Nella prima parte della tesi sono richiamate le basi teoriche necessarie per l'esecuzione delle procedure numeriche e delle prove sperimentali. Sono dunque presentati i risultati delle analisi numeriche per simulare la mobilità delle fondazioni dei motori diesel marini. I risultati delle analisi FEM sono stati validati mediante confronto dei risultati delle analisi numeriche con i dati ottenuti da una campagna di misure eseguite a bordo nave. Successivamente sono presentati i risultati di una serie di prove eseguite per collaudare una nuova macchina sperimentale per misurare l'impedenza meccanica degli elementi resilienti. Lo scopo del collaudo era definire una procedura per l'utilizzo della macchina e per l'esecuzione di prove sperimentali in accordo alla ISO 10846, che è considerata normativa di riferimento per questo tipo di prove. Si è dunque proceduto con l'esecuzione di prove sperimentali eseguite su un elemento resiliente per motori diesel marini. Le prove sono state eseguite a differenti carichi statici. I risultati di queste prove sperimentali sono stati utilizzati per settare un modello numerico che simuli il comportamento non-lineare del componente in gomma del resiliente.

I risultati ottenuti sia dalle prove sperimentali sia dalle simulazioni numeriche sono stati utilizzati per predire il rumore strutturale generato dai motori diesel, in accordo al single-point approach. I risultati ottenuti dall'applicazione del metodo sono stati confrontati con misure eseguite a bordo e sono stati discussi per evidenziare vantaggi e svantaggi dell'applicazione del metodo. Le procedure numeriche per la simulazione del comportamento dinamico del resiliente e della fondazione costituiscono un primo passo per l'ottimizzazione del sistema di isolazione del motore diesel marino.

Abstract

The high level of comfort that is required today on board cruise vessels and mega-yachts, leads the designers to focus their attention on structure-borne noise issues. Four-stroke diesel engines that are installed on board as main diesel engines for the propulsion system and as gen-sets, are usually the main sources of structure-borne noise. For this reason, the diesel engines are usually resiliently mounted in order to reduce the vibration energy generated by these sources and transmitted through the ship structures to the accommodation areas. These mounts decouple the noise and vibration source (diesel engine) from the means of wave propagation (ship structures) and so, they isolate the source from the receiving structures. The structure-borne noise levels measured at the diesel engine foundation depend on the velocity levels measured at the source (diesel engine feet), on the mechanical impedance levels of the resilient mounts and on the mechanical mobility levels of the diesel engine foundation.

The simplified theory of the single-point approach neglects the interaction among the resilient mounts. According to this theory, to decrease the structure-borne noise transmitted through the resilient mounts towards the ship structures, the mechanical impedance of the resilient mounts as well as the mechanical mobility of the diesel engine foundation are to be lowered. In other words the dynamic stiffness of the resilient mounts has to be decreased and the mechanical impedance of the diesel engine foundation has to be increased. To date, the mechanical impedance of real resilient mounts can only be obtained by laboratory tests and the mechanical mobility of the diesel engine foundation is usually measured when the ship is under construction, so it is not available for predictive analyses.

In the thesis, a procedure for simulating the structure-borne noise generated by marine diesel engine is discussed. The procedure is based on both experimental tests and numerical simulations. In the first part of the thesis, some notes on the

theoretical background are presented. Then, the results of FE analyses for simulating the mechanical mobility of a diesel engine foundation are shown. The FE models have been validated by the results of a measurement campaign carried out on board a ship. Then, the results of a series of tests performed to tune a new test rig, designed and built up at the University of Trieste for measuring the mechanical impedance of resilient mounts, are discussed. The campaign for tuning the test rig has been carried out in order to set an experimental procedure that allows achieving results in compliance with the ISO 10846 Standard, which is a sound reference for this kind of tests. As a case study, a large resilient mount for marine diesel engines has been tested to achieve its mechanical impedance curve at different static pre-loads. The outcomes of the experimental tests have been used for tuning the best numerical model of the resilient mount that properly takes into account the nonlinear behaviour of the rubber core. The data of the experimental tests carried out on board ships as well as in laboratory and the outcomes of numerical simulations have been used to predict the structure-borne noise according to the single-point approach. The outcomes achieved by the application of the method have been compared with on board measurements and pros and cons of the method are widely discussed. Moreover, the numerical procedures for the simulation of the dynamic behaviour of the resilient mount and the diesel engine foundation, pave the way for the optimization of the decoupling system of marine diesel engines.

Introduction

On board cruise ships where high levels of comfort are required, particular attention should be paid by the designers to the prediction of the noise and vibration sources due to the main disturbance sources. The diesel engine is a prominent source of vibration and of airborne and structure-borne noise. The latter is transmitted through the ship structures to the accommodation decks. In these areas, the noise generated by the vibration levels of the surrounding structures increases the overall noise of the environment and can affect the comfort levels on-board ships. For these reasons, it is of paramount importance to provide the designers with a straightforward procedure to predict the structure-borne noise due to the diesel engines and, in particular, to characterize the structure-borne noise source.

The aim of the thesis is to define a procedure to predict and simulate through numerical analyses, the structure-borne noise generated by a resiliently mounted marine diesel engine. Such procedure is based on the so-called single-point approach theory that treats the system source-isolator-receiving structures as a system with two degrees of freedom. This simplified approach neglects the mutual interaction between the isolators which decouple the diesel engine to the foundation. The system is sub-structured and the dynamic characteristics of each part are investigated individually and then the results, in terms of transfer functions, are used to predict the structure-borne noise. A more general theory that takes into account the mutual interaction among the resilient mounts is the multi-point approach that has been developed and presented by Fulford and Gibbs in 1997 [1]. According to this theory the vibration power transmitted by a source towards the foundation can be predicted if the magnitude and phase of the forces transmitted by the source in each connection point with the foundation are known. This approach leads to more accurate results but, as drawback, is more difficult to be practically applied. The difficulties are related to the measurement

of the transmitted forces in the audio-frequency range. Indeed, the measured data are often affected by high levels of background noise and, especially in the high frequency range, the coherence between the measured signals is low. For these reasons and since the aim of the thesis is to provide designers with a practical procedure to predict structure-borne noise, the procedure presented in the following chapters is based on the single-point approach, that is more easy to be applied from a practical point of view.

In this work, particular attention is paid to the dynamic characterization of the resilient mount. A test rig for the measurement of the dynamic transfer stiffness of isolators has been tested to verify its effectiveness in performing such laboratory tests. Then, a procedure to carry out laboratory tests on the resilient mount has been defined. The results of the laboratory tests have been used as reference in order to create a numerical model that, considering the non-linear behaviour of rubber and the contact between the rubber part and the resilient mount top and base casting, allowed simulating the dynamic transfer stiffness of the resilient mount under investigation.

The receiving structures have been characterized in terms of mechanical mobility. On-board measurements have been carried out and the results of the campaign have been used as reference in order to define an FE model that simulates the dynamics of the diesel engine foundation.

The results of the analyses have been used to predict the structure-borne noise generated by the marine diesel engine according to the single-point approach and the outcomes of the prediction have been compared with on-board measurements.

In the following chapters, after an introduction to the problem of the structure-borne noise generated by the diesel engines on board ships, some notes on the theoretical background are presented (Part I, Theoretical Background). In this first part of the work, special attention is paid to the theory of sub-structuring (Chapter 2) that has been used, in the research activity, to characterize the resilient mount (Chapter 3) as well as the structure-borne noise source (Chapter 4). Then the basics on the experimental characterization of resilient mount according to the direct and indirect methods are introduced (Chapter 6), as well as the basics on the experimental measurement of the diesel engine foundation

(Chapter 7). In Chapter 8 and in Chapter 9 the state-of-the-art on the simulation of the resilient mount and foundation dynamics is presented.

In the second part the work (Part II, Methods) the procedure to tune the test rig at the Ship Noise and Vibration Laboratory of the University of Trieste is outlined along with the results of the tests that prove the effectiveness of the new test rig in the measurement of the dynamic transfer stiffness of an isolator according to the indirect method (Chapters 10, 11 and 0). Then the procedure to carry out the experimental tests on an isolator is presented (Chapter 13). An iterative procedure to simulate the dynamic transfer stiffness of a resilient mount is outlined in Chapter 14. Chapter 15 and 16 present the method to measure and to simulate the mechanical mobility of a typical diesel engine foundation.

In the third part of the thesis (Part III, Results), the experimental and numerical results are presented (from Chapter 17 until Chapter 23). These are used to apply to a case study the single-point approach to simulate the structure-borne noise generated by a typical marine diesel engine.

General Background

On board ships, reciprocating machines are prominent sources of noise and vibration. These include particularly the four strokes marine diesel engines. The vibration and sound energy generated by the diesel engines are transmitted to the surrounding environment through a series of media [2]:

- Airborne noise: the noise is generated by the diesel engine in the air that surrounds the engine or by its exhaust gas system; the perturbation generated in the air is in the audio-frequency range, from 15 Hz till 16 kHz.
- Vibration energy transmitted through several paths such as resilient mounts, pipes and other devices that connect the diesel engines to auxiliary plants and the ship structure.

The vibration energy generated by the source and transmitted, propagated and radiated by means of waves in solid structures is termed structure-borne noise [3]. According to this definition, all the audio-frequency vibration phenomena of solid structures which are immersed in a fluid are encompassed by the term structure-borne noise [4].

To increase the comfort levels on board ships and in order to decrease the underwater noise pollution, the marine diesel engines are usually resiliently mounted. This solution allows isolating the diesel engines reducing the vibrational energy transmitted towards the ship structures, but on the other hand some vibrational energy is reflected back to the engine [5]. The latter must be controlled in order to prevent excessive vibration levels to cause damages to the engine. Other decoupling systems are also applied to connections between the engine and engine devices and auxiliaries, in order to avoid other propagation paths of vibrational energy. Such decoupling systems also preserve from the high vibrational levels of diesel engines, all that devices which must be rigidly

constrained to the hull structure. Such devices cannot often be exposed to high levels of vibrations that could lead to possible breakage. For instance, the gearbox is rigidly connected to the hull structures and it cannot be exposed to high vibration levels. To overcome that problem, decoupling devices are used in the connection between the diesel engine and the gearbox.

In Figure 1 the main transmission paths of structure-borne noise due to the marine diesel engine are shown. These transmission paths are labelled with progressive numbers. The resilient mounting system is labelled as 1; the airborne noise is labelled as number 2 while the flexible pipes that connect the engine with the auxiliary systems are labelled as number 3. The number 4 shows the flexible coupling between the diesel engine and the gear box, while the number 5 labels the flexible connection between the diesel engine and the exhaust gas system.

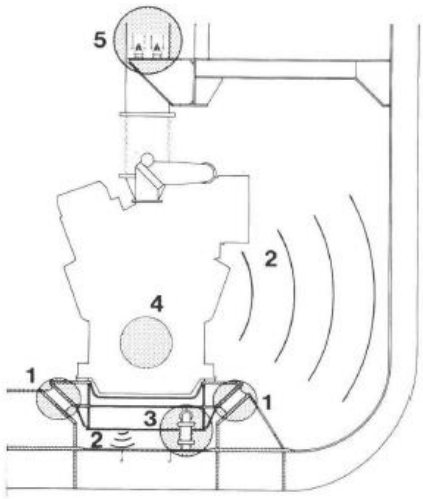

Figure 1- Structure-borne noise transmission paths, from the marine diesel engine towards the ship structures [2]

All structure-borne noise paths, save that one labelled as number 2, are referred to as first-order structure-borne noise, while the transmission path number 2 is referred to as second-order structure-borne noise. In the first-order structure-borne noise transmission paths, the vibrational energy is transmitted to the ship structures through solid structures. In the case of the second-order transmission

paths, the source radiates airborne noise in the surrounding environments; the sound waves propagate in the air medium and transfer energy to the ship structures that, in turn, propagate the energy by means of vibrational waves [4] [6].

In order to understand the transfer mechanism of the sound generated by the diesel engine, all the transmission paths of vibrational or sound energy should be investigated.

In recent years, several research activities have been addressed in order to define a straightforward method for characterizing the engine as a structure-borne noise source (e.g. [1] [7] [8] [9] [10] [11] [12] [13]). Moreover, other studies have been developed for understanding the physics of the transmission of the vibrational energy through the flexible connections, and for defining a straightforward method to simulate their dynamic behaviour (e.g. [14] [15] [16] [17] [18]).
The dynamics of the receiving structures has been deeply investigated in several research activities. In these studies, the researcher tried to define a measurement procedure as well as a method to simulate the response of the receiving structures to the engine excitation (e.g. [9] [19] [20] [21]).

Part I

Theoretical Background

In this part of the thesis, some theoretical backgrounds of the methods that are available today to predict the structure-borne noise are presented. In particular, after a brief mention to the concepts of transfer function and frequency response function, the attention is paid to the main frequency response functions (FRF) that are widely used in the thesis, e.g. the mechanical mobility, the mechanical impedance, the transmissibility.

Then, the concept of sub-structuring is introduced. According to the sub-structuring approach a complex system can be characterized studying the dynamics of each component that is decoupled from the system, and then summing up the results achieved for each component. This approach is the base of the single-point approach that has been applied in this work to predict the structure-borne noise of a resiliently mounted diesel engine.

Once these basic concepts have been introduced, the theoretical background for the experimental and numerical analyses of the resilient mount and of the diesel engine foundations are introduced. As regards the characterization of resilient mounts, the four-pole theory is presented. According to this theory, a passive resilient mount can be characterized once the driving mechanical impedances Z_{ii} and the transfer mechanical impedances Z_{ij} are measured. Then, the concept of power transmitted by the source is presented in the case of a SDOF system and of MDOF system. The latter allows to introduce the theory to study the diesel engine as a multi-point connected system. Even if that theory is not used in this study, it has been presented to show the state of the art of the theory to characterize a source of structure-borne noise. The basics for experimentally characterize a passive resilient mount is then presented in Chapter 6.

The basics for an experimental characterization of a typical diesel engine foundation for marine diesel engine is presented in Chapter 7 while in Chapter 8 and in Chapter 9 the numerical simulation of a resilient mount and the diesel engine foundation respectively are introduced. In Figure 2 a flow chart of the procedure to predict the single point approach is presented. The green blocks show the theoretical basics that are needed to understand the entire procedure along with the chapters of the thesis where such theoretical backgrounds are presented.

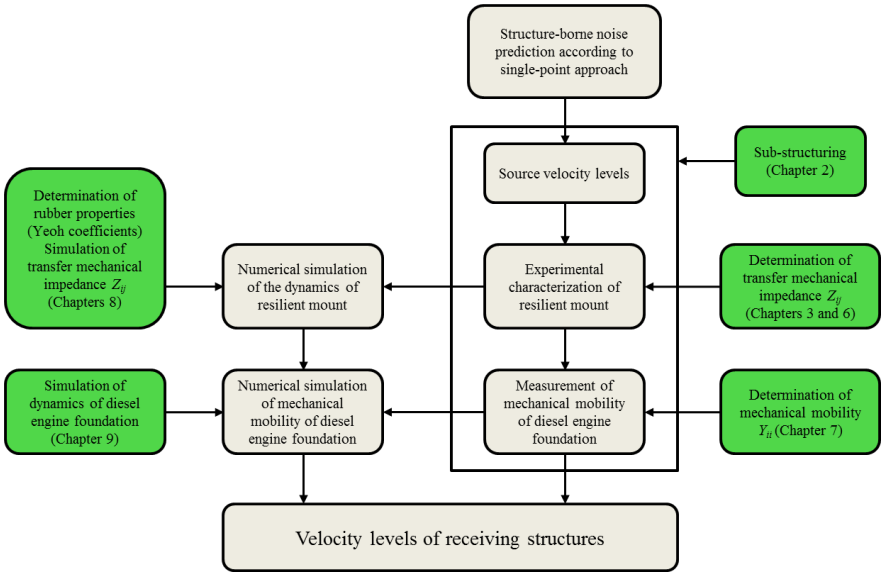

Figure 2 - Flow chart of the single-point approach; the green cells show the theoretical basics that have been applied in the thesis

1. Transfer function

A linear system, whose output characteristics are homogeneous and additive and which is time-invariant, can be dealt with in time domain or in frequency domain [4] [5]. A linear system is completely characterized by a unit impulse-response function that is the response $h(\tau)$ of a dynamic linear system at the time t to an unit-amplitude impulsive input applied at time $(t-\tau)$. It can be shown [5] that the response $y(t)$ of a dynamic linear system to a generic input excitation $x(t)$ is given by the convolution integral equation:

$$y(t) = \int_{-\infty}^{+\infty} x(\tau) h(\tau - t)\, \mathrm{d}t \qquad (1)$$

The Laplace transformation of the Equation (1) converts such equation into an algebraic relationship:

$$Y(s) = H(s)X(s) \qquad (2)$$

in which s is the Laplace variable $s = \sigma + j\omega$ and j is the unit imaginary number. In Equation (2), $Y(s) = \mathcal{L}\, y(t)$ is the Laplace transformation of the response of the dynamic linear system, $X(s) = \mathcal{L}\, x(t)$ is the Laplace transformation of the generic input excitation and $H(s) = \mathcal{L}\, h(t)$ is the Laplace transformation of the impulse-response function of the linear system. The latter, $H(s)$, is a unique characteristic of a linear system and, as well as the impulse-response function, completely represents it.

In a linear and time-invariant system, the input frequency does not change at the output side of the system, and only the amplitude and phase of the signal is changed by the system. This phenomenon is described by the frequency response function that is obtained by a frequency response function that is obtained setting the Laplace variable $s = j2\pi f = j\omega$ [5].The Equation (2) may be expressed as:

$$Y(s) = Y(\omega) = H(\omega)X(\omega) \quad (3)$$

where $X(\omega)$ and $Y(\omega)$ are the Fourier transforms of the input excitation and of the response of the linear system respectively, while $H(\omega)$ is the Frequency Response Function (FRF) of the linear system. The frequency response functions should be expressed by $H(j\omega)$ but, in this work, they are expressed by $H(\omega)$ for notational convenience. It should be noted that for a linear, time invariant system, the Frequency Response Function, the Transfer Function $H(s)$ and as the impulse response $h(t)$, completely represents the system [22].

1.1. Mechanical Mobility and Mechanical Impedance Functions

To define a transfer function of a mechanical system, any type of force or motion variable can be used as input as well as output variable [5]. In this work, the transfer functions, which will be referred to, are the mechanical mobility, the mechanical impedance and the transmissibility functions. These transfer functions are widely used in describing both the generation and the transmission of vibration in mechanical systems.

When the input variable is the force applied to the mechanical system $F(\omega)$, and the output variable is the velocity at a point of the system $v(\omega)$, the transfer function is called mobility function:

$$Y_{v,F}(\omega) = \frac{v(\omega)}{F(\omega)} \quad (4)$$

Indeed, if the output variable is the velocity $v(\omega)$ and the input variable is the force $F(\omega)$, the transfer function is called impedance function:

$$Z_{F,v}(\omega) = \frac{1}{Y_{v,F}(\omega)} = \frac{F(\omega)}{v(\omega)} \quad (5)$$

In frequency domain, velocity is related to acceleration and displacement through a factor of $j\omega$.

The compliance function $X_{x,F}(\omega)$ is defined as the frequency transfer function where the input variable is the force $F(\omega)$ applied to the mechanical system and the output variable is the displacement $x(\omega)$ measured at a point of the structure:

$$X_{x,F}(\omega) = \frac{Y_{v,F}}{j\omega} = \frac{x(\omega)}{F(\omega)} \quad (6)$$

The inverse function of the compliance is called dynamic stiffness $K_{F,x}(\omega)$:

$$K_{F,x}(\omega) = \frac{F(\omega)}{x(\omega)} \quad (7)$$

The transfer function obtained by the complex ratio of the acceleration $a(\omega)$, as output variable, and the input force $F(\omega)$, is called accelerance $A_{a,F}(\omega)$:

$$A_{a,F}(\omega) = Y_{v,F} \cdot j\omega = \frac{a(\omega)}{F(\omega)} \quad (8)$$

Its inverse is called dynamic inertia or effective mass $D_{F,a}(\omega)$:

$$D_{F,a}(\omega) = \frac{F(\omega)}{a(\omega)} \quad (9)$$

It can be shown that the structure-borne noise radiated from a structure can be found, if the input force $F(\omega)$ is known, according to the following equation [4] [13]:

$$H_{p,F}(\omega) = \frac{p(\omega)}{F(\omega)} \quad (10)$$

where $p(\omega)$ is the output pressure measured at a point and $F(\omega)$ is the input force applied to the structure.

Table 1 – Basics Frequency Response Functions

INPUT	OUTPUT	FRF	1/FRF
Force	Displacement	Admittance Compliance Receptance	Dynamic stiffness
	Velocity	Mobility	Mechanical Impedance
	Acceleration	Accelerance Inertance	Dynamic Mass Apparent Mass

1.2. Transmissibility Function

The transmissibility function is another important transfer function that is used in the treatment of the isolation of mechanical systems from unwanted vibration [5]. This function can be defined in two different ways: Force Transmissibility and Motion Transmissibility.

The force transmissibility can be easily defined considering a mechanical system (*e.g.* the diesel engine) that is decoupled from a rigid foundation (*e.g.* the diesel engine foundation) by means of a suspension system (*e.g.* the resilient mounting system). Applying a frequency dependent dynamic force $F(\omega)$ to the diesel engine, the force that is transmitted to the diesel engine foundation $F_s(\omega)$ is, in general, different from $F(\omega)$, and this is due to the presence of the resilient mounting system that alters the transmitted force. Hence the force transmissibility can be defined as follows:

$$T_F(\omega) = \frac{F_s(\omega)}{F(\omega)} \qquad (11)$$

In the case of a system that should be isolated from the motion of a vibrating structures which support it, the motion transmitted by the suspension system to the mechanical system can be described by the following transfer function:

$$T_v(\omega) = \frac{v_m(\omega)}{v(\omega)} \quad (12)$$

where v is the velocity of the supporting structures, v_m is the transmitted velocity and T_v is the motion transmissibility. It can be shown that these transmissibility functions (Equation (11) and Equation (12)) are equal, and this is due to the reciprocity characteristics of the linear systems [5].

The force transmissibility is widely used for investigating the dynamic properties of the isolators and their effectiveness in cutting-off the unwanted vibrations [2] [15] [18] [23] [24] [25] [26] [27] [28] [29] [30] [31]. The motion transmissibility is commonly used in defining the vibro-acoustics characteristics of the floating-floors that are usually installed on board ships to isolate the cabins form ship structures which vibrations could lead to decrease the comfort levels [32] [33] [34].

1.3. Mechanical Mobility and Impedance Matrices

Considering a multiple degree of freedom (MDOF) mechanical system, which is assumed to be linear and whose material behaves elastically, the set of the mechanical mobility functions $y_{i,j}$ is defined as follows:

$$v_i(\omega) = \sum_{j=1}^{n} y_{i,j}(\omega) \cdot f_j(\omega) \quad (13)$$

where v_i is the velocity of point i due to the force f_j applied at point j.

Equation (13) is valid for each point of the mechanical system, and so a set of equations can be defined for a MDOF system. Hence, a MDOF mechanical system is characterized by a set of mechanical mobility functions that allows describing the dynamic behaviour of the whole system. Each mobility function is an element of a tensor $\mathbf{Y}(\omega)$:

$$\vec{V}(\omega) = \mathbf{Y}(\omega) \cdot \vec{F}(\omega) \quad (14)$$

where $\vec{V}(\omega)$ is a column vector of the resultant velocities and $\vec{F}(\omega)$ is the column vector of the applied forces:

$$\begin{Bmatrix} v_1(\omega) \\ \vdots \\ v_n(\omega) \end{Bmatrix} = \begin{bmatrix} y_{1,1}(\omega) & \cdots & y_{1,n}(\omega) \\ \vdots & \ddots & \vdots \\ y_{n,1}(\omega) & \cdots & y_{n,n}(\omega) \end{bmatrix} \begin{Bmatrix} f_1(\omega) \\ \vdots \\ f_n(\omega) \end{Bmatrix} \qquad (15)$$

For the same system, we can define a set of mechanical impedance functions $z_{i,j}$ defined as follows:

$$f_i(\omega) = \sum_{j=1}^{n} z_{i,j}(\omega) \cdot v_j(\omega) \qquad (16)$$

And so it is possible to define the mechanical impedance tensor as follows:

$$\vec{F}(\omega) = \mathbf{Z}(\omega) \cdot \vec{V}(\omega) \qquad (17)$$

The terms of each row of the matrix $\mathbf{Z}(\omega)$ are the $z_{i,j}$ defined in Equation (16). From Equation (14) and Equation (17) it derives that $\mathbf{Z}(\omega)=\mathbf{Y}(\omega)^{-1}$. According to the properties of matrix operations, the general element $z_{i,j}$ of the impedance matrix $\mathbf{Z}(\omega)$ is not the inverse of the corresponding element $m_{i,j}$ of the mobility matrix $\mathbf{Y}(\omega)$.

2. Sub-structuring

A black-box approach is usually employed to characterize a structure-borne noise source [35] [13]. The source, *e.g.* a diesel-engine, is subject to internal generalized forces that are released by rotating mechanisms or generated by the reciprocating motion of pistons or by impacts or pressure variations. Such internal forces are usually very difficult to calculate or to measure. The large variety of internal forces and their simultaneous acting on the source structures lead to high uncertainty in the outcomes of their direct measurement, when the latter is possible. Moreover, the high number of non-linear phenomena which characterize a so complex structure entails troubles in the simulation of the transmission of the internal forces through the source structures. For these reasons, sources are described in terms of quantities (such as velocity or acceleration) which can be observed at the output of the source, at its interface with the receiving structures. If the source is not connected to other structures (free-free condition) and it is not subject to external forces, the velocity observed at the source interface can be related to the internal forces as follows:

$$Y_{t,s}(\omega) = \frac{v_s(\omega)}{F_{s,i}(\omega)} \qquad (18)$$

where $F_{s,i}$ is the total internal force developed by the source, v_s is the velocity measured at the source interface and $Y_{t,s}$ is the transfer mobility function that describes the relation between the resultant of the internal forces and the velocity caused by those forces.

Considering the source in its passive state which is subject to an external force F_s applied to a point s at the source interface, the resulting velocity v_s measured at the point s is related to the applied force F_s as follows:

$$Y_s(\omega) = \frac{v_s(\omega)}{F_s(\omega)} \quad (19)$$

where Y_s is the driving point mobility of the source in its passive state.

Similarly, a driving point function which describes the passive properties of the receiver can be defined as follows:

$$Y_r(\omega) = \frac{v_r(\omega)}{F_r(\omega)} \quad (20)$$

in which F_r is an external force applied to the receiver and v_r is the resulting velocity. Y_r is the driving point mobility of the receiving structures.

When the source and the receiving structures are coupled together, the velocity v_s measured at a point *s* depends on the boundary condition of the source as well as on the internal forces. According to Equation (18) and Equation (19), the source velocity v_s depends on the driving point mobility and on the transfer mobility as follows:

$$v_s(\omega) = Y_{t,s}(\omega) \cdot F_{s,i}(\omega) + Y_s(\omega) \cdot F_s(\omega) \quad (21)$$

If the source is rigidly coupled to the receiving structures, the source velocity v_s is equal to the receiver velocity v_r that, in turn, depends on the force applied to the receiver F_r and to the mobility of the receiver Y_r; then, $F_r = -F_s$.

Equation (21) allows to calculate the source velocity. Nevertheless, the transfer mobility $Y_{t,s}$ and the internal force $F_{s,i}$ are very difficult to calculate or to measure. In order to achieve the source velocity v_s the concepts of the blocked force F_b and of the free velocity v_f are introduced.

The free velocity v_f is the velocity measured at the source interface, when the source is in the free state, which means that no constrains are applied [35] [13]. Then, Equation (21) can be rewritten as follows:

$$v_s(\omega) = v_f(\omega) + Y_s(\omega) \cdot F_s(\omega) \quad (22)$$

When the source is rigidly coupled to the receiver, the transmitted force F_r can be obtained as follows:

$$F_r(\omega) = \frac{v_f(\omega)}{Y_s(\omega) + Y_r(\omega)} \quad (23)$$

and the velocity v_r:

$$v_r(\omega) = \frac{Y_r(\omega)}{Y_s(\omega) + Y_r(\omega)} v_f(\omega) \quad (24)$$

The blocked force F_b is defined as the force measured at the interface of the source in the blocked state, which means that the source velocity v_s is zero:

$$F_b(\omega) = -F_S(\omega)\big|_{v_s(\omega)=0} \quad (25)$$

and is related to the free velocity as follows [36]:

$$F_b(\omega) = \frac{v_f(\omega)}{Y_s(\omega)} \quad (26)$$

Equation (22) is then modified:

$$v_s(\omega) = Y_s(\omega) \cdot F_b(\omega) + Y_s(\omega) \cdot F_s(\omega) \quad (27)$$

and, considering a source rigidly coupled to the receiving structures, the force F_r transmitted by the source can be obtained by:

$$F_r(\omega) = \frac{Y_s(\omega)}{Y_s(\omega) + Y_r(\omega)} F_b(\omega) \quad (28)$$

and the velocity measured at the receiving structures:

$$v_r(\omega) = \frac{Y_s(\omega) Y_r(\omega)}{Y_s(\omega) + Y_r(\omega)} F_b(\omega) \quad (29)$$

In the thesis, all functions will be expressed in the frequency domain. For that reason, frequency functions will be assumed and so, hereafter, in all formulas (ω) will be dropped for clarity.

The blocked force can be practically measured when the source is constrained to an inert structure. The velocity v_r of the receiver can be approximated to zero and the forces at the source interface are measured by means of force transducers. Nevertheless, the introduction of these transducers can affect the rigid coupling between the source and the receiving structures and so they can alter the values of the measured forces. Moreover, the measurement of forces is more difficult than the measurement of velocity and the goodness of the data acquired by force measurement decreases with the increase of frequency.

Velocity measurement is usually easier to carry out and so it is almost always preferred to measure the free velocity instead the blocked force. To carry out these tests, the source has to be properly suspended in order to avoid the influence of the constraints in the source velocity. This can be easily done for small sources which can be suspended using elastic springs, and for big ones which can be installed on stiff foundation by means of a soft resilient mounting system. The downside of the free velocity method is that some sources cannot properly operate if they are not rigidly connected to the rigid foundation. The ISO 9611:1996 standardizes the measurement of the free velocity [37].

When the source is decoupled by the receiving structures by a resilient mounting system the Equation (21) is no longer valid and further considerations are needed.

3. Resilient mounts

In Chapter 2, the sub-structuring method has been introduced to study the rigid coupling of the source to the receiver. The source can also be coupled to the receiving structure by a resilient mount. This solution is widely diffused when the source has to be isolated by receiving structures in order to reduce the transmission of vibration energy. Figure 3 shows the source, the resilient element and the receiving structures as sub-structures. In the Figure, F_0 is the input force of the source, m_s is the mass of the source, F_s is the force transmitted by the source to the isolator, v_s is the source velocity, F_r is the force transmitted by the isolator to the receiver, m_r is the mass of the receiver and v_r is the receiver velocity. The stiffness of the isolator is labelled with k_0. In the following Sections the four-pole parameters theory is introduced to investigate how the resilient element alters the transmission of the energy towards the receiving structures.

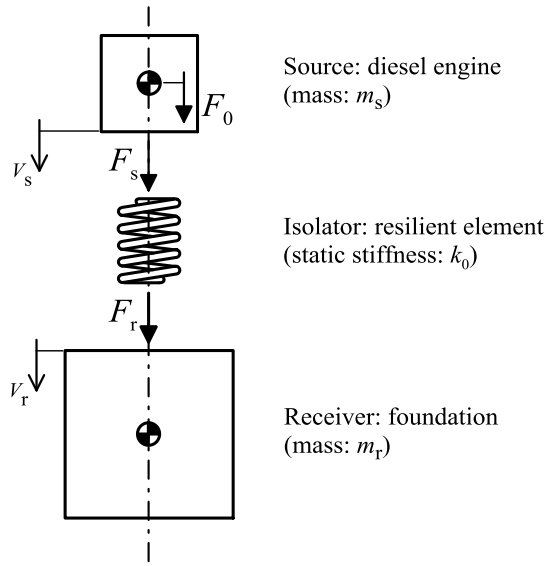

Figure 3 - Source-Isolator-Receiving structure system

3.1. Four-pole parameters theory

A complex mechanical system can be described with the so called four-pole parameters $\alpha_{i,j}$ [38] [24]. According to this approach, a mechanical system, which can be formed by several mechanical elements, can be described as a combination of linear lumped mechanical elements like masses and springs. Figure 4 shows a mechanical system characterized by an input force F_1 and an input velocity v_1 at terminal 1 and an output force F_2 and velocity v_2 at the output terminal 2.

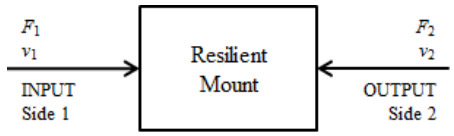

Figure 4 - Four-pole parameters for the characterization of a lumped mechanical system

The relations between the input quantities and the respective output ones are shown in the following equations:

$$\begin{cases} F_1 = \alpha_{11} F_2 + \alpha_{12} v_2 \\ v_1 = \alpha_{21} F_2 + \alpha_{22} v_2 \end{cases} \quad (30)$$

The four-pole parameters $\alpha_{i,j}$ can be obtained using the free velocity (which implies a null output force F_2) and the blocked force (which implies a null output velocity v_2) [38]:

$$\alpha_{11} = \left.\frac{F_1}{F_2}\right|_{v_2=0} \quad \alpha_{12} = \left.\frac{F_1}{v_2}\right|_{F_2=0}$$
$$\alpha_{21} = \left.\frac{v_1}{F_2}\right|_{v_2=0} \quad \alpha_{22} = \left.\frac{v_1}{v_2}\right|_{F_2=0} \quad (31)$$

According to the reciprocity theorem, the transfer mobility and the transfer impedance between two terminal pairs is independent of which terminal pair is considered the input or the output, and so Equations (30) can be rewritten as follows [39]:

$$\begin{cases} F_2 = \alpha_{11} F_1 + \alpha_{12} v_1 \\ v_2 = \alpha_{21} F_1 + \alpha_{22} v_1 \end{cases} \quad (32)$$

For a symmetric mechanical system it can be shown that $\alpha_{11} = \alpha_{22}$ [39].

3.2. Four-pole parameters of passive resilient mounts

When an isolator is used to decouple the receiving structure from the source, Equations (32) can be used to describe its action as linking structure. If the interface of the isolator with the source is called 1 and the interface of the isolator with the receiver is called 2, two impedance equations define the relations between the forces and the velocities as follows [2] [40]:

$$\begin{cases} F_1 = Z_{11} v_1 + Z_{12} v_2 \\ F_2 = Z_{21} v_1 + Z_{22} v_2 \end{cases} \quad (33)$$

Or, as a matrix equation:

$$F = \mathbf{Z} \cdot V \quad (34)$$

F_1 and F_2 are the input and output forces respectively and v_1 and v_2 are the input and output velocities respectively. The terms of the impedance matrix **Z** are the driving mechanical impedances Z_{ii} and the transfer mechanical impedances Z_{ij} of the resilient mount. In particular:

$$\begin{aligned} Z_{11} &= \left.\frac{F_1}{v_1}\right|_{v_2=0} & Z_{12} &= \left.\frac{F_1}{v_2}\right|_{v_1=0} \\ Z_{21} &= \left.\frac{F_2}{v_1}\right|_{v_2=0} & Z_{22} &= \left.\frac{F_2}{v_2}\right|_{v_1=0} \end{aligned} \quad (35)$$

where $Z_{21} = Z_{12}$ if the resilient mount can be considered a linear system and the reciprocity principle is valid.

The resilient mount is connected to the source, at the top, and to the receiver structure, at the bottom (see Figure 5).

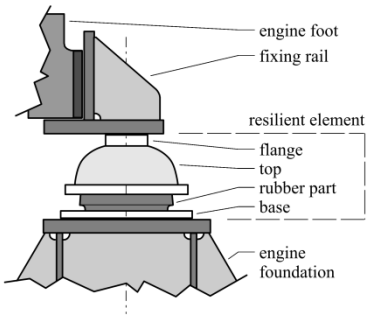

Figure 5 - Resilient mounting in marine application

At these interfaces, the resilient mount transmits forces with other structures and the following relations can be written:

$$F_1 = F_s \quad v_1 = v_s \tag{36}$$

with regard to the interaction between the resilient mount and the source, and:

$$F_2 = F_r \quad v_2 = -v_r \tag{37}$$

with regard to the interaction between the resilient mount and the receiving structures. The sings of Equations (36) and (37) follow from the Figure 6, where all the reported forces and velocities directions are positive.

From Equations (33) and (37), it follows that:

$$F_r = F_2 = \frac{Z_{21}}{1+\frac{Z_{22}}{Z_r}} v_s \tag{38}$$

Where *Zr* is the mechanical impedance of the receiver defined as:

$$Z_r = \frac{F_r}{v_r} \qquad (39)$$

Equation (38) shows that the force F_r transmitted from the source to the receiving structures is obtained if the mechanical impedance of the receiver Z_r is known, along with the driving point mechanical impedance Z_{22} and the transfer mechanical impedance Z_{21} of the isolator.

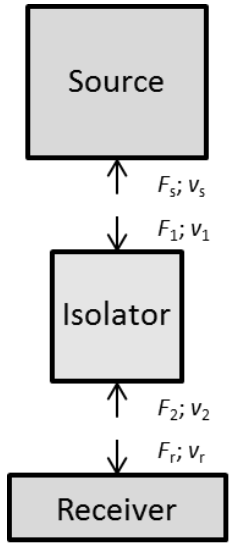

Figure 6 - Block diagram of unidirectional resilient mounting path

When the receiving structures are characterized by high value of mechanical impedance Z_r, if compared with the driving point mechanical impedance of the isolator Z_{22}, Equation (38) can be rewritten as follows:

$$F_r \cong Z_{21} \cdot v_s \qquad (40)$$

The condition that the mechanical impedance of receiving structures Z_r is larger than the mechanical impedance of the isolator is generally satisfied in order to guarantee the effectiveness of the isolators. But this condition is no longer satisfied in the frequency range in which standing waves occur in the rubber core

of the resilient mount. Indeed, these standing waves lead to an increase of the resilient mount mechanical impedance, and the condition $Z_r >> Z_{22}$ is no longer satisfied.

Equation (40) shows that the force F_r transmitted to the receiver can be obtained independently from the mechanical impedance of the receiver and only depends on the blocked transfer impedance of the isolator. Moreover, Equation (40) can be practically applied for obtaining the blocked transfer impedance by experimental tests, as described in Section 6.2.

3.3. Calculation of the receiver velocity

The velocity of receiving structures v_r can be calculated combining the Equations (33) and (37). From such combination it follows:

$$v_r = \frac{Z_{21}}{Z_{22} + Z_r} \cdot v_s \qquad (41)$$

Hence, the velocity of the receiving structures v_r depends on the velocity of the source v_s, on the driving point impedance of the output interface of resilient mount Z_{22}, on the transfer impedance of resilient mount Z_{21} and the driving point impedance of receiver Z_r. In the previous Section it has been explained that usually the mechanical driving point impedance of the output interface of the resilient mount is pretty much smaller than the driving point impedance of the receiving structures $|Z_{22}| \ll |Z_r|$. Then, Equation (41) can be written as follows:

$$v_r \cong \frac{Z_{21}}{Z_r} \cdot v_s \qquad (42)$$

The mechanical driving point impedance of receiving structures is the inverse of its mechanical mobility: $Z_r = Y_r^{-1}$, then:

$$v_r \cong Z_{21} \cdot Y_r \cdot v_s \qquad (43)$$

The advantage of Equation (43) is its immediate applicability to achieve the receiver velocity. The source velocity can be measured according to the free

velocity approach presented in Chapter 2, the mechanical transfer impedance of resilient mount can be measured with special laboratory tests, and the mechanical mobility of receiving structures can be measured carrying out field measurement campaign, before the source is installed on the foundation structure.

Equation (24) shows the relation between the source velocity v_s and the receiver velocity v_r, in terms of mobility of the source and of the receiver and in the case of a source directly connected to the receiving structures. Such Equation can be rewritten in terms of mechanical impedance as follows:

$$v_r = \frac{Z_s}{Z_s + Z_r} \cdot v_s \qquad (44)$$

It is worth pointing out that the insertion of the isolator between the source and the receiving structures implies the substitution of the driving point impedance of the source, at the numerator of Equation (44), with the transfer impedance of the resilient mount, that is considered as the new source of the system (Equation (41)).

3.4. Resilient mount characterization in the six degrees of freedom

In the previous Section, the characterization of a resilient mount using the four-pole theory has been explained for a single-point connected isolator, considered as a single degree of freedom system. Ten Wolde generalized such relations for a case with six degrees of freedom at each side of the isolator [40]. As results, a complete characterization of resilient mount can be carried out with a linear twelve-port. At the input and output points of resilient mount, it is possible to define two velocity vectors:

$$V = \left\{ \dot{x}_p, \dot{y}_p, \dot{z}_p \right\} \qquad (45)$$

$$\Omega = \left\{ \dot{\alpha}_p, \dot{\beta}_p, \dot{\gamma}_p \right\} \qquad (46)$$

Where the terms of vector V are the translation velocities of the point and the terms of vector Ω are the angular velocities of the point. For notational

convenience, we can define a generalized velocity vector whose 6 terms are the terms of the vector V and Ω respectively:

$$V_1 = \left\{ \dot{x}_1, \dot{y}_1, \dot{z}_1, \dot{\alpha}_1, \dot{\beta}_1, \dot{\gamma}_1 \right\} \quad (47)$$

$$V_2 = \left\{ \dot{x}_2, \dot{y}_2, \dot{z}_2, \dot{\alpha}_2, \dot{\beta}_2, \dot{\gamma}_2 \right\} \quad (48)$$

V_1 is the generalized velocity vector of the input side of resilient mount and V_2 is the generalized velocity vector of its output side. The first three terms of the vectors are the translational velocities and the fourth, fifth and sixth terms are the three angular velocities about the principal axes *x y* and *z* respectively.

Similarly, the generalized force vector at each side can be written as follows:

$$F_1 = \left\{ F_{x1}, F_{y1}, F_{z1}, F_{\alpha 1}, F_{\beta 1}, F_{\gamma 1} \right\} \quad (49)$$

$$F_2 = \left\{ F_{x2}, F_{y2}, F_{z2}, F_{\alpha 2}, F_{\beta 2}, F_{\gamma 2} \right\} \quad (50)$$

where F_1 is the generalized force at the side 1 of the isolator and F_2 is the generalized force at the side 2.

The impedance matrix is a 12 × 12 matrix and so contains 144 terms. Because of the reciprocity, impedance matrix can be divided in 4 sub-matrixes as follows [2] [41]:

$$\mathbf{Z} = \begin{bmatrix} [Z_{11}] & [Z_{12}] \\ [Z_{21}] & [Z_{22}] \end{bmatrix} \quad (51)$$

Z_{11} and Z_{22} are symmetrical matrices 6 × 6 and contain the driving point impedances of the two sides of the resilient mount, and Z_{12} and Z_{21} are 6 × 6 matrices which contain the transfer blocked impedances of the resilient mount.

Ten Wolde has shown that if the driving point impedance of receiving structures is much larger than the driving point impedance matrix of resilient mount, then the force transmitted to the receiver can be obtained as follows [40]:

$$F_2 \cong \mathbf{Z}_{21} V_1 \qquad (52)$$

Matrix Z_{21} contains 36 terms. Verheij has investigated on the simplification of matrix Z_{21} in the case of resilient mounts characterized by one or two planes of symmetry and he has rewritten the simplified matrix for some typical cases of resilient mounts [2].

4. Source power: characterization of a structure-borne noise source

The characterization of a structure-borne noise source is an issue that has been object of many studies in recent years (e.g. [1] [7] [8] [13] [10] [12]). The interest on this subject is due to the importance, at the design stage, of predicting the noise and vibration levels of a machine that has to be installed on board ships. Such problem has been already addressed to characterize the airborne noise sources, and straightforward analytical and numerical models have been established and they are widely used in acoustic engineering. The structure-borne noise generated by a machine depends on the characteristics of the source, along with the characteristics of the coupling elements (i.e. the resilient mounts) and the dynamics of the receiving structures. Indeed, as shown by Equations (44) and (52), the velocity of the receiver is related to the velocity of the source, to the driving point impedance of the source and of the receiver, and to the transfer blocked impedance of the isolator, if it is present.

To describe a structure-borne sound source, considered as a SDOF system, Cremer et al. [3] defined the complex transmitted power as follows:

$$Q = A + jB = \frac{1}{2} F_r \cdot v_r \qquad (53)$$

Where F_r is the complex force transmitted by the source to the receiver and v_r is the complex velocity of the receiver, at the contact point with the source. The real part of the complex transmitted power is the actual power flowing to the receiving structures, while the imaginary part B is the reactive part of the source power Q, and it is a part of the whole power that goes back and forth through the contact point.

The Equation (53) can be rewritten as follows [42, 12]:

$$Q = \frac{Y_r}{\left|Y_r + Y_s\right|^2}\left|v_f\right|^2 \qquad (54)$$

where v_f is the free velocity of the source. Equation (54) shows that the power flowing from the source to the receiver depends on the source and on the receiving structure characteristics.

Mondot and Petersson [43] introduced two functions to characterize the structure-borne noise sources: the source descriptor S and the source coupling function C_f. The source descriptor is:

$$S = \frac{v_f^2}{Y_s^*} \qquad (55)$$

and only depends on the source characteristics v_f and Y_s^*, that are the free velocity and the complex conjugate of source mobility. While the source coupling function C_f is defined as follows:

$$C_f = \frac{Y_s^* Y_r}{\left|Y_s + Y_r\right|^2} \qquad (56)$$

thus the source power, Equation (53) and (54) can be rewritten as:

$$Q = S \cdot C_f \qquad (57)$$

The experimental results presented by Mondot and Petersson showed that the source descriptor S is not a straightforward parameter for comparing different sources, as the active power transmitted to the receiver strongly depends on the coupling factor C_f [43].

4.1. Source power of a suspended machine

Petersson and Gibbs [12] showed that, in the case of a resiliently mounted source, the complex power transmitted by the source is obtained by:

$$Q = Q_0 \frac{\left|Y_s + Y_r\right|^2 \left|Y_{21}\right|^2}{\left|\left(Y_s + Y_{11}\right)\left(Y_r + Y_{22}\right) - Y_{12}Y_{21}\right|^2} \quad (58)$$

where Q_0 is the complex power of the source without the resilient mounts in place. Petersson and Gibbs defined the transmission efficiency of the isolators as:

$$t = \frac{\left|Y_s + Y_r\right|^2 \left|Y_{21}\right|^2}{\left|\left(Y_s + Y_{11}\right)\left(Y_r + Y_{22}\right) - Y_{12}Y_{21}\right|^2} \quad (59)$$

That can be approximated as:

$$t' = \left|Y_s + Y_r\right|^2 \frac{\left|Y_{21}\right|^2}{\left|Y_{11}Y_{22} - Y_{12}Y_{21}\right|^2} \quad (60)$$

if the isolator mechanical mobilities are much larger than the mechanical mobility of the receiver and of the source.

5. Multi-point connected sources

The relation presented by Verheij, Equation (52), allows to calculate the force transmitted by a single resilient mount to the receiving structures, i.e. the engine seating, for all the 6 degrees of freedom. The sources are usually connected to the receiving structures in several points (see Figure 7). For example, a diesel engine, installed on board ships, is usually suspended by a high number of isolators. The small four stroke diesel engines, whose power ranges from about 75 kW, when they are employed as prime movers of small pleasure crafts, till about 2000 kW for those ones employed as propulsion system of mega-yachts, can be connected to the receiving structures by 4 resilient mounts. The more powerful medium speed marine diesel engines are usually connected to the seating by a higher number of resilient mounts which can reach the number of thirty for diesel engines of about 19000 kW. For these reasons several studies have been undertaken in order to understand the mutual interactions of the resilient mounts and in order to provide methods for predicting the structure-borne noise due to a source that is connected to the seating in several points.

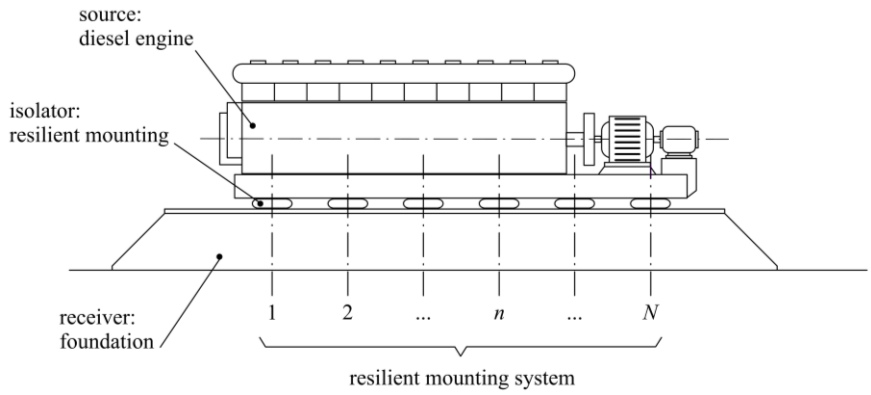

Figure 7 - A view of an actual multi-point-connected system [19]

5.1. Source power of multi-point connected systems

Equations (55), (56) and (57) defined by Mondot and Petersson allow to calculate the source power transmitted by a source connected to receiving structures in one single-point. Fulford and Gibbs generalized those equations to the case of a multi-point connected system [1] [7] [8]. The source has been supposed to move in all six degrees of freedom and to be connected to receiver in N connection points. Under these assumptions, the power transmitted by the source can be obtained by [1]:

$$Q_i^n = \frac{1}{2} \frac{\left(v_{fi}^n\right)^2}{\left|[\mathbf{Y}_s]\left\{F_j^m / F_i^n\right\} + [\mathbf{Y}_r]\left\{F_j^m / F_i^n\right\}\right|^2} \mathrm{Re}\left\{[\mathbf{Y}_r]\left\{F_j^m / F_i^n\right\}\right\} \quad (61)$$

where v_f is the free velocity of the source, $[\mathbf{Y}_s]$ is the $6N \times 6N$ matrix of the source mobility and $[\mathbf{Y}_r]$ is the $6N \times 6N$ matrix of the receiver mobility.

F_j^m / F_i^n is the ratio between the force acting in the j direction and in the m point and the force acting in the i direction and in the n point.

In order to help to address this complex problem, the effective mobility has been introduced as follows [44]:

$$Y_{ii}^{nn\Sigma} = Y_{ii}^{nn} + \sum_{m=1, m\neq n}^{N} Y_{ii}^{nm} \frac{F_i^m}{F_i^n} + \sum_{j=1, j\neq i}^{6} Y_{ij}^{nn} \frac{F_j^n}{F_i^n} + \sum_{m=1, m\neq n}^{N} \sum_{j=1, j\neq i}^{6} Y_{ij}^{nm} \frac{F_j^m}{F_i^n} \quad (62)$$

where the mobility Y_{ij}^{nm} is a mobility where the force is acting at the point m and direction j to the point n and direction i. The first term in the right hand side of the equation is the direct structure-borne sound transmission path, the second term is the contribution of the other points in the direction n, the third term is the contribution of the other direction at the point being considered and the fourth term is the contribution from other points in directions other than that being considered.

If only a one-direction translational motion is considered, Equation 4 simplifies and, under the assumption that forces have unity magnitude and zero phase, the effective mobility comes out to be [19] [20]:

$$Y_{ii}^{nn\Sigma} = Y_{ii}^{nn} + \sum_{m=1, m\neq n}^{N} Y_{ii}^{nm} \qquad (63)$$

This formulation is very simplified compared to that of Equation (62), and therefore easier to apply in practice, even if the contributions of the other points are still taken into account.

6. Experimental characterization of resilient mounts

In the Chapter 3, it has been shown that, to completely characterize a resilient mount in 6 degrees of freedom, the impedance matrix $\mathbf{Z}_{21}$ has to be known. Indeed, according to Equation (52), the force transmitted to the receiving structures through the resilient mount can be calculated once the impedance matrix $\mathbf{Z}_{21}$ is known along with the velocity of the source $\mathbf{V}_1$.

Matrix $\mathbf{Z}_{21}$ contains 36 elements, but if the resilient mount under investigation is characterized by axes of symmetry, many of these elements are null and other non-null elements are equal in magnitude [2] [41]. In those cases, fewer elements of the matrix have to be obtained in order to completely characterize the resilient mount. In practical cases, the resilient mounts are cylindrical or conical and the directions that are prominent in the transmission of the vibrational energy are the translational ones. So, just two or three terms of the impedance matrix are usually sufficient to characterize the resilient mounts.

A common standard for the test procedure and the design of the laboratory facilities is the ISO 10846 Standard "Acoustics and vibration - Laboratory measurement of vibro-acoustic transfer properties of resilient elements" whose relevant parts are Part 1 (Principles and guidelines) [41], Part 2 (on the direct method) [45], Part 3 (on the indirect method) [46] Part 4 (on resilient elements other than for translatory motion) [47] and Part 5 (on the driving-point method) [48].

The Part 1 of the Standard is an introduction to the theoretical background of the experimental characterization of the resilient mounts and is also a guide for the usage of the other parts of the Standard. According to that approach, the dynamic parameters of a resilient mounting system are defined by making reference to a three block system: the vibration source (i.e., the diesel engine), the N isolators and the receiving structure (i.e., the engine foundation). The application of the

procedure is subject to the main assumption that only passive linear-response resilient elements may be studied. It also supposes that the contact between the three blocks is a contact point and that a 6 component force vector and a 6 component displacement vector are assigned by each contact point. The Standard states that to characterize a resilient mount, its dynamic transfer stiffness k_{21} has to be measured. That quantity is defined as follows:

$$k_{21} = \frac{F_{2b}}{u_1} \qquad (64)$$

where F_{2b} is the dynamic force on the blocked output side of the isolator under investigation (i.e. the force F_2 when u_2 is null) and u_1 is the displacement of the source.

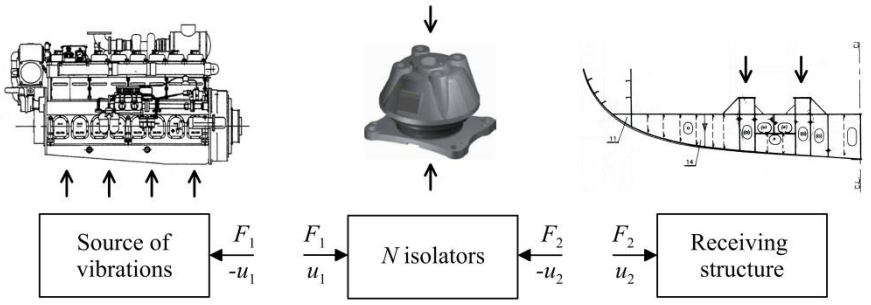

Figure 8 - Three block scheme of a source-isolator-receiver system

To prove the statement about the significance of the dynamic transfer stiffness, the simple case of a unidirectional transmission of vibrations through an isolator is considered in the following. If $k_{1,1}$ and $k_{2,2}$ are the driven-point stiffnesses when the resilient element is blocked at the opposite side (u_2 and u_1 are null, respectively), the equilibrium equations of the isolator can be written for each frequency as:

$$\begin{cases} F_1 = k_{11}u_1 + k_{12}u_2 \\ F_2 = k_{21}u_1 + k_{22}u_2 \end{cases} \qquad (65)$$

which, written in matrix form, becomes:

$$\{F\} = [K]\{u\} \tag{66}$$

In the three block system, the isolator excites the receiving structure with the force F_2 which may be derived by the definition of the driven-point stiffness of the receiving structure, that is $k_r = -F_2 / u_2$.

So, F_2 may be expressed as:

$$F_2 = \frac{k_{21}}{1 + \frac{k_{22}}{k_r}} u_1 \tag{67}$$

From a practical point of view, if $|k_{2,2}| < 0.1\ |k_r|$ it comes out that:

$$F_2 \cong F_{2b} = k_{21} \cdot u_1 \tag{68}$$

There is a clear correspondence among the Equations (65) (66) and (68) and the Equations (33) (34) and (40) respectively. Indeed, the Equations are related each other, considering that:

$$F_2 \cong F_{2b} = k_{21} \cdot u_1 = Z_{21} \cdot v_1 \tag{69}$$

6.1. Direct Method

The Part 2 of the ISO 10846 Standard specifies a direct method for the measurement of the dynamic transfer stiffness of a resilient mount in the normal and in the transversal directions, when the element is under a pre-load.

Figure 9 shows the layout of a test rig for the experimental tests according to the direct method. The frame of the test rig (labelled by number 2 in the Figure) is designed to support an actuator (number 1) that is the source of the vibration energy used to excite the resilient mount under test. The vibration energy is transmitted from the actuator to an excitation mass by a stinger rod (number 3). The excitation mass (number 5) is decoupled from the test rig frame by soft springs (number 4). That mass is used to provide a uniform vibration of the input

flange under dynamic forces and to enhance unidirectional vibration of the input flange [45]. The element to test is labelled with number 6 and is seated on a rigid foundation (number 7).

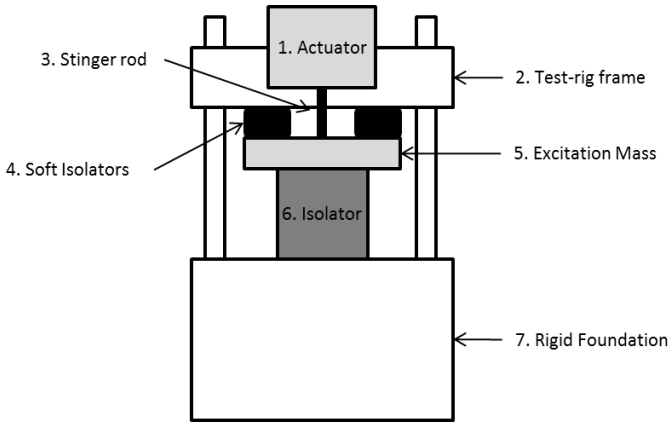

Figure 9 – Layout of a test rig for the direct measurement of dynamic transfer stiffness of a resilient mount

According to the direct method, the dynamic transfer stiffness is obtained measuring the output force F_2 at the interface between the output side of the resilient mount and the rigid foundation, and measuring the input acceleration a_1 at the excitation mass. Since the displacement u_1 can be calculated by the acceleration a_1 remembering that $a_1 = -\omega^2 \cdot u_1$, the dynamic transfer stiffness can be calculated using the Equation (68).

The main hypothesis, that is the basis of the direct method, is that the resilient mount lies on a rigid foundation. At high frequencies, the dynamic behaviour of the rigid foundation is influenced by its own first modes and it begins to behave as a deformable body. Moreover, at high frequencies, the frame of the test rig transmits vibration energy through the vertical columns and the results of the tests are altered. The test rigs that are designed to test large resilient mounts are characterized by an upper frequency limit f_3 of about 300 Hz, but this limit strongly depends on the test rig characteristics and so it varies for each test rig.

The dynamic transfer stiffness of a resilient mount in the low frequency range can be measured according to the so call driving point method. The layout of the test

rig is very similar to that one used in the direct method (see Figure 9), and the procedure of test is nearly the same, but in the driving point method, instead of the output force F_{2b} the measured force is F_1 at the input flange of the resilient mount. Thereby, the dynamic transfer stiffness is calculated as follows:

$$k_{21} = \frac{F_1}{u_1} \cong k_{11} \qquad (70)$$

Equation (70) is valid in a very low frequency range (usually f_3 is 100 Hz for large resilient mounts). Indeed, in that range the inertial forces are usually small, if compared to the damping and elastic forces and $k_{21} \cong k_{11}$ [41] [48].

6.2. Indirect Method

At high frequencies, both the direct method and the driving point method are no longer valid. To measure the dynamic transfer stiffness in the audio frequency range the indirect method is used [2] [41] [46].

In Figure 10 the layout of a test rig that is set up for the indirect method is shown. The vibration actuator is labelled with number 1 and is connected to the excitation mass (number 5) by a stinger rod (number 3). The excitation mass is decoupled from the frame of the test rig (number 2) by means of soft isolators (number 4). The isolator under test (number 6) is fitted between the excitation mass and the blocking mass (number 7) that is decoupled from a rigid foundation (number 8) by soft isolators (number 4).

Like in the case of direct method, the excitation mass is used to provide to the upper flange of the resilient mount, a point contact condition and to better control unwanted input vibrations that can alter the results of the tests. The blocking mass is also used to provide contact conditions at the output flange of the resilient mount, but it is also used to measure acceleration level at the output of the resilient mount a_2.

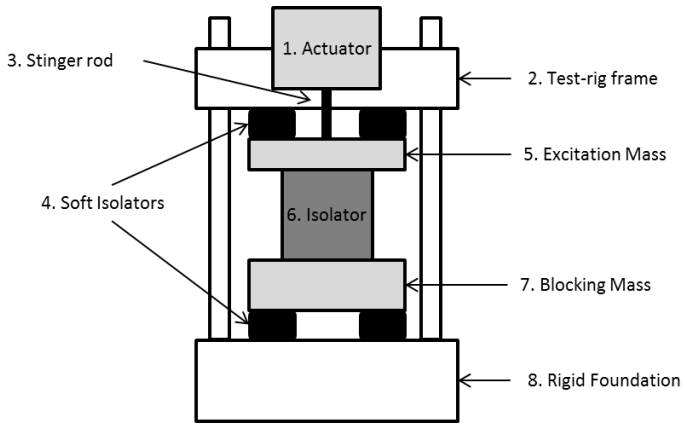

Figure 10 – Layout of a test rig to carry out measurement according to the indirect method

The decoupling of the blocking mass from the rigid frame of the test rig by means of soft isolators guarantees that the flanking transmission of vibration energy through the vertical columns does not affect the test outcomes. On the other hand, the mass/spring system formed by the blocking mass m_2, the isolator under test and the soft isolators, has its own six natural frequencies that can alter the acceleration a_2 measured at the output flange of the resilient mount. For these reasons, the mass and the rotational inertia have to be well below the test frequency range. Under these assumptions, the blocking force is equal to the force exerted by the isolator on the mass.

The ratio u_2/u_1 is called displacement transmissibility. The displacement transmissibility is related to the dynamic transfer stiffness by the Newton's law, as follows:

$$k_{21} \cong \frac{F_2}{a_1} = -(2\pi f)^2 m_2 \frac{u_2}{u_1} = -(2\pi f)^2 m_2 \frac{a_2}{a_1} \qquad (71)$$

The approach is still valid if tests are performed in a frequency range, which is not affected, at low frequencies, by the six resonance frequencies of the blocking mass that is constrained between a soft isolator bed and the resilient element. At high frequencies, the test frequency range is limited by the fact that the blocking mass no more behaves as a rigid-body.

A typical frequency range for the dynamic characterization of a large resilient mount in the audio frequency range is 100 Hz < f < 1000 Hz, but it strongly depends on the dynamic characteristics of the test rig.

The resilient mounting transfer function can be expressed as a dynamic inertia, and defined as the ratio between the force F_{2b} measured on the output side of the isolator, and the complex acceleration a_1 measured on the driven side. That quantity is related to the dynamic transfer stiffness by the following equation:

$$k_{21} \cong \frac{F_2}{u_1} = (2\pi f)^2 \frac{F_2}{a_1} = (2\pi f)^2 T_{2b,1} \qquad (72)$$

where the dynamic inertia is usually referred to as a dynamic transmissibility, and so denoted as $T_{2b,1}$, in consideration that it is an output to input force ratio where the input force is referred to a unit mass.

Figure 10 shows a typical transmissibility curve of a marine diesel engine resilient mounting [49]. The curve is represented in narrow band on a log-log scale. The solid line refers to measurements, carried out in a typical frequency range from about 100 Hz to about 1.0 kHz with the resilient mounting properly preloaded, while the dashed lines refer to extrapolated values.

The transmissibility curve is divided into three different parts. The first part of the curve shows a linear reduction of transmissibility, that gives evidence of an ideal spring-like behaviour of the resilient mounting. In the second part, the transmissibility curve deviates from ideal behaviour and shows two successive peaks where transmissibility increases. At last, in a third part, it resumes its original trend. Such behaviour is due to the presence of the rubber core, which is the cause of two different phenomena: on the one hand, stationary waves propagate in the rubber due to the natural vibration modes; on the other hand, the mass effect due to the rubber incompressibility implies a coupled transversal movement. From Equation 2, it is clear that such an increase in transmissibility corresponds to an increase of the resilient mounting impedance level and, therefore, to an increase in structure-borne noise measured on the engine foundation.

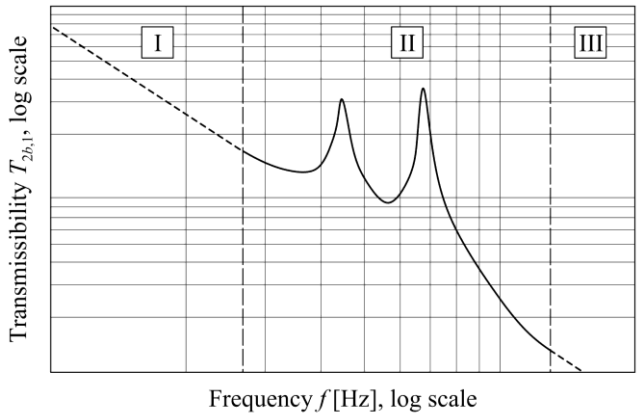

Figure 11 - Typical transmissibility curve of marine diesel engine resilient mountings

7. Mechanical mobility of the diesel engine foundation

Equation (43) shows that the velocity of receiving structures, i.e. the diesel engine foundation, depends on the velocity of the source, on the resilient mount impedance and on the mechanical mobility of the receiving structures, therefore to predict the structure-borne noise due to a source as a diesel engine, it is of paramount importance to measure or simulate the dynamic mechanical mobility of the receiving structures [50]. In Chapter 6, different methods of experimental tests to measure the dynamic transfer stiffness of a resilient mount have been presented; in this Chapter the methods to carry out measurements of the dynamic mobility of the receiving structures are presented. Since the ship's hull structures are usually made of steel, methods used to measure the dynamic mechanical mobility of the receiving structures are the classical methods used to characterize linear systems [5] [22] [50].

The ISO 7626 Standard is considered a reference in the measurement of the mechanical mobility of structures [51] [52] [53]. The first part of that ISO Standard defines the mechanical mobility as: "The frequency-response function formed by the ratio of the velocity-response phasor at point *i* to the excitation force phasor at point *j*, with all other measurement points on the structure allowed to respond freely without any constraints other than those constraints which represent the normal support of the structure in its intended application" [51].

The mechanical mobility Y_{ij} is called driving-point mobility, when it is the ratio of the velocity measured at a point *i* of the structure and the force applied at the same point (Y_{ii}), while the transfer mobility is the ratio of the velocity measured at point *i* and the force applied in another point of the structure *j* (Y_{ij}) [54].

According to the ISO 7626 Standard, two different methods can be used to measure the dynamic mobility of a structure: measurements using single-point

translation excitation with an attached vibration exciter [52], and measurements using impact excitation with an exciter which is not attached to the structure [53].

In both methods, the boundary conditions during the experiment are:

$$F_k = 0; \quad k \neq j \tag{73}$$

This means that when an excitation force is applied at point *j*, the forces at all the other *k* points of the structure are null. This boundary condition is easy to apply in practice, and the generic element of the mobility matrix is obtained as follows:

$$Y_{ij} = \left. \frac{v_i}{F_j} \right|_{F_k = 0;\ k \neq j} \tag{74}$$

where v_i is the measured velocity at point *i* and F_j is the applied force at point *j*.

The main difference between the two different methods proposed in the ISO 7626 Standard is the excitation source. The ISO 7626-2 Standard defines a method for the measurement of the mobility function using, as excitation source, an electrodynamic or an electrohydraulic actuator. The latter has to be connected to the structure under test by a drive rod that transmits the vibration energy from the source to the structure. Aatola presents an application of this method to a real case [55]. The ship under investigation is a 1000 DWT Ro-Ro carrier, and the aim of the experimental campaign is to find out the applicability of a method, that has been presented by Ohlrich [56], to predict the vibrational power energy transmitted by a source to the receiving structures.

The ISO 7626-5 defines a method for the measurement of the mechanical mobility using an impact excitation applied to the structure under test by an exciter that is not attached to the structure, such as a hammer. That method is the most used to carry out mobility measurements on board ships. This is due to practical considerations, such as the velocity in carrying out the measurement campaign, the ease in relocating the excitation source and the negligible influence of the excitation source on the structure response. On the other hand, using this

method the effectiveness of the results depends on the operator skills and the frequency range of measurements is limited.

From a practical point of view, on-board measurements of mechanical mobility of diesel engine foundation according to the method proposed by the ISO 7626-5 are carried out in the following phases: a series of relevant points is identify; at each point a sensor for measuring the response of the structure (usually an accelerometer) is attached and the structure is excited by an impact applied at each point. Figure 12 shows a typical cell of diesel engine foundation. Figure 13 shows a series of 8 measurement points. The foundation structure is divided in cells and for each cell two measurement points have been identified, one in the middle part of the cell (*e.g.* points 1, 3, 5 and 7) the others in correspondence of the supporting structures of the seating plate of the diesel engine foundation (*e.g.* points 2, 4, 6 and 8). Each point is excited, one at a time, by a hammer and the driving-point mobility and the transfer mobility are calculated for each point.

Figure 12 - Typical example of a cell element, part of the diesel engine foundation

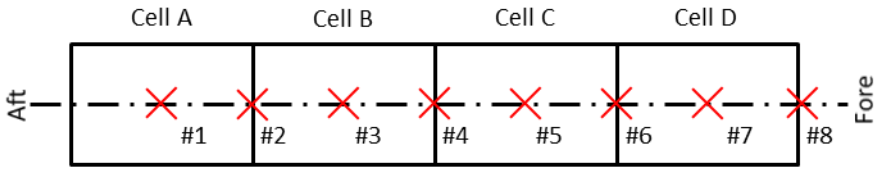

Figure 13 – Measurement points of a diesel engine foundation designed for marine diesel engine.

8. Simulation of rubber resilient mounts

To simulate the dynamics of a passive resilient mount, the non-linear behaviour of the rubber core has to be taken into account. The rubber commonly used in passive isolators is vulcanized natural rubber with carbon black filler.

The dynamic response of filled rubber depends on the exciting vibration amplitude [57] [58]. The presence of filler particles alters the behaviour of rubber. The filler particles are strongly bonded each other, forming the so called aggregates that, in turn are weakly bonded to other aggregates. That leads to two phenomena that are called the Mullins and the Payne effects.

The Mullin effect occurs when rubber undergoes to strain cycles with constant amplitude. In the first few cycles, a decrease in peak of the stress values of rubber appears and a dependence of the stress-strain curve to the maximum load applied previously to the rubber can be noticed.

The Payne effect can be noticed when filled rubber undergoes cyclic loading conditions. The shear modulus of rubber under test depends on its strain amplitude: when the strain amplitude is small (less than 0.1 %) the shear modulus is larger than that one observed if the rubber is subject to higher strain amplitude. The phenomenon is due to the break of the filler structure that occurs when the rubber is subject to large amplitude deformation. It depends on the quantity of filler inside the rubber material under test and increases with the increase of filler quantity. Several experiments and models have been carried through by Kari and Sjöberg who deeply studied these effects [26].

The rubber material behaviour also depends on temperature [59] [60]. The shear modulus and the loss factor change with the changing of temperature. Figure 14.a shows a typical shear modulus vs temperature graph. It is possible to identify three different regions: the glassy region, where the rubber is characterized by a high value of the shear modulus, a transition region, in which a strong decrease of

the shear modulus is shown and a rubber region, in which the shear modulus of rubber is almost constant. Figure 14.b shows a typical loss factor vs temperature graph. Also in this case, three regions can be identified: a glassy region, characterized by a loss factor that is almost constant, a transition region that is characterized by an increase of the loss factor value that then decreases and becomes constant again in the rubber region.

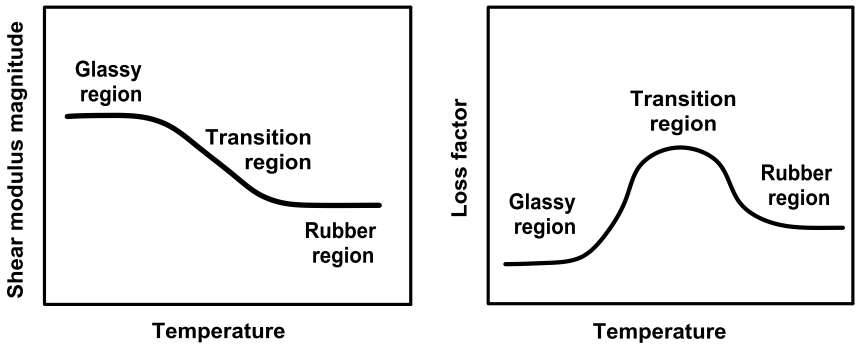

Figure 14 – a) Qualitative trend of the shear modulus vs temperature graph. b) Qualitative trend of the loss factor vs temperature graph [18]

The same three regions are shown also in a shear modulus vs frequency graph (see Figure 15.a) or in a loss modulus vs frequency graph (see Figure 15.b). In the former, at low frequency, the rubber region is characterized by a shear modulus that is almost constant and that increase, at higher frequencies, in the transition region. Increasing the frequency, the shear modulus becomes again constant in the glassy region. As regards the loss modulus, the rubber region is characterized by an almost constant value. Then the amplitude of the loss factor increases in the transition region and then decreases again till resumes to an almost constant value in the glassy region. The influence of the temperature in the stiffness value of rubber typically used in resilient mounts has been studied by Sjöberg and Kari [26] [27].

The dynamic transfer stiffness of a passive resilient mount, which core is made of rubber, is also characterized by a non-linear behaviour. At certain frequencies, standing waves appear inside the rubber core of the resilient mount and this leads to an increase of the dynamic transfer stiffness and so to an increase of the

transmissibility value (see Figure 11). The dynamic transfer stiffness of a resilient mount depends on the frequency, such as on the working temperature and on the static-preload applied to the resilient mount.

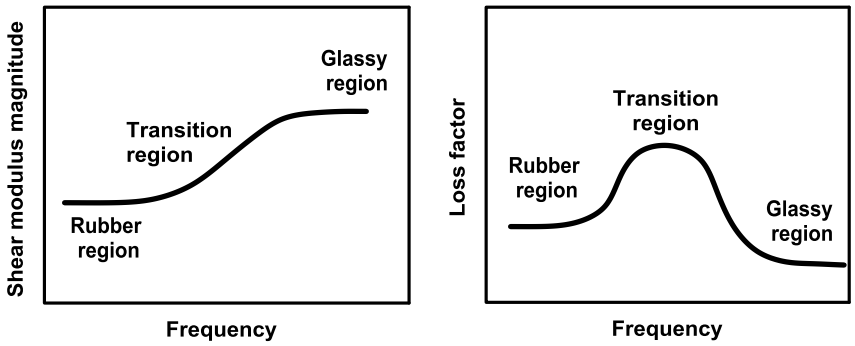

Figure 15 – a) Qualitative trend of the shear modulus vs frequency graph. b) Qualitative trend of the loss factor vs frequency graph [18]

In recent years, several studies have been done in order to simulate the dynamic behaviour of passive resilient mounts. In all these studies, the rubber has been considered a homogeneous, isotropic, nearly incompressible material. The effect of the temperature has been neglected, considering the rubber of the resilient mount working at constant temperature that is always in the rubber region of the shear-modulus vs temperature graph. Moreover, the Mullins and Payne effects are neglected since the rubber is considered time invariant and the strain amplitude is considered small.

The analytical solutions or numerical methods to simulate the dynamic stiffness of the resilient mounts, good results have been obtained only in the case of isolators with simple geometric shapes. Dickens has investigated a dynamic model as a function of the compression ratio of its rubber element. The dynamic model has been validated with data acquired by laboratory tests [15, 61]. Kim and Singh used the theory of the Timoshenko beam to simulate the vibration transmission through a rubber isolator [62].
Kari has studied the non-linear, preload-dependent dynamic stiffness of an isolator made of two circular plates (top and bottom interfaces) and a rubber cylindrical core. Also in this study, the results of the model have been compared

with the experimental data [17]. In another study, Kari proposed a scaling load for predicting the variation of the dynamic stiffness of a cylindrical resilient mount due to a geometrical shift [63]. The problem of the dynamic transfer stiffness simulation of a cylindrical resilient mount in the audible frequency range has been addressed by Kari in the vertical direction using non-linear FEM method [64].

Beijers and de Boer have proposed an iterative procedure for carrying out FE simulations of a cylindrical shaped passive isolator at different static pre-loads [30]. They have also set another iterative procedure to identify the material parameters of the rubber core if those are not available for the definition of the numerical model [29]. The results obtained by these studies have been used in a modelling approach proposed by Beijers to study the hybrid isolation of structure-borne sound [18].

9. Simulation of the dynamics of diesel engine foundations

The diesel engine foundations are usually made of steel or, on board of small pleasure craft, of composite materials. In this work, the attention is paid to the dynamics of the diesel engine foundations that are made of steel. The foundation is composed by simple cells (see Figure 12) that are welded together. When the receiving structures are excited by the vibrations generated by the diesel engine and transmitted through the resilient mounting system, the amplitude of the displacements are usually very small. For this reason, and considering that the steel can be treated as a homogeneous, isotropic material, an FE linear dynamic analysis can be used to simulate the mechanical mobility of the receiving structures. Lin, Pan, O'Shea and Mechefske studied the vibration characteristics of ship structures and focused their study on the mobility of diesel engine foundations. The example for this study is a 30 m aluminium crew vessel. The mobility of the diesel engine bed has been simulated in low and medium frequency range (0 – 250 Hz) and the study has been carried out including or excluding the deck and hull plating. As conclusion, the authors stated that there is no significant difference between the results obtained by the complete model (i.e. the model with deck and hull plating) and the simplified model and they verify that the vibration response of ship structures can be controlled by structural modification of the diesel engine foundation structures [65].

The governing equation for the computation of the frequency response of the ship's structure to a time varying applied set of forces is given by [66] [67]:

$$(\mathbf{M}+\mathbf{M}_{\mathbf{A}})\boldsymbol{a}+\mathbf{C}\boldsymbol{v}+(\mathbf{K}+\mathbf{K}_{\mathbf{G}})\boldsymbol{u}=\boldsymbol{f} \qquad (75)$$

where $\mathbf{M}$ is the structural mass matrix, $\mathbf{M}_{\mathrm{A}}$ is fluid added mass matrix, $\mathbf{C}$ is the damping matrix, $\mathbf{K}$ is the stiffness matrix, $\mathbf{K}_{\mathrm{G}}$ is the geometric stiffness matrix, u is the displacement vector and f is the force vector. As for the interaction between

ship and the surrounding fluid, it can be dealt with by a linear approach and FE software can take into account the added mass effect using boundary element method, by which a set of sources are distributed over the outer boundary, each producing a simple solution to the differential equation. If there is no coupling between structure and a fluid domain ($\mathbf{M}_A = 0$) and if the structure experiences geometrically linear vibrations ($\mathbf{K}_G = 0$), the system reduces to a linear system.

The setting of the damping properties in modelling an entire ship or large portion of the hull, consisting of the hull structures, equipment and cargo, is a demanding task. A rather accurate mathematical representation of the structural damping can be made by assuming a viscous damping mechanism, described by the constant value of the logarithmic decrement δ for all frequencies [68]. Structural damping may then be magnified for considering component damping and cargo damping. This leads to assume the structural system experiences a linear proportional damping, for which the Rayleigh model is accepted:

$$\mathbf{C} = \alpha\mathbf{M} + \beta\mathbf{K} \qquad (76)$$

By developing Equation (75) for the case of unforced analysis ($\boldsymbol{f} = 0$) it leads to the determination of the natural frequencies and mode shapes:

$$[\omega^2(\mathbf{M} + \mathbf{M_A}) - (\mathbf{K} + \mathbf{K_G})]\boldsymbol{\phi} = \mathbf{0} \qquad (77)$$

where ω is a natural frequency and $\boldsymbol{\phi}$ the corresponding mode shape. In case of a high modal density, to predict which modes will play a dominant role in the response of a structure, the modal effective mass of each mode shape has to be calculated. Modes with relatively high effective masses can be readily excited by a base excitation. The modal effective mass vector $\boldsymbol{\varepsilon}^2$ is derived as a vector of scaling factors for the vector $\boldsymbol{\Phi}$ (made by the eigenvectors ϕ) in order to obtain a rigid body vector $\mathbf{D}_R$:

$$\mathbf{D}_R = \boldsymbol{\Phi}\boldsymbol{\varepsilon} \qquad (78)$$

Analysis of the dominant mode shapes can be useful when, in correlating two FE models or in updating an FE model with experimental data, the aim is to identify the global modes of the structure, on which to focus the setting process.

The running time to solve the dynamics problem of large ship's structures is very costly and produces a large amount of data, which are only in a limited amount necessary for the evaluation of the structure behaviour. Therefore, FE solution of Equation (76) can be carried out right after the reduction of the given FE dynamic model to one with fewer degrees of freedom, while maintaining the dynamic characteristics of the system. An effective reduction technique extensively used in correlation is based on the static Guyan condensation process, by which a reduced stiffness matrix $\mathbf{K}_r$ is obtained by applying a proper transformation $\mathbf{T}_S$ to relate the master degree of freedoms u_m to the deleted ones u_d. In the case of linear systems, to the mass matrix **M** and the damping matrix **C** can be applied the same transformation to obtain $\mathbf{M}_r$ and $\mathbf{C}_r$ respectively to account for the effects of mass inertia and damping associated with the deleted degree of freedoms. The condensation leads to a new model given by:

$$\begin{cases} \mathbf{M}_r \boldsymbol{a}_m + \mathbf{C}_r \boldsymbol{v}_m + \mathbf{K}_r \boldsymbol{u}_m = \boldsymbol{f}_m \\ \boldsymbol{u} = \boldsymbol{u}_m + \boldsymbol{u}_d \end{cases} \qquad (79)$$

The approximation occurs only on the inertial terms and the quality of the eigenvalue approximation highly depends on the location of the points preserved in the reduced model - and calculated eigenvalues are always higher than those of the original system. The approximation is poor if mass associated to the omitted nodes is significant, it decreases as the mode number increases and becomes unacceptable for systems with high mass/stiffness ratios.

The dynamic characterization of a time-invariant and linear system leads to the determination of the frequency response functions (FRF) at any given grid point of the structure. As for the ship structures dealt with in this study, the vibration analysis is normally carried out by referring to the mechanical mobility $m_{ij}(\omega)$ which is defined as the ratio between the vibration velocity FRF $\mathbf{V}_i(\omega)$ read out on the i-*th* grid point and the force spectrum $\mathbf{F}_j(\omega)$ applied to j-*th* grid point.

Part II

Methods

10. Testing of the test rig at the Ship Noise and Vibration Laboratory

At the Ship Noise and Vibration Laboratory (NVL) of the University of Trieste, in recent years several research activities on the dynamic response of passive resilient mounts have been carried out. In particular, a test rig for the dynamic characterization of isolators has been designed and built up. The peculiarity of such test rig is that it has been designed to carry out the measurement of the dynamic transfer stiffness according to the indirect method of small isolators as well as of very large isolators for marine diesel engines.

Once the test rig has been designed and built up, it has been tuned in order to set a procedure to carry out the laboratory measurements.

10.1. Description of the test rig at the NVL Laboratory

Figure 16 shows the main parts of the test rig that has been built at the University of Trieste. The parts are: (A) crossheads for shaker support placed on the top of the (B) heavy and rigid main frame of the test rig, (C) trunnion hanged by isolators to the crossheads, (D) electrodynamic vibration generator, (E) mobile crosshead and static load upper support plate, (F) moving system between upper and lower isolator beds, (G) static load lower support discs and (H) static force transducers and cylinder for hydraulic preload.

The core of the test rig are the vibrating bodies (see Figure 17), whose assembling is the so called moving system. The moving system, being tightened by a hydraulic piston between an upper and a lower elastic bed of auxiliary isolators, may move under the action of an electrodynamic shaker. The moving system is made by the resilient element supported by a blocking mass and holding on the top the excitation mass, by which the whole system is connected to the elastically

suspended shaker. In Figure 17 a moving system is shown, arranged for testing steel springs.

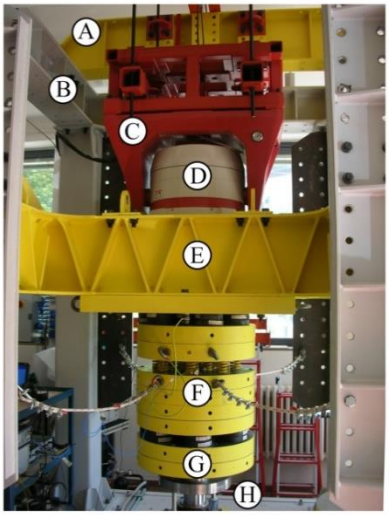

Figure 16 -- Test rig facility at the NVL

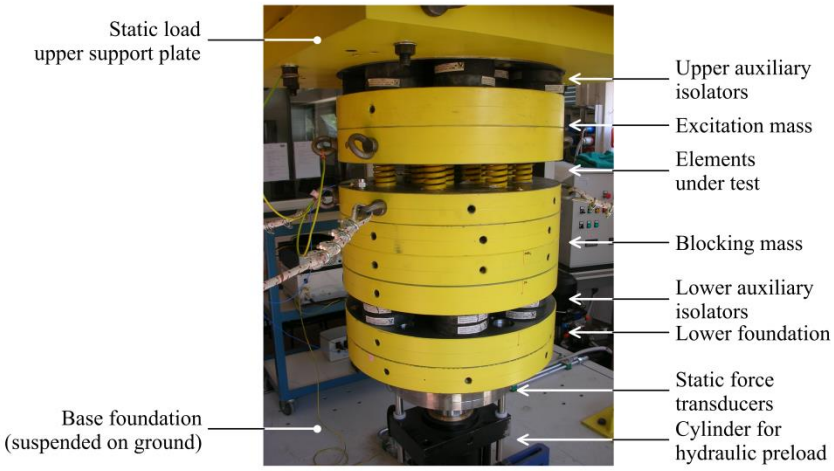

Figure 17 - Moving system of the test rig

Connection between moving system and shaker (see Figure 18) is a very significant part and is made by a “stinger” rod. Through the stinger, vibrational energy is transmitted to the excitation mass. Mechanical connection among such elements has been designed to avoid local resonance frequencies in order to preserve measurements from such noise sources. In Figure 18 a connection chain is shown, arranged for testing on low-stiffness elements.

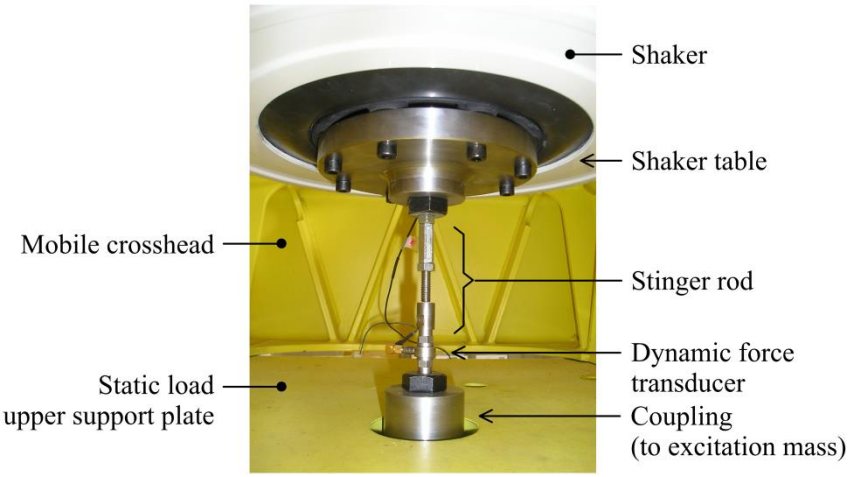

Figure 18 - Connection between the moving system and the shaker

Laboratory tests can be developed on small to big resilient elements as test controlling parameters may be adjusted in a wide range of values. The most distinctive feature of the test rig lies in its capacity of performing tests on the biggest resilient mountings today used in the suspension systems of marine engines, with a static load capacity up to 150 kN and a maximum dynamic load capacity of 4 kN up to a frequency of 2 kHz, which range largely covers the typical frequency range taken into account in the investigations on medium-speed marine diesel engines. Dimensions of test rig are remarkable too, being supporting frame for moving masses very large, so allowing tests to be carried out on resilient mountings 0,5 metres wide and weighting about 1 kN placed on a foundation of up to 8 kN weight.

Figure 19 shows a schematic layout of the test rig for the measurement of the dynamic transfer stiffness according to the indirect method.

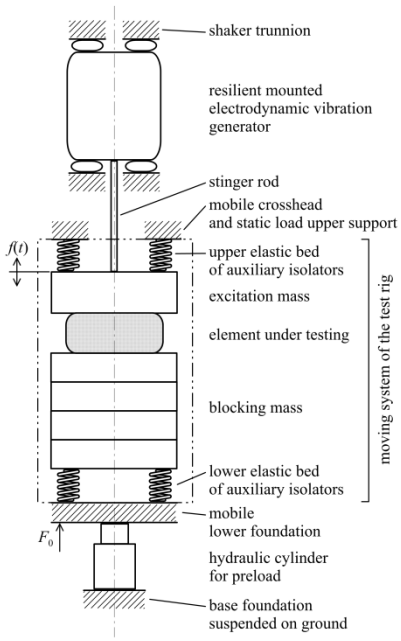

Figure 19 - Test rig layout for the laboratory experiments according to the indirect method.

10.2. Excitation system

The excitation mass of the test rig is excited by an electrodynamic shaker through a stinger rod. The electrodynamic shaker used at the Ship Noise and Vibration Laboratory is able to provide a dynamic force of 2.9 kN (peak) when generating a sine signal, 1.9 kN (RMS) when the shaker generates a random force. The acceleration developed by the shaker reaches 66.3 g (peak) in sine signal generation and 44.9 g in random.

The signal generated by the shaker is controlled using a closed-loop active control system.

10.3. Acquisition system

The measurement of the acceleration signals is carried out using piezoelectric accelerometers and the data are acquired by a 12-channels data acquisition system. The acquired data are processed in real time or in post-processing using a software package for signal analysis. The dynamic force applied by the shaker to the moving system is measured by a dynamic load cell that is placed between the shaker table and the stinger rod (see Figure 18), while the static preload is measured by three static load cells that are placed between the lower side of the seismic mass and the upper plate of the hydraulic piston that applies the static preload (see Figure 16).

11. Prescription for test accuracy

According to the ISO 10846-3 Standard, the approximation in the definition of the dynamic transfer stiffness of an isolator in the audio frequency range shall be accurate within the 12% (1 dB) of the magnitude of the calculated stiffness. This requirement limits the frequency range of the test.

In order to guarantee that accuracy in the calculation of the dynamic transfer stiffness magnitude, the following inequality has to be fulfilled:

$$\Delta L_{1,2} = L_{a1} - L_{a2} \geq 20 \text{ dB} \qquad (80)$$

where L_{a1} is the acceleration level of the input side and L_{a2} is the acceleration level of the blocking mass.

In the low frequency range, the natural frequencies of vibration modes of the system consisting of the isolator under test, the blocking mass and the soft bed isolators increase the vibration levels L_{a2} and the Inequality (80) is no more valid. For these reasons the natural frequencies f_n of that system have to be calculated and then verified by measurements. Since the natural frequencies f_n alter the outcomes of the tests in the low frequencies a lower limit f_2 of the test frequency range can be defined as follows:

$$f_2 \geq 3 \cdot f_{n,\max} \qquad (81)$$

where $f_{n,\max}$ is the highest natural frequency of the rigid body motions, in the six degrees of freedom of the blocking mass. The natural frequencies of the system depend on mass m_2 of the blocking mass and on the stiffness of the resilient mount under test and of the soft bed isolators. The soft isolators are to be selected in order to lower the frequencies f_n and so the lower limit of the frequency range f_2, but at the same time, they should be able to withstand the static preload applied to the moving system.

As for the upper limit of the frequency range f_3, it depends on the mass and the shape of the blocking mass. At a certain frequency the blocking mass no more behaves as a rigid body and so the Equation (71) is modified as follows:

$$k_{21} \cong \frac{F_2}{a_1} = -(2\pi f)^2 m_{2,eff} \frac{u_2}{u_1} = -(2\pi f)^2 m_{2,eff} \frac{a_2}{a_1} \qquad (82)$$

where $m_{2,\mathrm{eff}}$ is the effective mass of the blocking mass, that is defined as the frequency-dependent ratio between the force transmitted by the resilient mount under test and the acceleration a_2 of the blocking mass. In order to do not affect the accuracy of the measurements, the deviation of the effective mass $m_{2,\mathrm{eff}}$ from the mass m_2 should not exceed the 12 % (1 dB):

$$|\Delta L| = \left| 10 \log \frac{m_{2eff}^2}{m_2^2} \right| \text{ dB} \leq 1 \text{ dB} \qquad (83)$$

Experimental measurements have to be performed in order to calculate the effective mass of the blocking mass.

The accuracy of the measurements can be affected by unwanted input vibrations that increase the acceleration levels at the input side of the isolator under test in a direction different from the driving one. For this reason, the difference between the acceleration levels measured in the excitation direction L_a should exceed the vibration levels in the other perpendicular directions $L_{a'}$ of 15 dB or more:

$$L_a - L_{a'} \geq 15 \text{ dB} \qquad (84)$$

12. Procedure for the test rig testing

In order to test the effectiveness of the new test rig at the NVL laboratory and to define a procedure to measure the dynamic transfer stiffness of a resilient mount, a series of tests and studies has been carried out. The aim of these studies was to investigate the dynamics of the test rig components and to define the best set up of the machine. This means that the moving system has to guarantee to provide a unidirectional excitation to the isolator under test and a useful frequency range of the tests. In particular, the elements that have to be properly selected are the following:

- *Stinger rod*: The stinger rod has to be selected in order to properly couple the electrodynamic shaker to the moving part of the test rig, and in particular to the excitation mass;
- *Excitation mass*: The excitation mass has to be selected in order to guarantee a point contact with the upper flange of the isolator and so to homogeneously distribute the excitation force on it.
- *Blocking mass*: The dynamics of the blocking mass influences the experimental frequency range. Its inertia m_b influences the lower limit of the frequency range. Indeed, the blocking mass is constrained by the resilient mount, on the top, and a bed of soft isolators, at the bottom side, and so, in the low frequency range the measurements are affected by the resonances of the system composed by blocking mass, the soft isolators and the test element. Above a certain frequency, the blocking mass no more behaves as a rigid body and so it no more provides a uniform vibration of the output flange of the isolator under test.
- *Soft isolators*: the soft isolators have to decouple the moving part of the test rig by the rigid structure of its frame. Their stiffness has to be properly selected so that the resonance of the system composed by the blocking mass, the resilient mount, and the soft isolators.

– *Flanking transmission of vibration energy*: the vibration energy transmitted through the rigid frame of the test rig can alter the results of the tests limiting the accuracy of the results.

12.1. Stinger rod

The connection rod has been selected in order to transmit the vibration energy generated by the actuator to the moving system of the test rig. The energy provided by the actuator should excite the moving system only in the driving direction, avoiding unwanted input vibration that could excite the system in other directions.

Four different types of stinger rods have been used and the outcomes of the tests have been compared. The connection rods are shown in Figure 20: the rod in the left hand side of the figure is made of nylon, the others are made of steel and are characterized by different sections: (from left to right) M8 rod, M12 rod and M20 rod.

Figure 20 – Different types of stinger rods: (from left to right) nylon rod, M8 steel rod, M12 steel rod, M20 steel rod

The outcomes of the tests, carried out using the different types of connection rods, show that the increase of the stiffness of the rod leads to an increase of the vibration energy transmitted to the moving system and so to an increase of the vibration excitation of the resilient mount. Moreover, the tests carried out using a threaded nylon stinger show that, on the one hand, the electrodynamic shaker is

decoupled by the moving system of the test rig and so the dynamics of the shaker mass does not affect the dynamics of the moving system, but, on the other hand, such a weak coupling leads to an increase of the shaker mobility that, transmitting the vibration energy through the test rig rigid frame, increases the flanking transmission and so the background noise during the test. The decrease of the vibration levels transmitted to moving system and the simultaneous increase of the background noise affect the outcomes of the tests decreasing their accuracy.

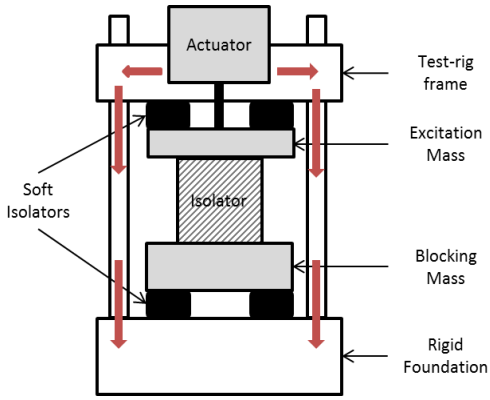

Figure 21 - Flanking transmission of vibration energy

The outcomes of the tests performed using steel stingers characterized by different diameters (see Figure 20) show that the accuracy of the results increases stiffening the coupling between the shaker and the moving system. For these reasons, the measurements of the dynamic stiffness of the resilient mounts have been carried out using the M20 steel stinger rod.

To verify the connection between the stinger rod and the excitation mass, an operational deflection shape (ODS) analysis has been carried out. The M20 stinger rod has been screwed in a threaded hole in the geometrical centre of the upper surface of the excitation mass. The results of the ODS analysis have showed a deflection shape at the connection point between the stinger rod and the excitation mass at about 700 Hz. Such behaviour led to an increase in the vibration levels in the x and y directions and the Equation (84) was no more satisfied. For this reason, the connection between the stinger rod and the excitation mass has been improved. A steel sleeve has been designed in order to

stiffen that connection and supply the vibrational energy generated by the shaker in a more uniform way. Figure 22 shows the connection sleeve fixed to the excitation mass. The red rows show the vibrational energy provided by the shaker and transmitted through the stinger rod to the system. The wider section at the base of the sleeve guarantees a uniform supply of the energy to the moving system that implies the decrease of the vibrational energy in the *xy* plane. An ODS analysis has been performed once that the sleeve has been fixed to the excitation mass and the results show an improvement in the connection of the stinger rod to the excitation mass, since the deflection shape at 700 Hz has been shift out of the range of measurements (i.e. above 1000 Hz), and the vibration levels in the horizontal plane have been lowered.

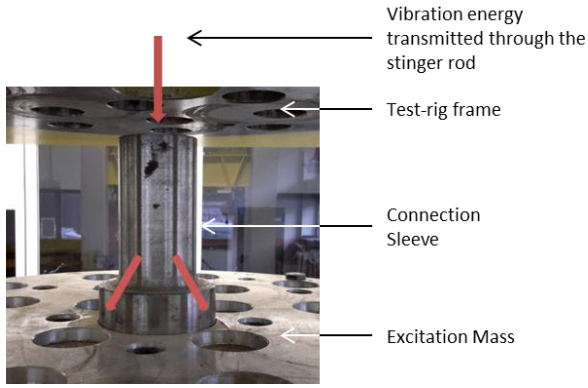

Figure 22 - Steel sleeve designed to improve the connection between the stinger rod and the excitation mass

12.2. Excitation mass

The excitation mass is used to provide a contact point to the top casting of the resilient mount in order to guarantee a uniform transmission of the vibration levels. For this reason, it should behave as a rigid body in the frequency range of the test, otherwise the contact surface between the excitation mass and the flange of the resilient mount top casting should be altered by the deformation of the mass. As shown in Figure 17 the excitation mass of the NVL test rig is composed by aluminium disks that are joined together to create a cylinder. To study the

dynamics of the excitation mass, a series of dynamic linear analyses has been performed to achieve the mode shapes and the natural frequencies of the disks. In Figure 23 the FE model of the aluminium disk is shown. In Figure 24, Figure 25 and Figure 26 the three mode shapes of the disks are shown. The disk is not constrained during the analysis and so a free-free analysis has been carried out. The outcomes of the FE analysis have been validated by experimental tests.

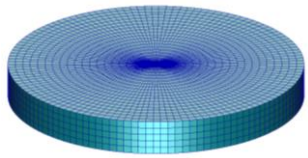

Figure 23 - FE model of an aluminium disk of the excitation mass

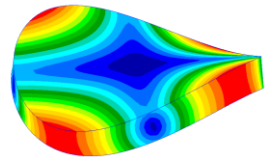

Figure 24 - First vibration mode shape (1026 Hz)

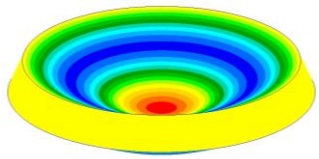

Figure 25 - Second vibration mode shape (1695 Hz)

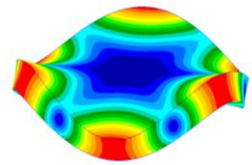

Figure 26 - Third vibration mode shape (2243 Hz)

A dynamic FE analysis has been performed to calculate the natural frequencies and the mode shapes of the exciting mass composed of two and three aluminium disks. These are bolted together to form a cylinder. The results of the analysis have been compared with the outcomes of the experimental modal analysis. In general, by joining together the disks, the natural frequencies of the excitation mass appear at higher frequencies, and so it behaves as a rigid body in a wider frequency range. In Figure 27 the FE model of the excitation mass composed by three aluminium disks is shown. Figure 28, Figure 29 and Figure 30 show the first three vibration mode shapes of the excitation mass. The results of the simulations disagree with the outcomes of the experimental tests. The latter show that the first three natural frequencies of the excitation mass are lower than the calculated ones. This is due to the connection between the disks that are bolted together. In order to overcome that problem, several simulations have been

carried out merging the nodes of the surfaces of the disks just in a circular area that surrounds the bolts used to connect the different disks. For each simulation a different area of the contact surfaces has been merged. The iterative procedure terminated once the numerical outcomes showed the best conformity with those ones obtained by the experimental tests. The numerical model that led to the best conformity of the numerical results with the experimental ones is characterized by a circular contact area around each bolt of 70 mm radius.

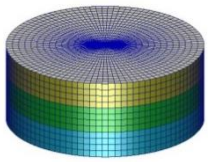

Figure 27 - FE model of the excitation mass made of three aluminum disks

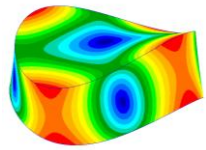

Figure 28 - First vibration mode shape (2567 Hz)

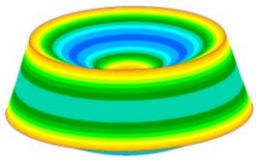

Figure 29 - Second vibration mode shape (3926 Hz)

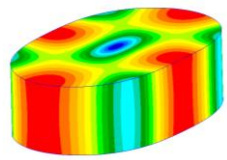

Figure 30 - Third vibration mode shape (4210 Hz)

Table 2 shows the natural frequencies of the first and second vibration modes achieved by the experimental tests compared with those ones achieved by numerical simulations.

Table 2 – Comparison of the experimental and the numerical natural frequencies of the excitation mass

MODES	Experimental tests [Hz]	Numerical simulations [Hz]
Mode I	2150	2193
Mode II	2800	2877

12.3. Blocking mass

The blocking mass provides a contact point at the output flange of the isolator under test. Moreover, the dynamic behaviour of the blocking mass affects the frequency range of the tests. Indeed, the lower frequency limit f_2 depends on the highest natural frequency $f_{n,\max}$ of the mass-spring system composed by the isolator under test, the blocking mass and the soft isolators, according to the Inequality (83). The highest frequency limit f_3 depends on the dynamic characteristics of the blocking mass and it is the lowest frequency at which the Inequality (83) is no more valid.

In order to select a blocking mass that assures a wide frequency range of testing, a series of FE linear dynamic simulations has been carried out. The blocking mass has been built using steel disks of 125 kg that have been bolted together to form a cylinder. In this case too, the numerical analyses have been performed to study the dynamics of the cylinder made of two, three and four disks. The results of the analyses permitted to identify the blocking mass made of four disks as a good solution to perform the experimental tests with the indirect method, since the first mode shape of the cylinder appears at 2350 Hz.

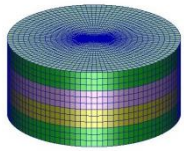

Figure 31 - FE model of the blocking mass made of three steel disks

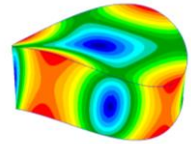

Figure 32 - First vibration mode shape (2567 Hz)

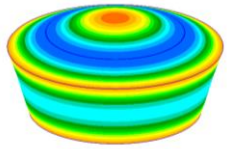

Figure 33 - Second vibration mode shape (3926 Hz)

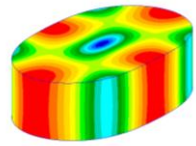

Figure 34 - Third vibration mode shape (4210 Hz)

Experimental tests have been carried out to determine the effective mass $m_{2,eff}$ of the blocking mass. These tests have been performed according to the ISO 10846-3 Standard [46]. The blocking mass, made of 4 steel disks, has been supported by soft isolators. The soft isolators have been properly selected in order obtain a natural frequency in the vertical direction of the mass-spring system that was lower than 10 Hz. Then, the blocking mass has been excited with an impact hammer equipped with a load cell to measure the applied dynamic force. Two accelerometers have been placed on the upper surface of the blocking mass, symmetrically to the vertical axis through the mass centre, and with a spacing of:

$$D = \sqrt{A} \tag{85}$$

where A is the contact surface between the output flange of the isolator and the blocking mass. Figure 35 shows a scheme of the experimental tests for the measurement of the effective mass.

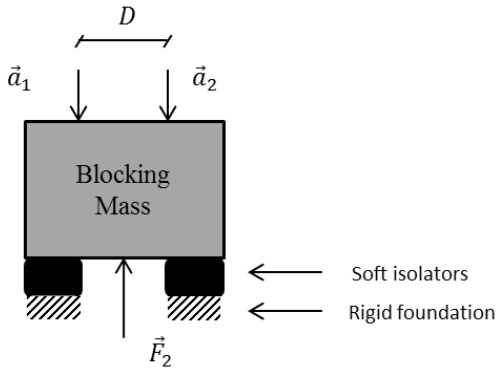

Figure 35 - Scheme of the experimental test for the measurement of the effective mass

The effective mass is achieved as follows:

$$m_{2,eff} = \frac{2F_2}{(a_1 + a_2)} \tag{86}$$

Figure 36 shows the experimental curve of the blocking mass. The blocking mass is composed of 4 steel disks of 125 kg. The experimental tests have been carried

out according to the scheme shown in Figure 35. The Inequality (83) is satisfied till 1550 Hz, that is the upper frequency limit f_3 of the test.

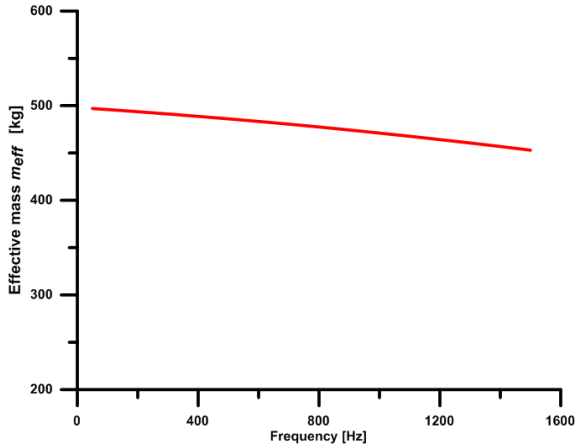

Figure 36 - Experimental curve of the effective mass of the Blocking mass

12.4. Soft Isolators

The soft isolators are used to decouple the moving system from the rigid frame of the test rig. Their stiffness should guarantee that the natural frequencies of the mass-spring system composed by the blocking mass, the isolator under test and the soft isolators are below the lower frequency of the frequency range of the test; they also should withstand the static preload applied to the isolator.

Experimental measurements have been carried out to verify the effectiveness of the soft isolators used to decouple the moving system. A first series of tests has been carried out decoupling the moving system by means of steel springs (see Figure 37). The outcomes of the tests show that such a solution guarantees the decoupling in low frequency range but, at higher frequencies, the springs do not damp down the flanking vibrations that are transmitted through the test rig frame, as shown in Figure 21. For these reasons, in the high frequency range the difference between the acceleration levels L_{a2} and the background noise levels measured at the rigid foundation was less than 20 dB.

Figure 37 – Steel springs used as soft isolators to decouple the moving system by the rigid frame of the test rig

To improve the quality of the measurements, the same test has been carried out isolating the moving system with rubber disks instead of the steel springs, as shown in Figure 38. A proper number of disks have been put in series in order to lower the natural frequencies of the mass-spring system, and in parallel, so that they could withstand the static preload.

Figure 38 - Rubber disks used as soft isolators

The results of the experimental campaign show an improvement of the quality of the measurements. The acceleration levels L_{a2} of the blocking mass, measured in the driving direction, are 20 dB higher than the background noise measured at the rigid foundation, in the whole frequency range of the test.

12.5. Centring of the moving system of the test rig

In order to guarantee a unidirectional excitation of the moving system, a device for the centring and the alignment of the shaker table with the excitation mass has been designed. The alignment and the centring of the components also preserve the shaker table by loads perpendicular to driving excitation direction that can damage the shaker table. Moreover, a good alignment of the moving system with the actuator improves the accuracy of the measurements as the vibration levels in the directions perpendicular to the driving direction decrease in magnitude and so the Inequality (84) is valid. Figure 39 shows the device designed and built to centre and align the shaker table with the moving system of the test rig. The device is composed by two disks, one is screwed to the shaker table and it is centred with the lower surface of the shaker table, the other one is screwed to the upper surface of the excitation mass and it is centred with that surface. A hole has been made at the centre of both disks so that a cylinder can enter both the holes when the whole system is centred and aligned. The design of the device has been carried out in order to guarantee a certain tolerance of parallelism and concentricity between the actuator and the excitation mass.

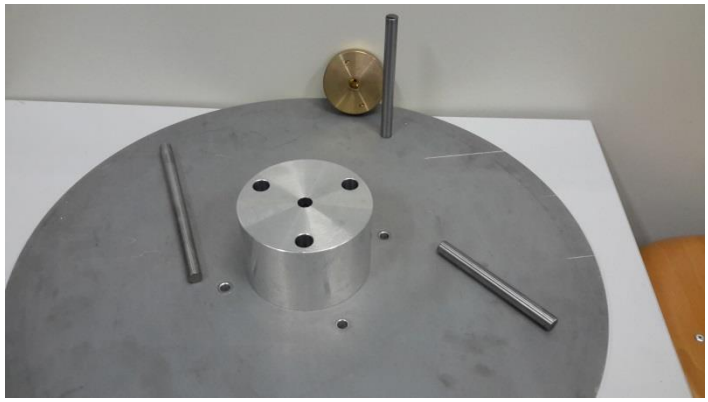

Figure 39 – Device for the centring and the alignment of the shaker table with the moving system of the test rig

The procedure to centre the systems has been developed in the following steps:

- The moving system of the test rig is set up according to the prescription above described;

- The two disks of the device designed for the alignment and centring of the system are installed on the upper surface of the excitation mass and on the output surface of the shaker table;
- The cylinder is inserted in the hole of the disk connected to the shaker table;
- The shaker table is moved to be centred with the upper disk installed on the excitation mass;
- When the cylinder enters, at the same time, in the hole of both the disks the system is centred and aligned.

In Figure 40 the scheme of the device for the alignment and the centring between the shaker table and the moving system is shown. At the top of the Figure, the disk to be connected to the output side of the shaker table is shown. The hole for the housing of the steel cylinder is specified using a dashed curve. At the bottom of the Figure, the disk to be connected to the excitation mass is shown; once again, the dashed curve shows the housing hole of the steel cylinder.

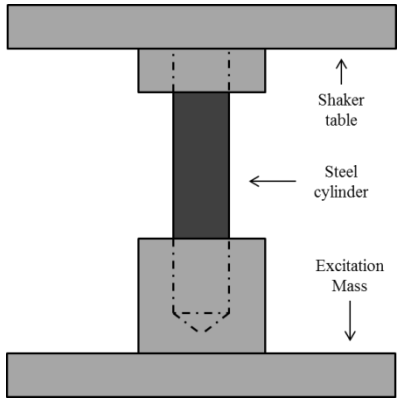

Figure 40 – Scheme of the device for the alignment and centring between the shaker table and the moving system.

13. Experimental Tests for the measurement of the dynamic transfer stiffness of a resilient mount

At the NVL laboratory, the experimental tests for the measurements of the dynamic transfer stiffness of a large resilient mount, designed to support the marine diesel engines installed on board ships, have been carried out. The tests have been performed to achieve the dynamic transfer stiffness in the normal and transversal directions. All the experimental campaigns have been accomplished according to the ISO 10846-3 Standard [46]. Before the tests, FE dynamic linear analyses have been carried out to study the dynamic behaviour of the top casting and of the base casting of the resilient mount under tests. These elements are usually made of steel or cast iron. That study allows understanding the behaviour of the steel parts of the resilient mounts in the frequency range of the tests. Thereby, in Figure 41 the FE model of a conical resilient mount for marine diesel is shown. In the Figure the coordinate system used in the analyses that are presented in the following chapter is shown. The *z* axis is the vertical one, while the *x* and *y* axes lie on the horizontal plane. All the axes are parallel to the corresponding axes of the coordinate system used in the analyses of the diesel engine foundation. In Figure 42 a section of the same resilient mount is shown, where the rubber core of the resilient mount is the white part of the FE model. The resilient mount has been modelled with brick elements. The mesh size has been set in such a way that the lowest wave length λ of the excitation signal can be properly simulated in each part of the isolator. For these reasons, the mean mesh size is about 6 mm.

The resilient mount is preloaded with the design load 24 hours before the test is carried out so that the test will be not affected by the relaxation of the rubber. During the 24 hours, the applied static load is continuously checked and, when required, it is adjusted to maintain the applied load constant. As regards the temperature, the environmental temperature is checked in the 24 hours before the test is carried out and also during the tests for the measurement of the dynamic

transfer stiffness of the isolator. The environmental temperature of the laboratory cannot be set at the temperature value at which the resilient mount is exposed when it is installed on board and usually the environmental temperature of the laboratory is about 20°C, but, according to the graph shown in Figure 14, the behaviour of rubber usually used in the isolators for marine diesel engines, does not vary considerably in the temperature range that includes the environmental temperature of the laboratory and that one of the engine room of a ship (no more than 40°C). In the following Sections, the procedure for the experimental tests to measure the dynamic transfer stiffness of resilient mount is presented.

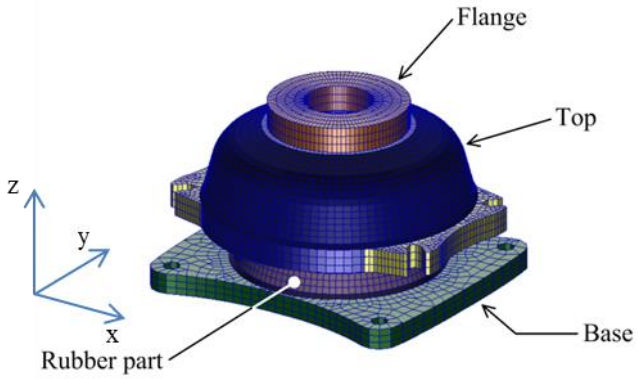

Figure 41 - FE model of a conical resilient mount for marine diesel engine

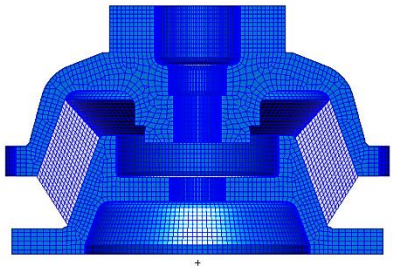

Figure 42 - Section of an FE model for marine diesel engine. The cast iron parts are blue and the rubber part of the resilient mount is white

13.1. Experimental tests for the measurement of the dynamic transfer stiffness in the normal direction

An experimental campaign has been carried out to measure the dynamic transfer stiffness of a large resilient mount in the normal direction.

The blocking mass used in the tests is made of four steel disks. The soft isolators to decouple the blocking mass by the rigid frame of the test rig have been selected to lower as much as possible the highest natural frequency f_0 of the mass-spring system composed by the blocking mass, the soft isolators (the rubber disks) and the isolator under tests. Such natural frequencies have been calculated in Matlab. In particular, the system has been considered as a lumped parameter system composed by the blocking mass connected to the rigid foundation by the soft isolators and to the excitation mass by the resilient mount under test. The soft isolators and the resilient mount have been considered as ideal springs (hypothesis that is considered valid in the case of small displacements and low frequency analysis) and the blocking mass has been considered as a lumped mass characterized only by its inertia. So a simple script has been created in Matlab to identify the optimum combination of soft isolators in order to lower as much as possible the natural frequency f_0.

An approximate formulation for the calculation of frequency of the lowest internal resonance of the resilient mounting is the following:

$$f_e = 0.5\sqrt{\frac{k_0}{m_{\mathrm{el}}}} \qquad (87)$$

where k_0 is the low-frequency dynamic stiffness of the resilient mounting and m_{el} is the mass of its elastic part.

According to the ISO 10846 Standards, measurements are valid for frequencies higher than f_e /3, but just if the resonance frequency f_0 is lower than f_e /10.

As for the upper limit, the ISO 10846-3 Standard provides the frequency values f_3 for steel blocking masses of cylindrical or cubic shape. Upper frequency limit may be also determined by means of experimental tests and referring to the concept of effective mass. When the effective mass $m_{2,\mathrm{eff}}$ has been determined,

the upper frequency limit f_3 has to be chosen as the lower frequency value where the effective mass does not vary more than 12 % from the mass value m_2.

Moreover, both background noise level and unwanted vibration levels related to the degrees of freedom other than the investigated one have to be taken low. These noises are controlled by setting a series of physical parameters of the moving system. This setting is made through a comprehensive prediction of the moving system behaviour.

With regards to the background noise, as required in the ISO 10846-3 Standard, acceleration levels measured in vertical direction at the blocking mass, when the vibration source is turned on, must be 15 dB [ref. 10-6 mm/s2] higher than the corresponding levels measured while the vibration source is turned off. The second check has been carried out to control the transverse acceleration levels (i.e. horizontal accelerations). The acceleration levels measured at the excitation mass in directions orthogonal to the driving direction must be 15 dB [ref. 10-6 mm/s^2] lower than those measured in the driving direction. If that is not verified, the unwanted accelerations of the excitation mass could cause, on the blocking mass, accelerations which are a linear combination of the excitation mass transverse and vertical accelerations. Unwanted horizontal accelerations have been measured on the excitation mass according to procedure given in the ISO Standard (see Figure 44) [69].

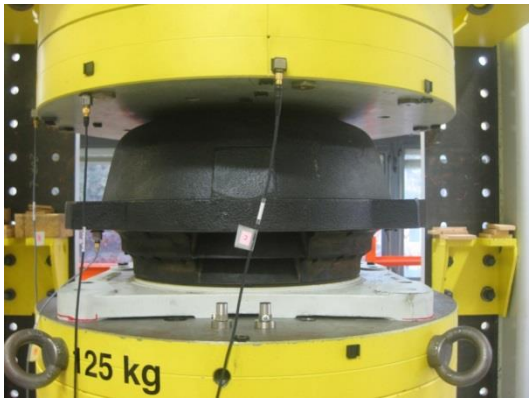

Figure 43 - Resilient mount under test

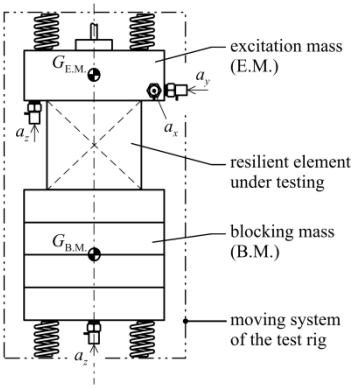

Figure 44 - Plan of acceleration transducers on the moving system (E.M.: excitation mass, B.M.: blocking mass).

13.2. Experimental tests for the measurement of the dynamic transfer stiffness in the transversal direction

Figure 45 shows the set-up of the test rig for the measurement of the dynamic transfer stiffness in the transversal direction. The prescriptions that have been presented for improving the accuracy of the measurements are still valid. The driving direction lies on the *x* or *y* axes and the unwanted input vibrations to be checked during the experimental campaign are measured in the *y* and *z*, or in the *x* and *z* directions respectively.

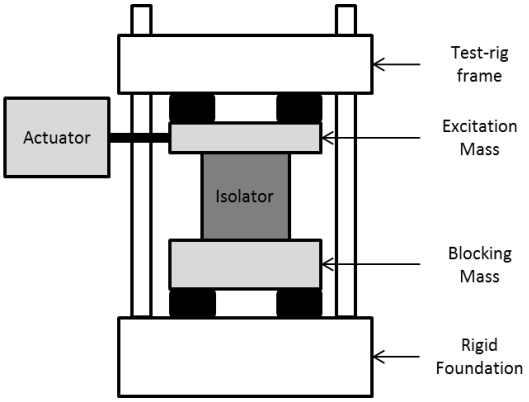

Figure 45 - Set up of the test rig to carry out the measurement of the dynamic transfer stiffness in the transversal direction

With regard to the effective mass, the procedure to carry out the measurements is that one already presented for the measurement of the dynamic transfer stiffness in the vertical direction, but it is performed according to the scheme presented in Figure 46. The measurement of the effective mass is used to define the upper limit f_3 of the frequency range of the test.

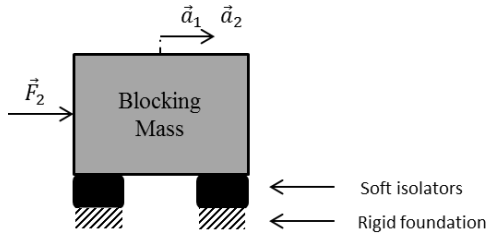

Figure 46 - Scheme of the experimental test for the measurement of the effective mass of the blocking mass in the transversal directions

14. Simulation of the dynamic transfer stiffness of a resilient mount

14.1. Dynamic behaviour of rubber

In order to properly simulate the dynamic behaviour of rubber in the high frequency range, a suitable constitutive model to describe the rubber material has to be used.

Rubber behaves as a visco-elastic material and so it combines the viscosity of the liquids with the elasticity of the solid materials. When rubber undergoes deformation, it exhibits time-dependent strain. Moreover the material behaviour strongly depends on temperature, frequency range of the excitation and on pre-deformation. Several models have been developed to describe the behaviour of rubber. The visco-elastic models usually take into account both the viscous and the elastic behaviour of the resilient mount, while the hyper-elastic models provide a mean to model the non-linear stress-strain relationship of the rubber.

The Yeoh model [70] is a hyper-elastic model that is widely used to simulate the rubber stress-strain relationship. According to this model, if the material to be simulated is nearly incompressible, its strain energy density function W depends on the first strain invariant I_1 as follows:

$$W = \sum_{i=1}^{3} C_{i0} (I_1 - 3)^i \qquad (88)$$

To completely characterize the rubber, three material coefficients are needed: C_{10}, C_{20} and C_{30}. For the consistency condition with linear elasticity, it can be shown that the first material coefficient C_{10} is equal to half of the initial shear modulus μ.

The material coefficients are usually obtained carrying out laboratory tests on rubber standardized specimen for the achievement of the stress-strain curve. Unfortunately, these data are often not available or they are strictly confidential.

The dynamic parameters of the material which characterize rubber like materials are the storage modulus E' and the loss modulus E''. The former measures the stored energy, representing the elastic portion of the material, the latter, measures the energy which is dissipated as heat and so it represents the viscous portion. These parameters can be measured performing the Dynamic mechanical analysis (DMA) tests. Tests facilities can usually perform this kind of measurement in a low frequency range, and these results cannot be extrapolated at higher frequency range.

14.2. Outline of the numerical procedure

In order to set a numerical model which simulates the dynamic behaviour of a resilient mount, the characteristic material data of the rubber core are needed. These data can be obtained by DMA tests, but they are usually confidential and so they are often not available to properly identify the material coefficients of the rubber part of the resilient mount. Beijers [29] set a procedure to identify the Yeoh coefficient C_{10}, C_{20} and C_{30} starting from static force-deformation compression tests. This procedure is based on static non-linear simulations and it has been tested in the case of a small resilient mount with a cylindrical shape. Then, a second set of numerical simulation were carried out to characterize the dynamic behaviour of the rubber, and so to obtain the loss modulus E'' of the rubber, starting from the experimental curve of the dynamic transfer stiffness of the same resilient mount. The procedure defined by Beijers has been reused by the authors and generalized to be applied in the more general case of a conical resilient mount for large marine diesel engine.

The procedure can be divided into several steps. First of all, non-linear static simulations are carried out to find the static coefficients that characterize the rubber material C_{10}, C_{20}, C_{30}. Such simulations reproduce the static compression test of a resilient mount and a Force-Displacement curve is obtained as result. The latter is to be compared with an experimental force-displacement curve, obtained

as results of a compression test carried out on the resilient mount under investigation. The first step is to fit the numerical curve with the experimental curve in the interval of the latter where the non-linear behaviour is negligible. In this way the linear coefficient of Equation 7, i.e. C_{10}, is set. Then the fitting procedure carries on in order to find the non-linear terms of Equation (88), i.e. C_{20} and C_{30}. The procedure terminates when the quadratic error between the measured reference curve and the simulated one (both have been sampled at constant intervals) is minimized (percentage error less than 5%).

Once the static non-linear simulations are completed and all the three coefficients of the Yeoh models are set, the second step of the procedure can begin. The resilient mount is preloaded with the work static load and then a series of non-linear dynamic simulations is carried out. Such simulations take into account the non-linearity due to the contact between the resilient mount top casting and the rubber core, and between the latter and the resilient mount base casting. The viscous behaviour of rubber affects the dynamic response of the resilient mount. Since the rubber material has been modelled using the Yeoh constitutive law, i.e. a hyper-elastic model, the damping is taken into account defining a damping coefficient of the rubber part ξ which strongly depends on frequency. A procedure has been developed to define such coefficient. In this procedure, a measured curve of the dynamic stiffness of the resilient mount has been taken as reference. For each frequency step of about 10 Hz, a harmonic acceleration a_1 in the vertical direction has been imposed to the flange of the resilient mount top casting. The constraint force that results at the resilient mount base casting constraint, in the vertical direction, is the output force F_2 to be used in the calculation of the simulated dynamic transfer stiffness, once the displacement of the top casting u_1 is obtained from a_1. The value of the damping coefficient to be used in the model is tuned, minimizing, for each frequency step, the quadratic error between the calculated values and the measured ones [71, 71]. The flow chart in Figure 47 shows the presented procedure for the simulation of the dynamics of the resilient mount. On the left hand side of the flow chart, the steps to define the coefficients that characterize the materials are shown (green boxes). On the right hand side of the flowchart, the steps to be followed in order to simulate the dynamic transfer stiffness of the resilient mount are presented (blue

boxes). The dashed curves show the steps of the workflow in which iterative calculations are needed.

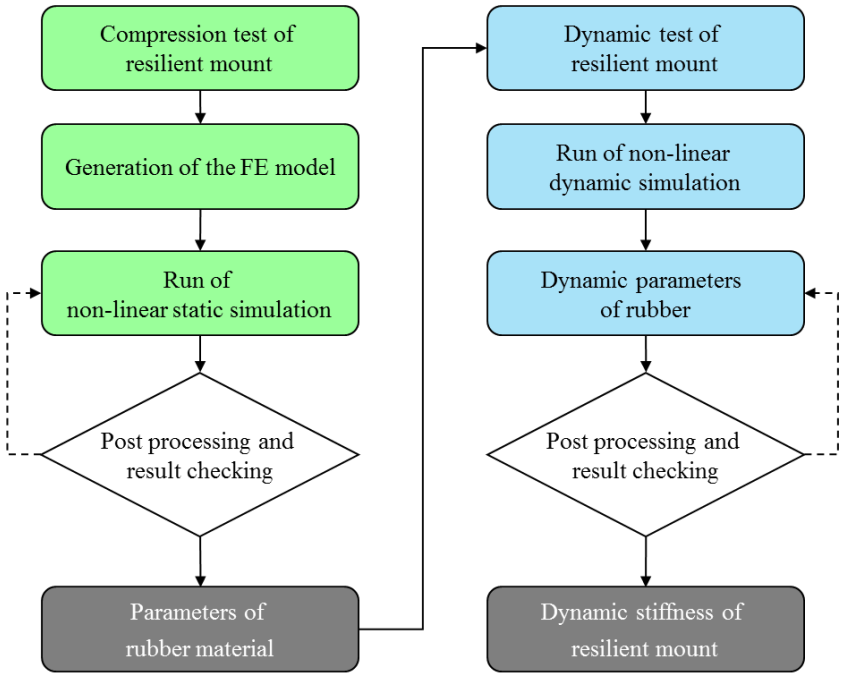

Figure 47 - Flow chart of the iterative procedure for the simulation of the dynamic transfer stiffness of the resilient mount

15. Measurement of the mobility of the diesel engine foundations

The mechanical mobility of a diesel engine foundation is achieved carrying out impact tests on board ships. Figure 48 shows the upper plate of a diesel engine foundation. On such plate, four accelerometers have been attached in order to carry out the experimental measurement of the mechanical mobility of the diesel engine foundation. In Figure 49 a typical foundation for marine diesel engine is shown.

Figure 48 - measurement points on a diesel engine foundation

Figure 49 - example of diesel engine foundation for marine diesel engines

Each driving-point frequency transfer function is derived by a test in which output velocity is measured on a spot located near to the point where vibrations are excited by an instrumented impact hammer. Analogue signals of both the accelerometer and impact hammer are elaborated by a data acquisition system in order to get the frequency response functions in the frequency range of interest. During the measurement stage, for each impact test, the force spectrum, the

velocity (or acceleration) spectrum and the driving-point frequency transfer function together with the relevant coherence function are checked. The narrow band spectra describing the frequency response functions are further elaborated in order to have the one-third octave-band spectra, as usual in the treatment of the structure-borne noise.

16. Dynamic Simulation of the diesel engine foundation

Many drawbacks have to be overcome when proceeding with the numerical evaluation of the dynamics of the engine foundations on board ships. These are related with two orders of difficulties: on one hand, setting of the FE model by correlation with measures taken on the real structure is not so easy, due to the uncertainties typical of the measurements taken on large and complex structures; on the other hand, the dynamics of the foundation can be satisfactorily understood only if the FE model includes the foundation surrounding structures, so leading to solve a large model characterized by a high modal density.

As for the measurements, it has to be pointed out that they are usually just performed to evaluate the foundation mobility levels, that the measurement technique is based on the excitation of the structure by an instrumented hammer, and that the measures are taken on the foundations before the installation of the engine above them, when the ship blocks placed in the dry dock are only partially joined together. Therefore, it follows, in order, that: the updating of an FE model through measured data can be only performed in terms of mobility levels; the range of measurement is such as to cover the resonance controlled region, while the stiffness controlled region is more difficult to characterize due to the measurement procedure, so acquired data can only partially cover the typical frequency range of investigation; and that current condition of the engine foundation during measurement, which remarkably differs from the operative working condition, is not clearly known in term of masses, perimeter constraints and keel blocks positions.

In this frame, a not negligible support for the interpretation of the foundation mobility measurements is given by the conclusion of an experimental study which has been carried out in test room with the diesel engine both placed or not on the foundation. This shows that the difference between the natural frequencies

of the foundation obtained in the two situations is less than 10%, that the modal shapes are correlated, and that a slightly lower damping factor is found when the mobility is measured without the engine. This all leads to conclude that, even though foundation dynamics can be measured in good approximation for general purposes, it should be carefully regarded as a benchmark when updating a numerical model.

In second place, designer has to face the problem of a burdensome calculation and data processing. To solve the question, a setting procedure needs to be implemented to define the most cost-effective FE model, by comparing FE models which differ in extensions, constraints and mesh fineness. With this objective in mind, different FE models should be created by increasing the mesh refinement while reducing the model extension, in order to perform a series of modal analyses, each of them can be limited to a proper frequency range. Correlation between FE models are established by first comparing natural frequencies and mode shapes and then direct and cross mechanical mobility.

The updating of FE models by experimental data is carried out by changing the material properties, like the elastic modulus and the volumetric mass density, and the system properties like the structural and component damping. The question on how to update an FE model through experimental data and how to set the most cost-effective FE model for the purpose of structure-borne noise analyses, are intrinsically connected.

In a first step it is essential to define the frequency range in which analyses should be performed, in order to evaluate the maximum size of the elements and how to extreme the condensation process. Then, the basic FE model is generated, which is the model of the engine foundation alone, including only bed plates and relevant supports standing out from the double bottom plating. Next step is to widen the model extension while controlling the increase of the mesh size.

Various methods are available for the purpose of performing a systematic comparison between two sets of vibration data within a model correlation or updating process. This can be done, in practice, in two steps, starting from the analysis of the mode shape correlation of a set of grid points by the Modal Assurance Criterion (MAC) and using then the Frequency Response Assurance

Criterion (FRAC) applied to the mechanical mobility FRF's in order to analyse the frequency response of the modelled structure. Both the criteria provide a measure of the least-squares deviation or 'scatter' of the points from the straight line correlation. Minimum threshold to consider a good correlation depends on the quality of the calculated and measured data.

Moreover, to compare the frequency response of every FE model with the real data, the level of correlation can be effectively evaluated using the Local Amplitude Criterion (LAC), which quantifies such correlation as a frequency function for each individual degree of freedom:

$$LAC_{ij}(\omega) = \frac{2\left|H^{*}_{Xij}(\omega)H_{Aij}(\omega)\right|}{\left(H^{*}_{Xij}(\omega)H_{Xij}(\omega)\right)+\left(H^{*}_{Aij}(\omega)H_{Aij}(\omega)\right)} \qquad (89)$$

where *i* and *j* are the response and excitation coordinates, $H_{Aij}(\omega)$ is the predicted FRF value and $H_{Xij}(\omega)$ is the corresponding measured FRF value, both at frequency ω (and * denoting complex conjugate). By this criterion it is possible to individually evaluate the frequency correlation for each frequency response function.

A complementary and basic analysis of the correlation of single FRF's can also be performed by simple indices measuring, for each of the first mode shapes, the shift of correlated natural frequency $\delta f = (f_A - f_X)/f_X$ and the difference in relevant damping ratio $\delta\zeta = (\zeta_A - \zeta_X)/\zeta_X$ between the calculated *A* and experimental *X* data.

A first analysis on the matching among calculated and experimental data can also be done by visual inspection of the FRFs curves by overlaying the measured and the numerically generated FRFs as magnitude curves. This analysis gives an overall but subjective and qualitative measure of the level of correlation.

In this thesis, a series of numerical analyses has been carried out to study the dynamics of a typical foundation design to support a medium speed diesel engine. Several FE models have been created; these differ each other for the fineness of the mesh, for the type of elements (shell elements and brick elements), for the boundary conditions and for the extension of the ship structures to simulate. The

results of the simulations have been validated by outcomes of experimental tests and applying the LAC criterion as shown before.

Part III

RESULTS

17. Resilient mount under investigation

A series of tests has been carried out to measure the dynamic transfer stiffness of a conical passive resilient mount designed for marine diesel engines. Figure 50 shows a typical resilient mount for marine diesel engine. Figure 51 shows the components of such resilient mount: the Base Casting is made of cast iron and guarantees the coupling of the resilient mount with the diesel engine foundation and so with the ship structures; the rubber core, that is made of filled vulcanized natural rubber, is the passive isolator element of the resilient mount and the Top Casting, that is also made of cast iron and guarantees the coupling between the resilient mount and the diesel engine foot. Sometimes, the resilient mount top is adapted to house a flange which allows the adjustment of resilient mount in height, by means of a ring nut [69].

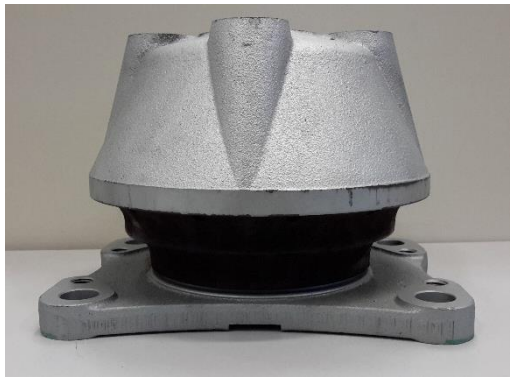

Figure 50 - Passive resilient mount for marine diesel engine

In this work, a large conical passive resilient mount has been investigated. Such isolator has been specifically designed for medium speed marine diesel engine of a rated power of about 16000 kW, that are usually employed as prime mover or as

diesel generator on-board cruise ships or RoPax ferries. The rubber core of the resilient element has a hardness of 65 Shore A.

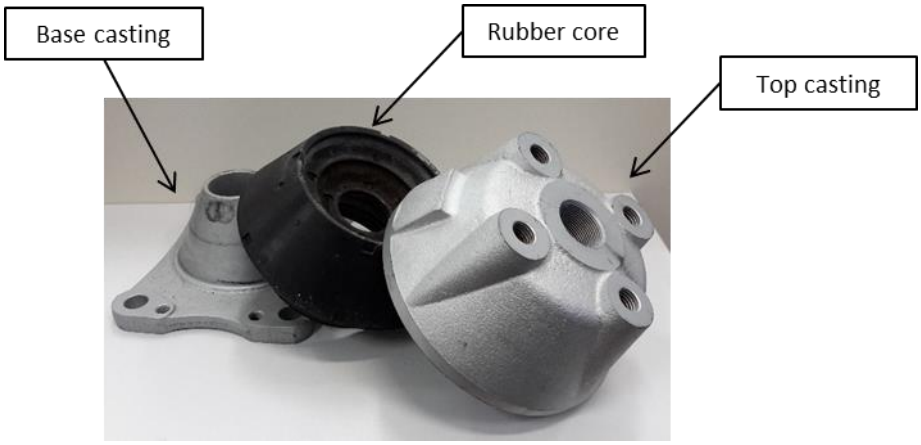

Figure 51- Components of conical passive resilient mount for marine diesel engine

Figure 52 shows the Force-displacement curve achieved by a static compression test carried out at the NVL Laboratory. The test has been performed increasing the compression static force at fixed steps. For each force step, the measurement of the relative displacement between the top casting and the base casting of the resilient mount has been done after 24 hours, so that the relaxation phenomenon of the rubber did not altered the measured data (i.e. the compression force has been maintained constant during each force test for a length of time that has been considered sufficient to cross the relaxation phenomenon; after that, the relative displacement of the top casting and the base casting of the resilient mount has been measured) [71].

The isolator under test has been designed to withstand a static load of 150 kN. In this work, the dynamic transfer stiffness of the resilient mount has been measured with the resilient mount loaded at the expected working load of 75 kN. That one is the typical load that a resilient mount had to withstand, when it is installed under a medium-speed diesel engine, on board ships.

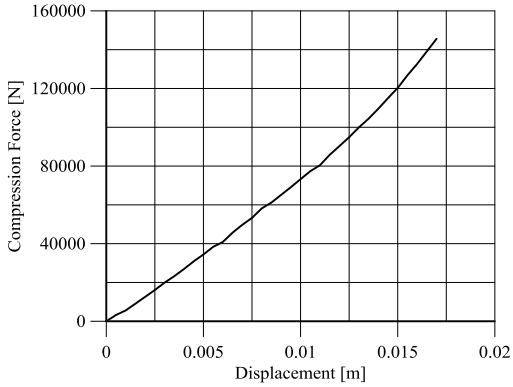

Figure 52 - Force-displacement curve of the resilient mount under investigation

17.1. FE linear dynamic analysis of the cast iron components of the resilient mount

A preliminary analysis has been carried out to investigate the dynamic behaviour of the top casting and of the base casting of the resilient mount [72]. An FE model of the two components of the isolator has been created and a series of free-free numerical modal analyses has been performed. Figure 53 shows the FE model of the top casting of the resilient mount; Figure 54, Figure 55, Figure 56 show the first, the second and the third mode shape of the top casting respectively. The Figures report the top casting of the resilient mount in the *xy* plane. In Figure 57 the FE model of the resilient mount base casting is reported. Figure 58, Figure 59 and Figure 60 show the first, the second and the third mode shape of the resilient mount base casting. All the FE analyses have been solved in MSC.Nastran.

The outcomes of the analyses show that in the frequency range of the test (100 Hz – 1000 Hz), the top casting of the resilient mount is characterized by a two lobes shape at 964 Hz. The base casting has the first natural frequency at 953 Hz, but, as shown in Figure 58, the conical part of the base casting is not affected by that mode shape. Another series of analyses has been carried out to study the mode shapes of the resilient mount base casting when it is bolted to a rigid foundation. Figure 61 shows the two lobe shape of the conical part of the resilient mount base

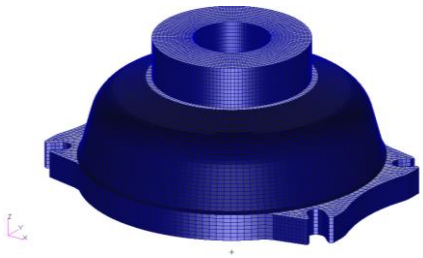

Figure 53 - FE model of the resilient mount top casting

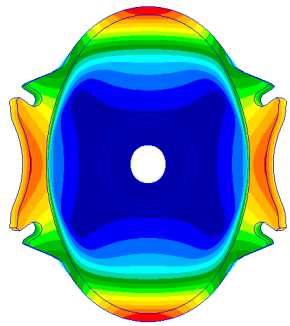

Figure 54 - First vibration mode shape (964 Hz)

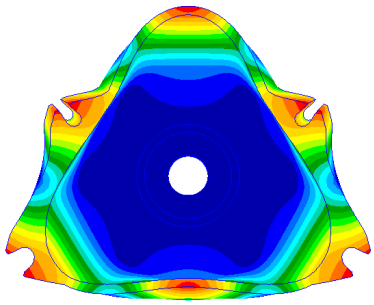

Figure 55 - Second vibration mode shape (1677 Hz)

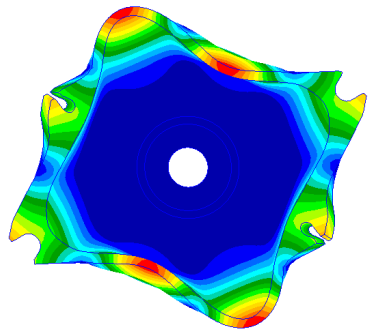

Figure 56 - Third vibration mode shape (1864 Hz)

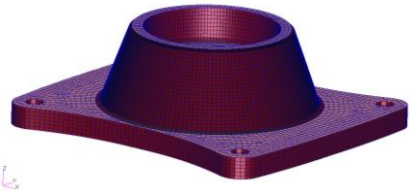

Figure 57 - FE model of the resilient mount base casting

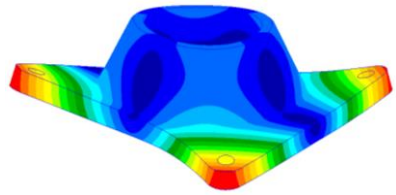

Figure 58 - First vibration mode shape (953 Hz)

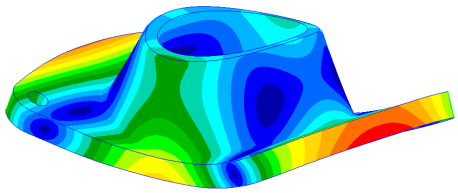

Figure 59 - Second vibration mode shape (1381 Hz)

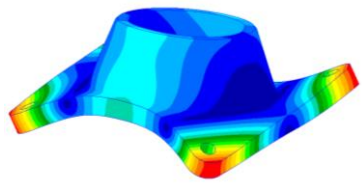

Figure 60 - Third vibration mode shape (1912 Hz)

casting at 5674 Hz. That frequency is out of the measurement frequency range and so it does not affect the measurement results.

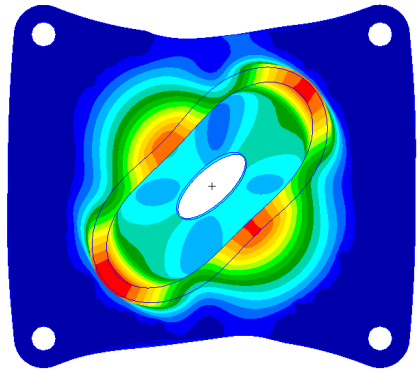

Figure 61 - First mode shape of the base casting of the resilient mount, when it is bolted to a rigid foundation (5674 Hz)

18. Outcomes of the experimental tests for the dynamic characterization of a resilient mount in the normal direction

An experimental campaign has been carried out to measure the dynamic transfer stiffness of the resilient mount under investigation according to the procedure presented in Chapter 13.

18.1. Frequency range of the experimental tests

First of all, the test rig has been set up according to the prescriptions of the ISO 10846-3 Standard [46] and the considerations presented in Chapter 11 and 0.

An analysis of the mass-spring system composed by the excitation mass, the isolator under test, the blocking mass and the soft isolators, has been done in order to define the lowest frequency of the frequency range of the test. Considering that the lowest internal resonance of the isolator under test, calculated according to the Equation (87), appears at f_e = 450 Hz and considering that the highest natural frequency of the system f_0 in the six degrees of freedom is 35 Hz, according to the procedure presented in Section 13.1, the lowest frequency of the measurement frequency range is 100 Hz. All the tests have been performed using the blocking mass made of 4 steel disks bolted together and presented in Section 12.3. According to the outcomes of the experimental tests for the measurement of the effective mass $m_{2,\text{eff}}$, the upper frequency limit f_3 of the test is 1550 Hz. Nevertheless, as will be shown in the following, the outcomes of the tests are considered valid till 1000 Hz, since, at higher frequencies, high levels of unwanted input vibrations affect the outcomes of the laboratory tests.

18.2. Test for linearity

In order to verify the effectiveness of the outcomes achieved by the experimental campaign, a test to prove the linearity in dynamic response of resilient elements under different static loads has been carried out.

Three different static loads have been applied (60 kN, 70 kN and 80 kN), characterizing a range of usual design working loads. Figure 62 shows that the relevant vertical transmissibility curves have the same trend and do not diverge significantly from each other. A slight increment in dynamic stiffness due to an increment in static load is clearly appreciable both in a higher transmissibility at low frequencies and in higher resonance frequencies. Results are expressed in terms of dynamic transmissibility levels L_T, calculated as 20 log ($T_{2b,1}$) = 20log (F_{2b}/a_1) and expressed in dB [ref. 1 kg] in consideration that $T_{2b,1}$ is an output to input force ratio [49] [73].

The check for verifying the linearity in the dynamic response of the resilient element has been also carried out by varying levels of the applied dynamic loads. This test has been performed at the design static load of 75 kN.

Outcomes of this test are shown, in terms of dynamic transmissibility, in Figure 63. The three different curves of dynamic transmissibility are referred to three different levels of excitation dynamic loads, which correspond three different levels of acceleration a_z (100 dB, 105 dB and 110 dB [ref 10-6 mm/s^2]) measured on the base of the excitation mass [73].

It is worth pointing out that once again the three transmissibility curves do not diverge significantly from each other and that they maintain the same trend in the investigation frequency range. Such behaviour of the resilient mounting under different dynamic loads of excitation proves the linearity in the dynamic response of the resilient element.

Figure 64 shows the transmissibility curve measured at the design static load (75 kN).

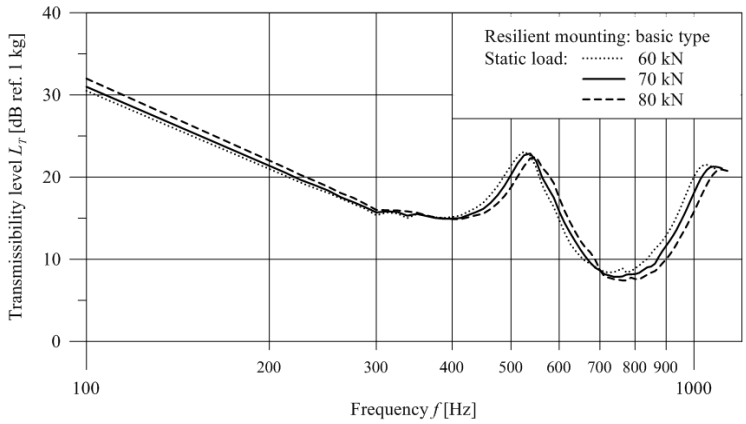

Figure 62 - Vertical Transmissibility at different static loading

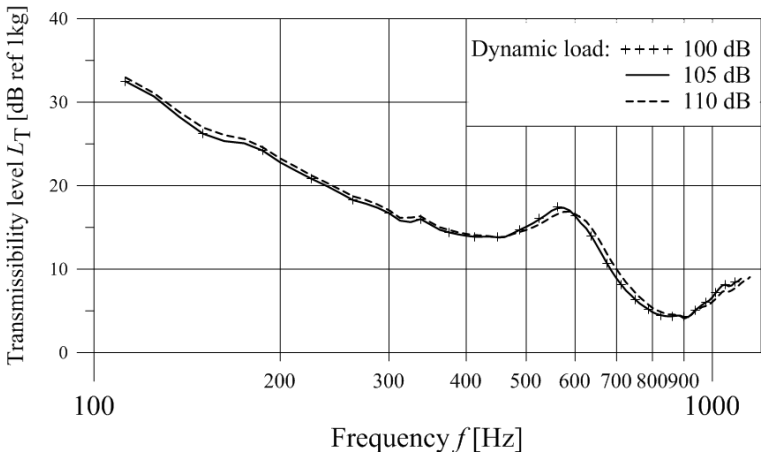

Figure 63 – Vertical Transmissibility curve at different dynamic loads (a_z levels)

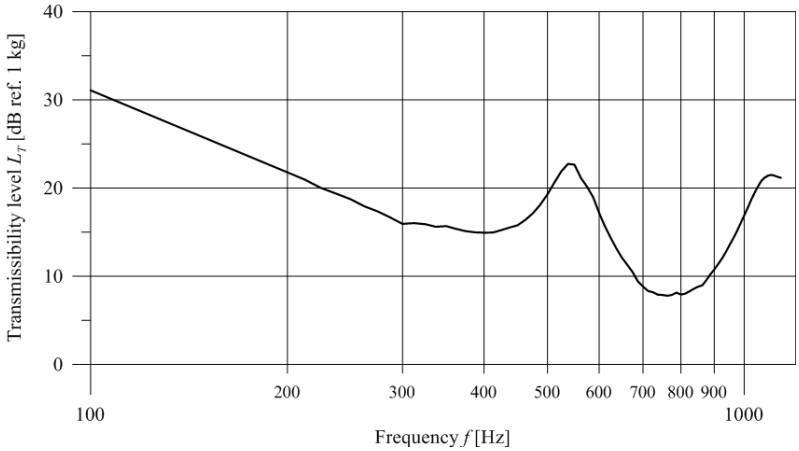

Figure 64 - Vertical transmissibility curve at the design static load of 75 kN

18.3. Unwanted input vibration

According to the prescription of the ISO 10846-3 Standard, the acceleration levels a_y and a_z of the excitation mass have been measured during the test to verify if the input vibration applied in directions different from the driving one could affect the effectiveness of the results. Figure 65 shows the accelerometers layout for the measurement of the acceleration levels of the excitation mass in *x* and *y* directions.

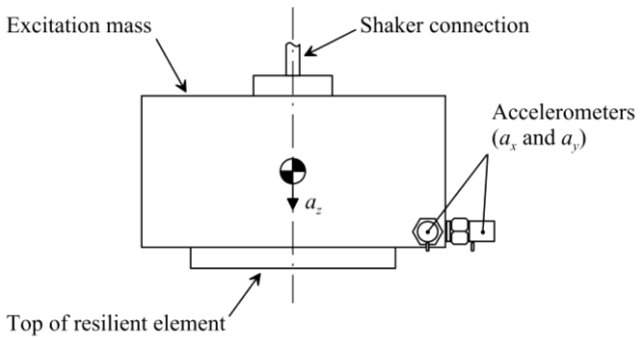

Figure 65 - Accelerometers layout for the measurement of the acceleration levels of the excitation mass in *x* and *y* directions

Unwanted horizontal accelerations have been then compared with the vertical acceleration as shown in Figure 66 [49]. Even if the acceleration levels a_x and a_y increase with the frequency and they show two picks at about 950 Hz, till 1100 Hz, the Equation (84) is satisfied. Above that frequency, the transversal accelerations increase and the difference between the vertical acceleration and the transversal accelerations is no more satisfied. For these reasons, the upper frequency f_3 in the high frequency range has been no more considered valid and the frequency range of the laboratory tests has been limited, in the high frequency range to 1000 Hz.

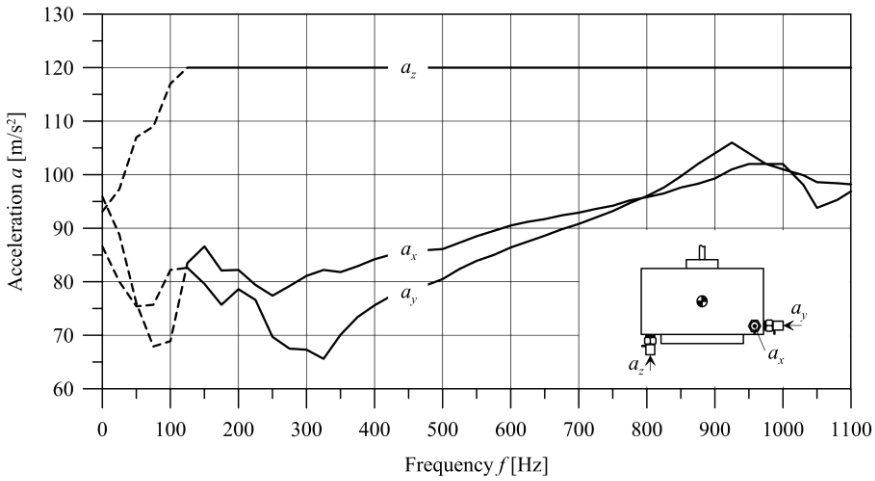

Figure 66 - Acceleration levels of the excitation mass in *x*, *y* and *z* direction

19. Coupling between the top casting of the resilient mount and the excitation mass

In some configurations, resilient mounts are equipped with fixtures for the adjustment of resilient mount in height, by means of a ring nut, for a better engine alignment and an easier on board installation below the engine. While the resilient mount base is rather large and tightly joined to the bed plate of the foundation, the resilient mount top with its adjustment flange may be weak to transverse flexural deformations. Being resilient mount top and fixing rail of the engine foot firmly fastened each other, gives rise to a dynamic coupling of the two parts and so to coupled modes of vibration.

A comparative experimental research has been carried out in order to evaluate the influence of different boundary conditions at the top of the resilient element on its dynamic response, and in this Section the outcomes of such experimental campaign are presented [69].

Figure 41 shows an FE model of the resilient mount under test equipped with the fixture for the alignment in height and Figure 43 shows the resilient mount, installed in test rig, without the fixture on its top casting. The two different configurations of the resilient mount have been studied, by applying or removing the fixture on the top casting. Removal of the flange on the top of the resilient mount has been considered to try and evaluate the mechanism by which a dynamic coupling appears between top casting and the exciting mass.

The acceleration levels of the excitation mass measured when the resilient mount without the fixture on its top casting has been tested, have been presented in Figure 66. Figure 67 shows the acceleration levels measured during the experimental campaign for the dynamic characterization of the same resilient mount fitted with the flange. Also in this case, the accelerometers have been installed on the excitation mass according to Figure 65.

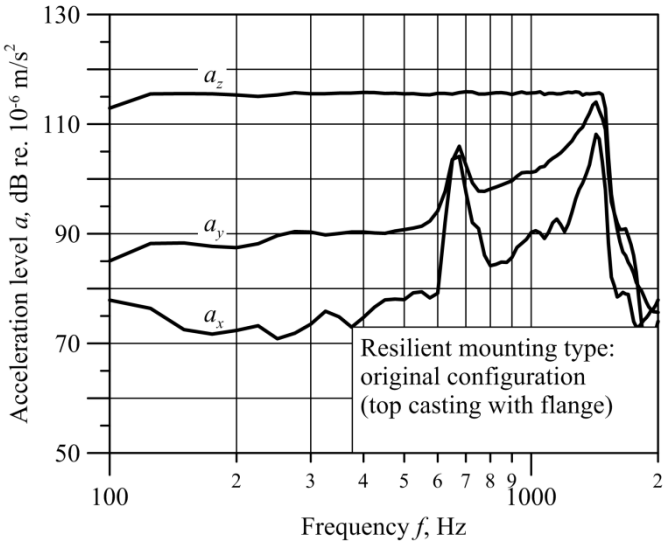

Figure 67 - Accelerations measured on the exciting mass (resilient element fitted with the top flange)

In Figure 67, the a_x and a_y curves show to maintain a difference of more than 15 dB [ref. 10^{-6} mm/s^2] lower than that one measured in the driving direction. Unfortunately, an unexpected disturbance has been detected, being the output relevant to the horizontal linear motion in both coordinate directions unsatisfactory due to the presence of a peak at about 681 Hz. Their shapes diverge significantly from the previous ones since the latter do not show any clear peak in the useful frequency range, except for the smooth peak at about 950 Hz.

Clearly, the low difference in the levels of the vertical and horizontal accelerations is not due to the resonance of the exciting mass itself which, as discussed in Section 12.2, behaves as a rigid body in the whole frequency range. Comparison of the results of the two tested configurations of the same resilient element points out that the two tested configurations have a different dynamic behaviour and differently interact, through the top casting, with the upper body which they are in contact with. So, new experiments have carried out to understand reasons of discrepancy in the accelerations relevant to the horizontal motions, and the results are presented in the following sections.

19.1. The ODS based analysis

First of all, special attention has been paid to the correct functioning of each element of the moving system of the test rig. A comprehensive measurement of movement and deflection has been carried out on all the masses, and in particular on the excitation mass and on its connection to the shaker by the stinger rod. Such an analysis has been performed by the Operational Deflection Shape (ODS) technique.

This method allows to obtain, basing on the displacement cross spectra derived by a series of acceleration measurements, the identification of each mode shape and its animate for each single body of the moving system.

This technique has been applied by acquiring the cross spectra of accelerations at a series of significant points of the moving mass, while the shaker was producing, through the stinger rod connected to the top of the exciting mass, a flat acceleration autospectrum. A total of 8 and 4 points located at the same distance each other on the outer edge of both top and base surface of the exciting mass and blocking mass respectively was detected; as for the resilient mounting, just 4 points have been used to characterise motion and deformation of its top casting.

After processing the measured values, it has been ascertained that in general all the parts move perfectly in the direction of the driving force and that they behave like rigid bodies within the investigation frequency range. At the same time, a transverse movement has been detected on both exciting mass and top casting of the resilient mounting at the frequencies close to 681 Hz, as shown in Figure 68.

At this frequency range a pronounced transverse deflection of the top casting of the resilient element has been observed, so identifying an in-phase coupled mode of oscillation between top casting and exciting mass.

Results of the analysis based on the ODS technique put a suggestion on the reason why an unwanted oscillation is triggered on the exciting mass, but further investigations are needed to prove the hypothesis about the dynamic coupling of the two parts.

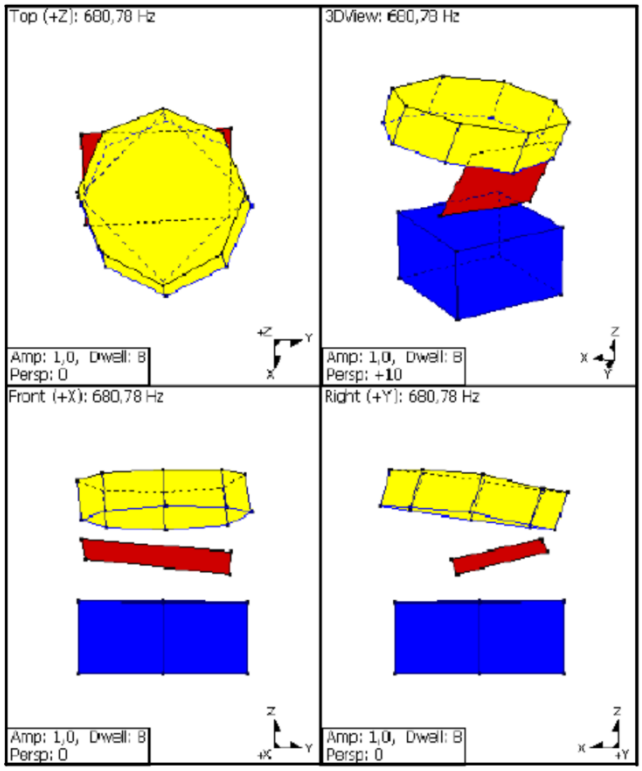

Figure 68 - Mode shape of the bodies of the moving system at the resonance frequency of about 681 Hz (resilient element fitted with the top flange).

19.2. The FEM simulation of the moving system

A further analysis has been performed by a numerical simulation of the whole moving system of the test rig, performed within the linear elastic approach. The FE model has been specially designed to acquire information on the dynamic coupling between the top casting of the resilient element and the exciting mass. This means that for some parts a fine mesh model has been generated, with a special attention to their vibrational response, while others have been just roughly modelled.

The exciting mass, the blocking mass, the top casting and the base of the resilient mounting have been explicitly modelled by brick elements (hexahedral and

tetrahedral elements) so giving an accurate modelling of their geometry and mass distribution. The rubber part of the resilient mounting has been simulated by a number of linear springs, so overcoming the difficulty of the simulation of the contact between rubber and inner and outer castings.

The interactions between the other bodies in contact have been solved by two different ways: by the merging of all the nodes shared by the two bodies in contact, when the bodies are expected to remain perfectly in contact at any modal vibration frequency – that is the case of the contact between the base of the resilient element and the blocking mass; or by merging only a selected part of the nodes in common between the bodies, when the bodies are expected to undergo relative perpendicular movements at a given modal vibration frequency – that is the case of the contact between the top casting of the resilient element and the exciting mass. In the latter case, the number of nodes to be merged has been chosen by an iterative process aimed to minimize the gap between the measured and the predicted lowest coupled resonance frequencies.

The strategy of allowing a free relative movement to the nodes belonging to the two bodies in contact has been proven to be the key for the interpretation of the dynamic coupling between the two bodies. The FE model, which is not accurate enough to give a proper prediction of the frequency response of any parts of the moving system, has been proven to be adequate to reproduce the mechanism by which a high transverse vibration arises at a given frequency on the exciting mass.

The main results of the numerical modal analysis are the mode shapes of the whole moving system at the lowest coupled resonance frequencies. As for the interaction between the top casting of the resilient element and the exciting mass, a dynamic coupling between the two bodies has been identified at a frequency of 775 Hz (+10 % with reference to the peak identified by the ODS technique), very close to the frequency of the peak in the cross-spectrum of the acceleration levels a_x and a_y measured in the laboratory test on the base of the exciting mass. The corresponding mode shape is that shown in Figure 68, an angular oscillation around a horizontal axis of the two bodies moving with opposite phase.

The deformation calculated on the two bodies is in perfect agreement with that one directly derived, by the ODS technique, from the measured accelerations. The clear agreement between the outcomes of the mode shape analysis carried out through the ODS technique and the FE simulation, points out that the coupled mode of vibration identified by the FE simulation is the explanation of the transverse movement of the exciting mass observed in the laboratory test.

The same modal analysis has been performed on the modified resilient mounting, where the flange has been removed. In this case, the lowest coupled resonance frequency between the exciting mass and the top casting is calculated at a frequency of about 980 Hz, a +3 % with respect to the measured value. The mode shape is shown in Figure 69.

Also in this case, the FE analysis gives a real contribution to the interpretation of the experimental results, showing that the smooth peak at about 950 Hz in the acceleration levels a_x and a_y (see Figure 66) is due to the repositioning to higher frequencies of the same disturbance measured on the resilient element without top flange, caused even now by the dynamic coupling of the two parts.

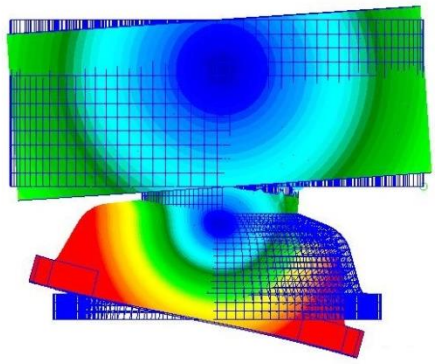

Figure 69 - Coupled mode shape of the exciting mass and the top casting (without flange) at the frequency of about 780 Hz.

20. Outcomes of the experimental tests for the dynamic characterization of a resilient mount in the transversal direction

The procedure presented in Chapter 13 to carry out the measurement of the dynamic transfer stiffness of a resilient mount and applied to carry out such experimental tests in the normal direction (see Section 13.2) has been also applied to carry out the measurement for the dynamic characterization of the resilient mount in the transversal direction. The layout of the test rig has been properly modified and the actuator has been connected to the excitation mass in such a way to excite the moving system in the transversal direction. The outcomes of an ODS analysis performed to verify the proper movement, at each frequency step, of the moving system of the test rig, showed some oscillations of the excitation mass. Those movements have been confirmed by some tests carried out to verify the accuracy of the measurements.

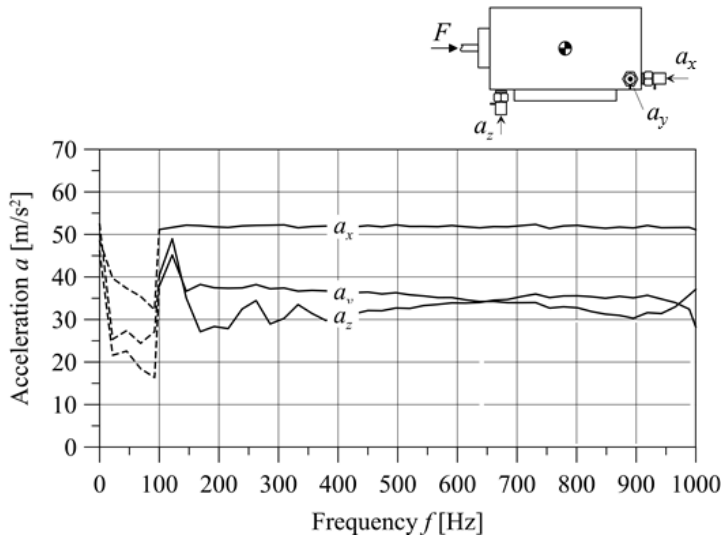

Figure 70 - Accelerations on the excitation mass (transverse driving direction)

For these reasons, a second actuator has been connected on the opposite side of the excitation mass and the two electro-dynamic shakers have been actively controlled so that the signals generated by the actuators were half a cycle out of phase. Such solution guaranteed the control of the movement of the excitation mass and so the accuracy of the outcomes of the measurement campaign. Figure 70 shows the acceleration levels of the excitation mass that have been measured during the test for the dynamic characterization of the resilient mount in the transversal direction. Figure 71 shows the dynamic transmissibility of the resilient mount obtained as outcomes of the laboratory measurement.

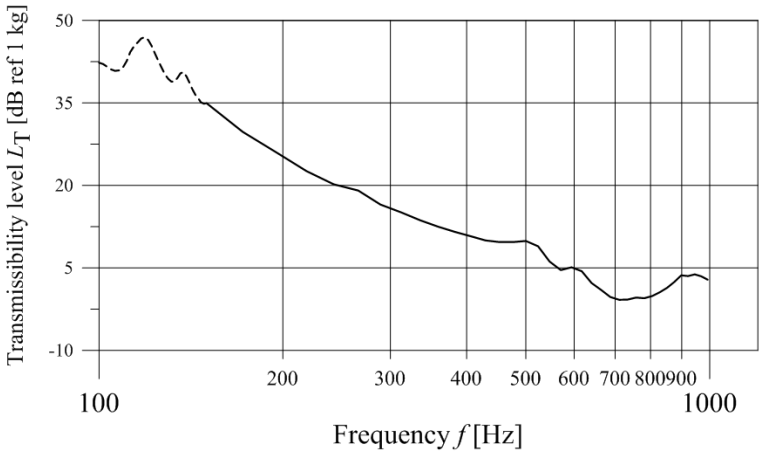

Figure 71 - Dynamic transmissibility of the resilient mount

21. Outcomes of the numerical simulations

21.1. Numerical Simulation of the compression test: identification of the main parameters of rubber material

A numerical model has been created to simulate the dynamic behaviour of a resilient mount. Such model has been defined according to the procedure presented in Chapter 14 [71].

An FE model of the resilient mount has been created. In Figure 72 the FE model has been sectioned by a vertical plane of symmetry.

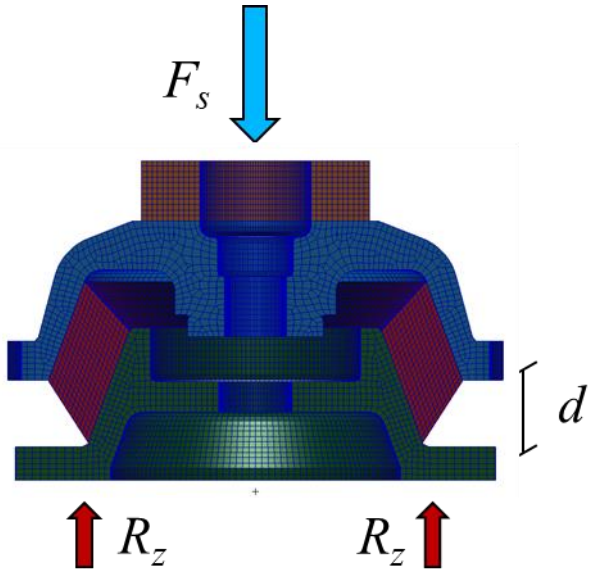

Figure 72 - Section of the FE model of the resilient mount under test. Ring nut (brown), top casting (blue), rubber core (red), base casting (green).

The resilient mounting top (blue part) holds a flange for the coupling with the engine foot (brown part), whose flange allows the adjustment of resilient

mounting in height, by means of a ring nut, for a better engine alignment. The rubber part (in red) is a conical-shaped toroid body which is coupled by a conical-shaped seat with the resilient mounting base (green part). The base is bolted to the diesel engine foundation on the ship inner bottom. In Figure 72, the border lines between the rubber part and the top and bottom casting belong to the contact surfaces between the parts. The top and the base casting of the resilient mount are made of cast iron whereas the isolator part is made of carbon filled rubber.

The resilient mount has been modelled using constant stress solid elements. Penalty contact interfaces have been defined between the rubber part and the top and base steel parts. The mesh size has been set in such a way that the lowest wavelength λ of the excitation signal can be properly simulated in each part of the isolator. Since the upper frequency range that has been investigated in this study is 800 Hz, the mean mesh size is about 6 mm. All the analyses have been carried out in LS-Dyna.

A first series of simulations has been carried out in order to obtain the characteristic parameters of rubber simulating the compression test. A second series of simulations has been done with the aim to obtain the damping coefficient and so to completely define a dynamic non-linear model of the resilient mount. Figure 72 shows how the resilient mount under investigation has been loaded for the non-linear static simulations. At the top of the resilient mount a static load F_s has been applied and, for each static load, the deflection d has been calculated in order to create the force-deflection curves. In the Figure, the constraint forces are labelled as R_z.

In Figure 73 some relevant curves of the first series of simulations are shown. It is worth pointing out that the first part of the experimental curve (dashed curve), in the neighbourhood of the graph origin is almost linear and that its non-linear behaviour arises at higher loads. That curve has been used as reference in the numerical runs that simulates such test. The curve fitting carried out in the first series of runs leads to the individuation of the first characteristic parameter C_{10} of the Yeoh model. The point-dashed curves are the outcome of some runs and the continuous curve is obtained with the coefficient C_{10} that has been achieved once the optimization process has been accomplished.

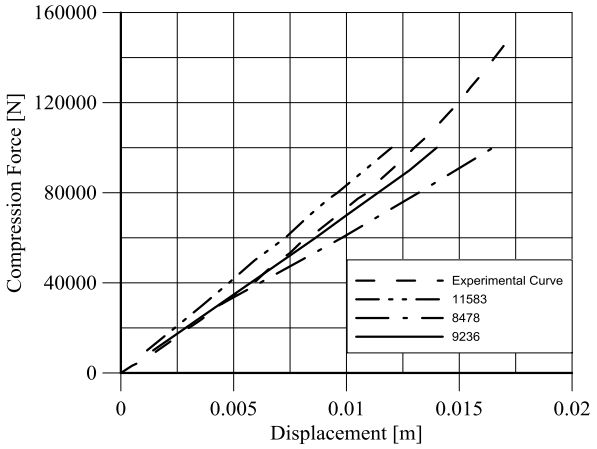

Figure 73 - Force-displacement curve obtained by compression experiments (dashed curve) and by simulations (point-dashed and continuous curves) with different values of the C_{10} coefficient. The continuous curve has been achieved with the coefficient obtained at the end of the fitting procedure.

Figure 74 and Figure 75 show some force-displacement curves obtained by runs done to achieve the second and the third parameters, C_{20} and C_{30} respectively.

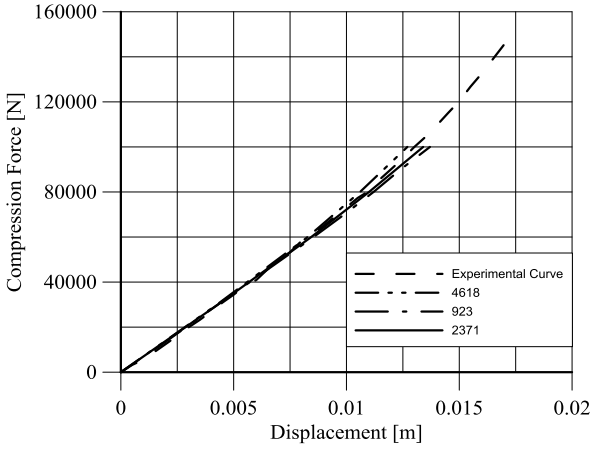

Figure 74 - Force-displacement curve obtained by compression experiments (dashed curve) and by simulations (point-dashed and continuous curves) with different values of the C_{20} coefficient. The continuous curve has been achieved with the coefficient obtained at the end of the fitting procedure.

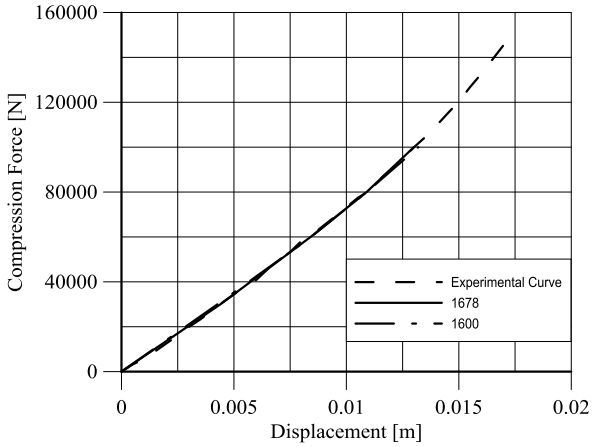

Figure 75 - Force-displacement curve obtained by compression experiments (dashed curve) and by simulations (point-dashed and continuous curves) with different values of the C_{30} coefficient. The continuous curve has been achieved with the coefficient obtained at the end of the fitting procedure.

The Figure 11 shows the force-displacement curve obtained by a numerical simulation in which the rubber part of the model is characterized by the three Yeoh coefficients obtained as results of the optimization process.

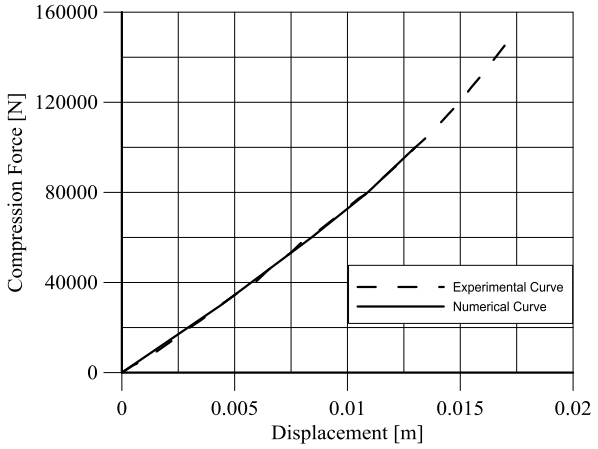

Figure 76 - Force-displacement curve obtained by compression experiments (dashed curve) and by simulations (continuous curves) carried out with the three different coefficients obtained once the numerical procedure has been completed.

The values of the coefficients obtained once the iterative procedure has been completed, are shown in Table 3.

Table 3 - Yeoh coefficient of the rubber part of resilient mount

Coefficients	Estimated values
C_{10}	9236
C_{20}	2371
C_{30}	1678

21.2. Numerical simulation of the dynamic response of rubber

The FE model that has been defined in the static simulations has been used to simulate the dynamic response of the resilient mount. The numerical simulations have been carried out according to the procedure explained in Chapter 14.

Figure 77 shows a section of the FE model of the resilient mount considered as a case study. The FE model has been loaded as shown in the Figure. At the top casting has been applied an acceleration $a_z(t)$, while the forces transmitted has been calculated at the constraint at the base casting of the resilient mount, in the vertical direction $Fz(t)$.

The experimental curve of the dynamic transfer stiffness achieved by the experimental tests (see Figure 78) has been used as reference. Figure 79 shows the excitation levels of the tests. Those are shown in terms of accelerations. In the same figure the accelerations of the unwanted vibrations are shown to give evidence about the effectiveness of the results. The same vibration levels have been applied to the top casting of the FE model to reproduce, in the simulation, the excitation condition of the experimental tests. Figure 80 shows the results of the non-linear dynamic simulations, once the damping coefficient has been set for each frequency step.

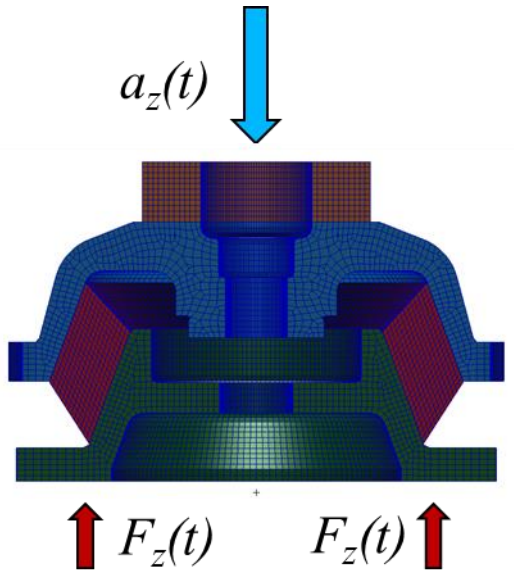

Figure 77 - Section of the FE model of the resilient mount with the loads applied for the dynamic symulations. Ring nut (brown), top casting (blue), rubber core (red), base casting (green).

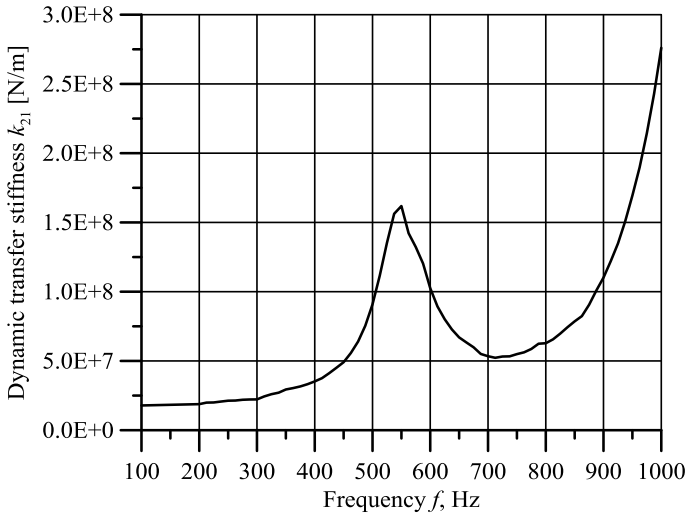

Figure 78 - Measured dynamic transfer stiffness k_{21}

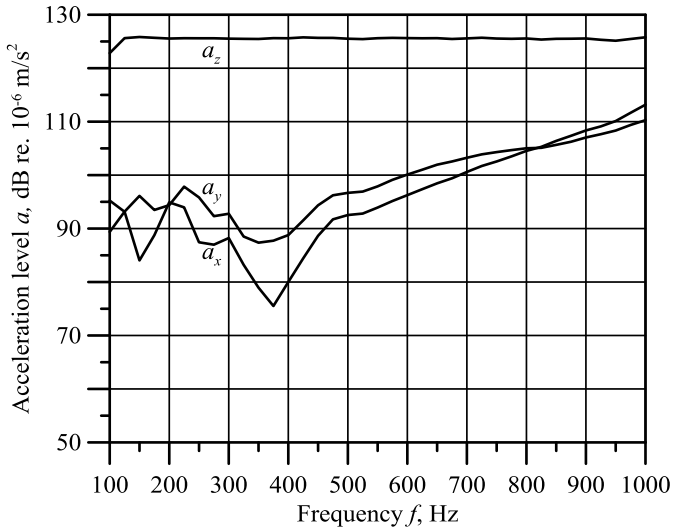

Figure 79 - Acceleration levels a_x a_y a_z measured during the experimental tests on the excitation mass: the acceleration levels a_z have been used as input acceleration in the numerical simulations.

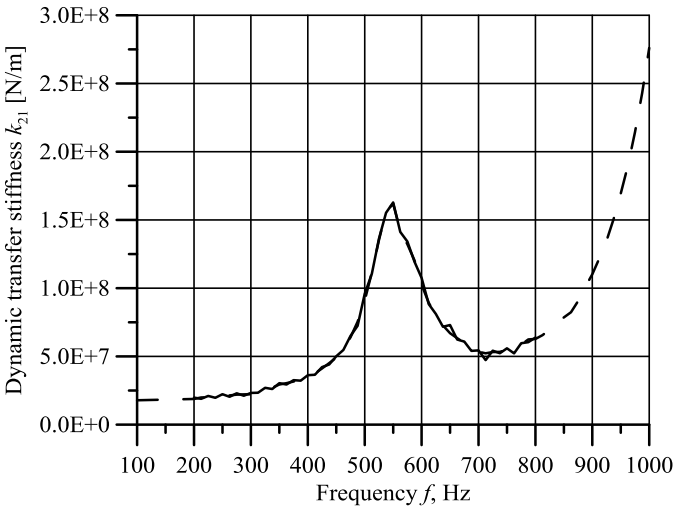

Figure 80 - Measured (dashed curve) and simulated (continuous curve) dynamic transfer stiffness

22. Simulation of the dynamics of the diesel engine foundation

To validate the discussed method for setting and updating FE simulations of diesel engine foundation (see Chapter 16), a case study has been carried out. The subject of such case study is a typical foundation of a medium speed diesel engine of a genset installed on board cruise ships or RoPax ferries. The study is addressed to define a numerical FE model for the prediction of the mechanical mobility of foundations [67] [74].

Four different FE models have been generated to simulate the dynamics of the diesel engine foundation. In Table 4 the main characteristics of the generated FE models are described. Such models differ in extensions, constraints and mesh fineness. The foundation cell has been shown in Figure 12. In Figure 81 half foundation, made of one bed plate and their supports, is shown and in Figure 82 the FE model of the foundation and the whole double bottom is presented.

Table 4 - FE models used in the updating process

FE model	Description	Mesh size [mm]	Condensation [yes/no]
Level -1	Foundation cell (the portion between two consecutive transverse supports)	20x20	no
Level 0	Half Foundation (one bed plate and their supports)	20x20	no
Level 1	Foundation & the underlying hull double bottom	≤250x250	no
Level 2	Foundation & the whole hull double bottom extended over the engine room	≤250x250	yes

Figure 81 - Half foundation (FE model level 0)

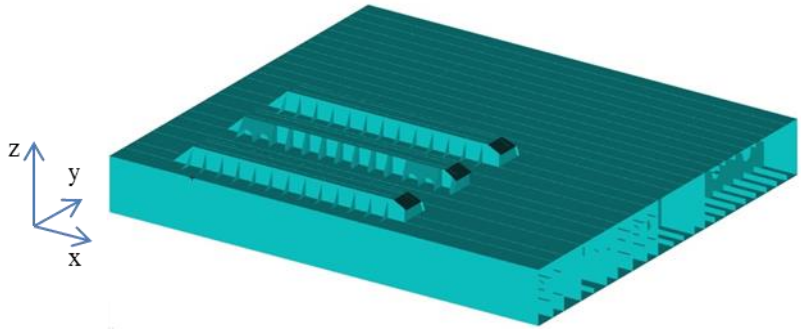

Figure 82 - Foundation & the whole hull double bottom extended over the engine room

First of all, a series of analyses has been carried out to investigate the dependence of the outcomes on the type of FE element [75]. Two FE models have been created, one made of brick elements, the other one made of shell elements. Both the models represent a singular cell of the foundation, *i.e.* the portion between two consecutive transverse supports. All the nodes at the base of the cells have been constrained in all the 6 degrees of freedom ($u_x = 0$, $u_y = 0$, $u_z = 0$, $u_\alpha = 0$ $u_\beta = 0$ $u_\gamma = 0$) in order to simulate high stiffness of the double bottom. All the other sides of the cell have been constrained with symmetric restraints that allow symmetric displacement condition. This means that the displacement vector

component perpendicular to the plane of symmetry is zero and the rotational vector components parallel to that plane are zero. In the case of the upper horizontal plate of the foundation cell, the following boundary conditions have been set: $u_x = 0$, u_y = free, u_z = free, u_α= free u_β= 0 u_γ= 0 . The mesh size is 3 mm and has been chosen to simulate the dynamics of the foundation till about 1000 Hz.

In the following Figures (from Figure 83 till Figure 90), the first four natural modes of the foundation cell are shown as result from the analyses carried out using the two different FE models. The images show the correspondence of the modes and the little discrepancy in the calculated natural frequencies (as also reported in Table 5).

A frequency response analysis has been carried out to compare the dynamic response of the foundation cell modelled using shell elements, with that one of the foundation cell that has been modelled using brick elements. Frequency response analyses have been carried out selecting some relevant points on the upper plate of the foundation cell and applying a unit-amplitude, frequency dependent force in each one of the selected points. The results of the analysis are shown in Figure 91. The outcomes, expressed in terms of driving point mobility, are the velocity calculated in a relevant point in the vertical direction *z* and due to a unit-amplitude force applied in the same point. The results show the equivalence of the two models since, in the frequency range of interest, the two mobility curves have the same trend. Figure 92 shows the results of the frequency response analyses in the transversal direction *y*. The results are expressed in terms of driving point mobility that is the point velocity in the *y* direction due to a unit-amplitude force applied in the same point and in the same direction. Once again the results show the equivalence of the two models. The comparison of the results has been carried out in several points to ensure the equivalence, in the frequency range of interest, of the dynamic response of the two models.

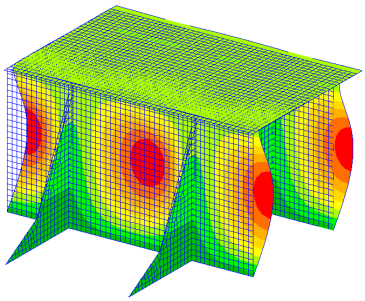

Figure 83 – Normal mode shape at 311 Hz

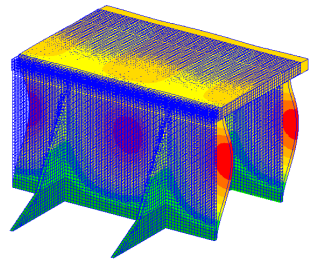

Figure 84 – Normal mode shape at 313 Hz

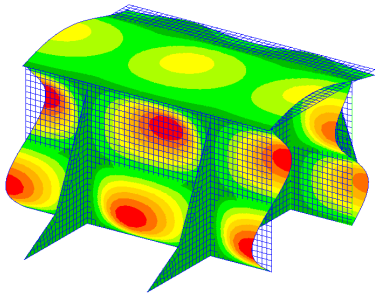

Figure 85 – Normal mode shape at 645 Hz

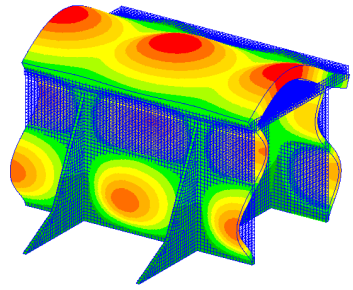

Figure 86 – Normal mode shape at 664 Hz

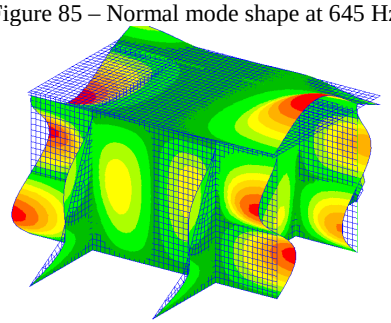

Figure 87 – Normal mode shape at 680 Hz

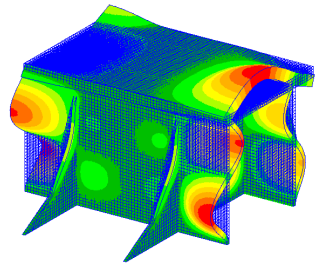

Figure 88 – Normal mode shape at 704 Hz

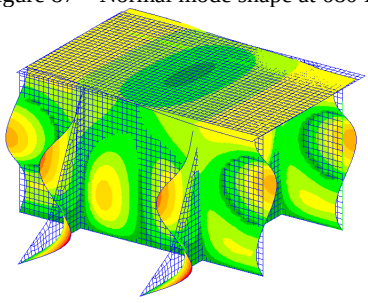

Figure 89 – Normal mode shape at 776 Hz

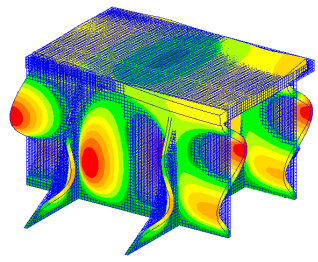

Figure 90 – Normal mode shape at 820 Hz

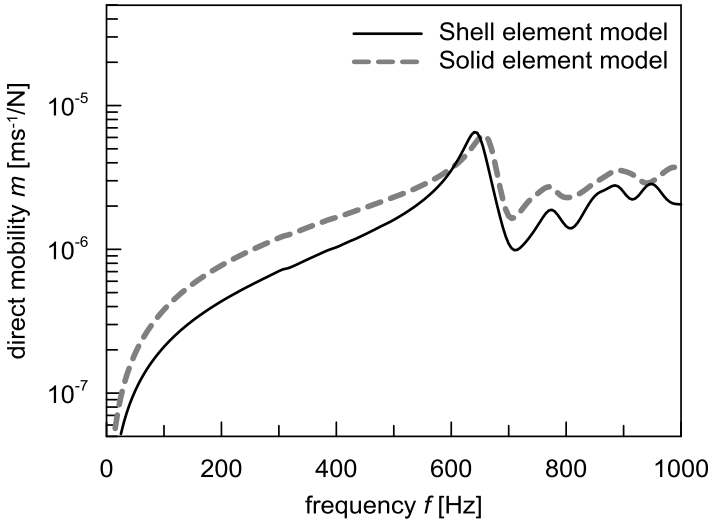

Figure 91 - FRF in the vertical direction

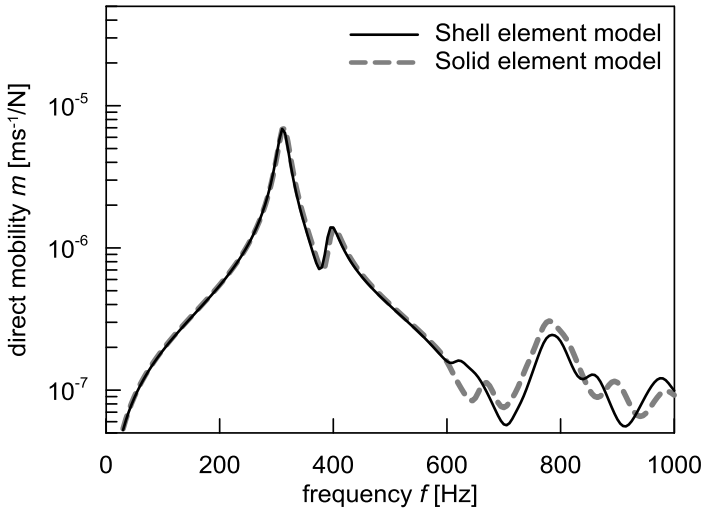

Figure 92 - FRF of resilient mount in transversal direction

Table 5 - Comparison between the first normal modes of the FE models of foundation cell; one is made of shell elements, the other one of brick elements.

Modes	Shell Elements Frequency [Hz]	Brick Elements Frequency [Hz]	Difference %
1	311	313	0.64
2	645	664	2.86
3	680	704	3.4
4	776	820	5.37

Then a series of frequency response analyses has been carried out to simulate the dynamic response of the diesel engine foundation. The driving point mobility of the foundation has been simulated in the *y* and *z* directions and the results achieved by the different FE models have been compared with the measured driving point mobility according to the procedure presented in Chapter 16 [67].

In Figure 93 the direct mobility curves in the frequency range of interest (up to 1 kHz), based on both calculated and measured values, relevant to the transverse vibration are shown for a significant spot (measurement point 3Y), located on the upper surface of the bed plate at the connection with a transverse stiffeners. A first analysis on the matching among calculated and experimental data has be done by visual inspection and by measuring the shift of first correlated natural frequencies (correlation if $\delta f \leq 10\%$). Then the MAC criterion has been applied to correlate mode shapes of FE models (correlation if MAC ≥ 0.8), a not easy task because, having the FE models different extension, their number of modes is different. Then, a deeper analysis has been performed by using the LAC criterion to correlate numerical and experimental direct mobility field (correlation if LAC ≥ 0.8). As an example, in Figure 94 it is shown the LAC calculated for the Level 1 FE model on the same measurement spot: it gives the measure of the frequency range within the FE model can accurately simulate the real structure behaviour. In Figure 95 the direct mobility curves relevant to the vertical vibration are shown for the same significant spot 3, but relevant to the vertical vibration. In Figure 96 the LAC calculated for the Level 1 FE model is shown.

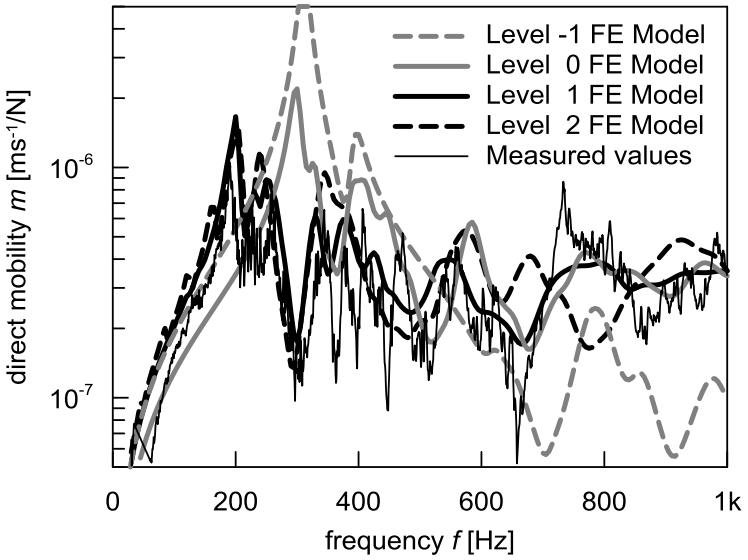

Figure 93 - Mobility curves, measurement point 3Y.

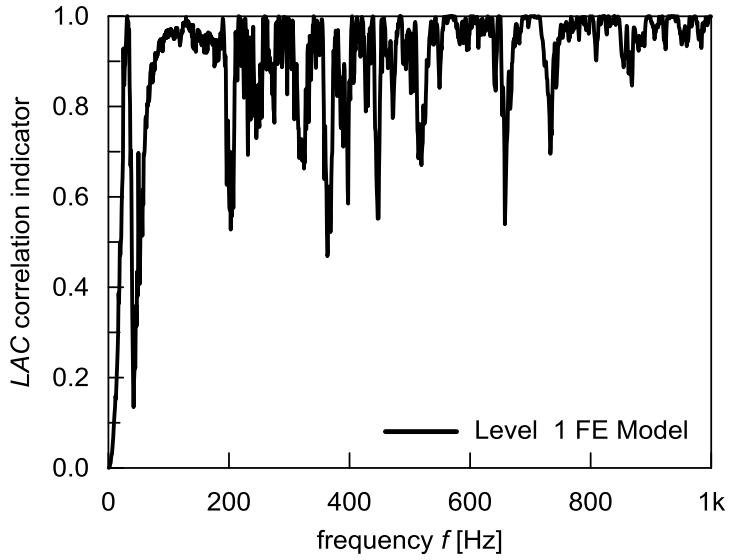

Figure 94 - LAC correlation indicator, measurement point 3Y, Level 1 FE model.

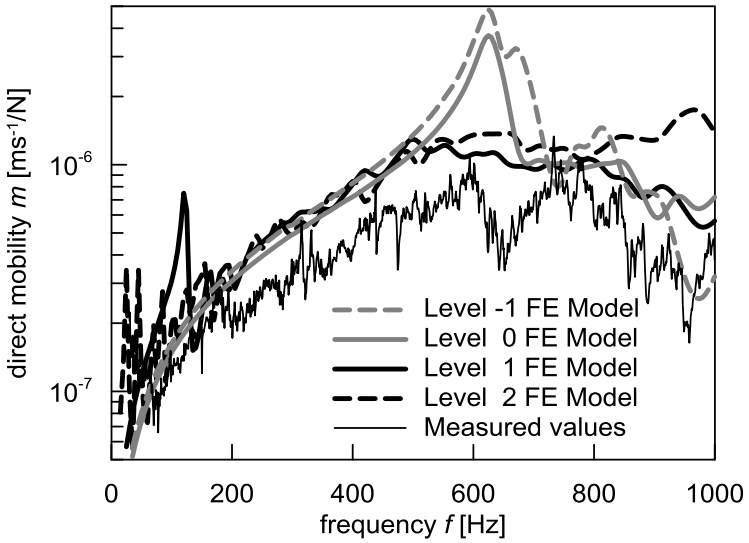

Figure 95 - Mobility curves, measurement point 3Z.

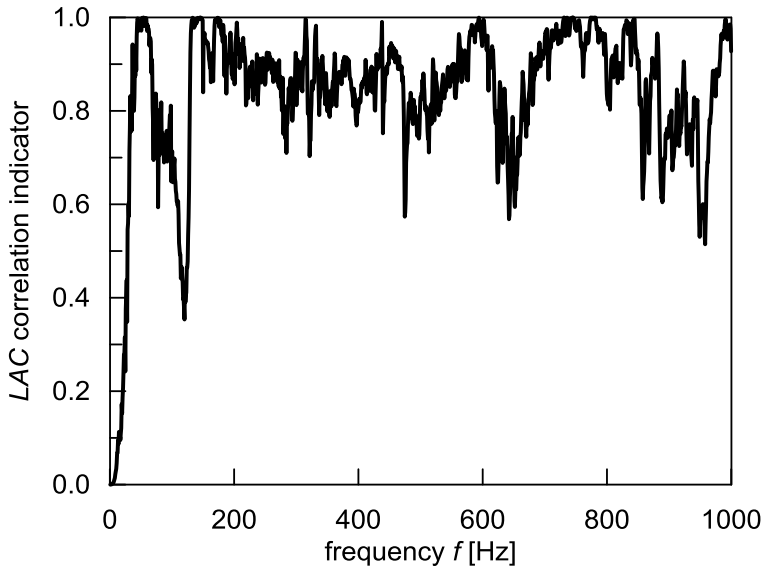

Figure 96 - LAC correlation indicator, measurement point 3Z, Level 1 FE model.

23. Structure-borne noise prediction according to the single-point method

In the previous Chapter, the dynamic characterization of the diesel engine foundation and of the resilient mount has been carried out by experimental tests. Moreover, numerical models have been set up to carry out the simulation of the dynamics of the two components. Equation (43) shows that the velocity level of the diesel engine foundation v_r can be calculated once the velocity levels of the source v_s is known along with the mechanical impedance of the diesel engine foundation Y_r and the mechanical impedance of the resilient mount Z_{21}.

Equation (43) can be rewritten in a more practical form as follows:

$$L_{v,r} = L_{v,s} + L_{Z_{21}} + L_{Y_r} \qquad (90)$$

where foundation velocity level $L_{v,r}$ is evaluated by summing up source velocity level $L_{v,s}$, resilient mounting mechanical impedance level L_{Z21} and foundation mobility level L_{Yr}.

The tests and the numerical simulations allowed the author to achieve the main terms of the Equation (43), *i.e.* the mechanical mobility of the diesel engine foundation Y_r and the mechanical impedance of the resilient mount Z_{21}.

In the following, the theory of the single-point approach has been applied to a case study. The structure-borne noise levels on the bed plate of the foundation of a diesel engine have been predicted by applying the previously discussed practical method which considers the engine-isolators-foundation system as a series of 2-DOF systems. Results of simulations have then been compared with the structure-borne noise levels measured on board the ship [76]. All the results are expressed in terms of levels, in order to directly apply the Equation (90).

The study has been performed on a medium speed diesel engine of a genset installed on board a large cruise ship. In the genset, the two machineries (diesel engine and electric generator) are mounted on a common baseframe. This configuration is typical on board modern cruise ships, where gensets supply electric power to the electric propulsion motors and to all on-board services while diesel engine delivers the maximum continuous rating (MCR).

The measurement campaign has been performed when the diesel engine was running on board the ship during the sea trials performed by the shipyard before the delivery of the ship. Accelerations have been recorded at the six resilient mountings located at both ends and in the middle of the engine block; detection points where established on the engine feet and on the bed plate, close to each resilient element top and base respectively; detection points were the same while engine was running in the test room and on board the ship. Foundation direct mobility has been assessed in the same points before installing the diesel engine.

Among all the measured data, the only results presented in this thesis are for the vibration transmission path taking place along the resilient mounting located at the forward end (non-drive end) of the starboard bed plate (position 1-STB). The calculated structure-borne noise has been obtained by applying a 2-DOF model to the engine-isolator-foundation system whose dynamic input parameters are (*i*) the source velocity levels V_s and (*ii*) the foundation mobility Y_r measured close to the resilient element at position 1-STB, on the engine feet and the base plate respectively, and (*iii*) the isolator mechanical impedance Z_{21} derived from the vertical dynamic transfer stiffness measured in the laboratory tests.

In Figure 97 the source velocity level $L_{V,s}$ [dB ref. 10^{-9} m/s] measured on board the ship is shown. In Figure 98 the foundation mobility level $L_{Y,r}$ [dB ref. 1 (m/s)/N] is shown as obtained by measurements on two points within the contact area of the 1-STB resilient element base, precisely on the bed plate upper surface (*i*) between two consecutive supporting stiffeners (*i.e.* in the cell center) and (*ii*) in correspondence of a stiffener. In Figure 99 the resilient mounting dynamic transmissibility level L_T [dB ref. 1 kg] is given as obtained by the measurement of the dynamic transfer stiffness in the vertical direction $k_{2,1}$; the resilient mounting impedance level L_{Z21} is derived by applying Equation (72). In Figure 100 the

three dynamic parameters $L_{V,s}$, $L_{Z,i}$ and $L_{Y,r}$ of the 2-DOF system simulating the engine-resilient-foundation interaction are represented, which summed up, as shown in Equation (90), give the predicted value of the structure-borne noise level $L_{V,r}$. Figure 101 shows a comparison among the predicted and the measured structure-borne noise levels. In Figure 102 the receiver to source velocity ratio is reported in terms of level difference ($L_{V,r} - L_{V,s}$), which measures the coupled effect of resilient mounting bed and foundation. Curves refer to the two cases analyzed (measured on board and predicted).

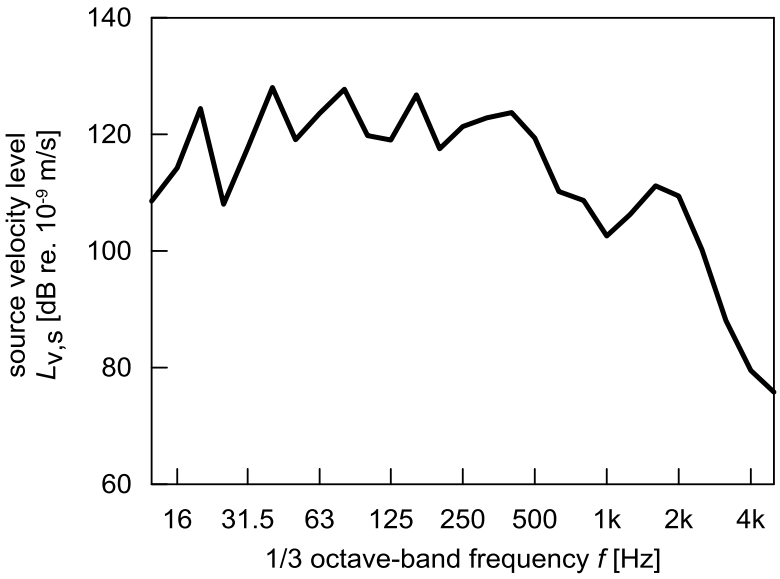

Figure 97 – Source velocity level

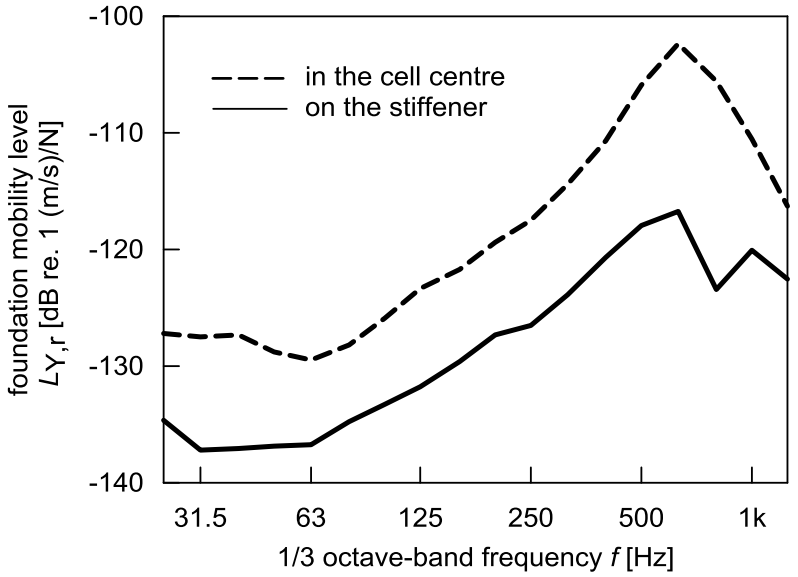

Figure 98 - Foundation mobility levels

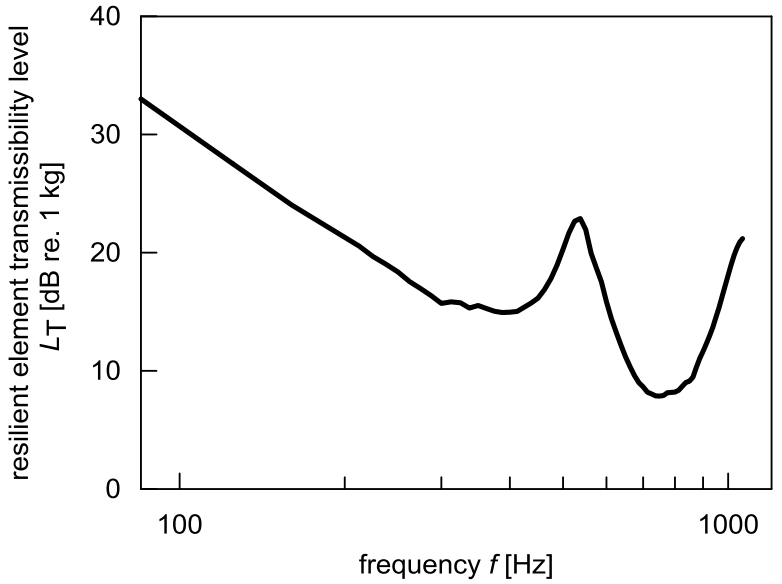

Figure 99 - Resilient mount transmissibility levels

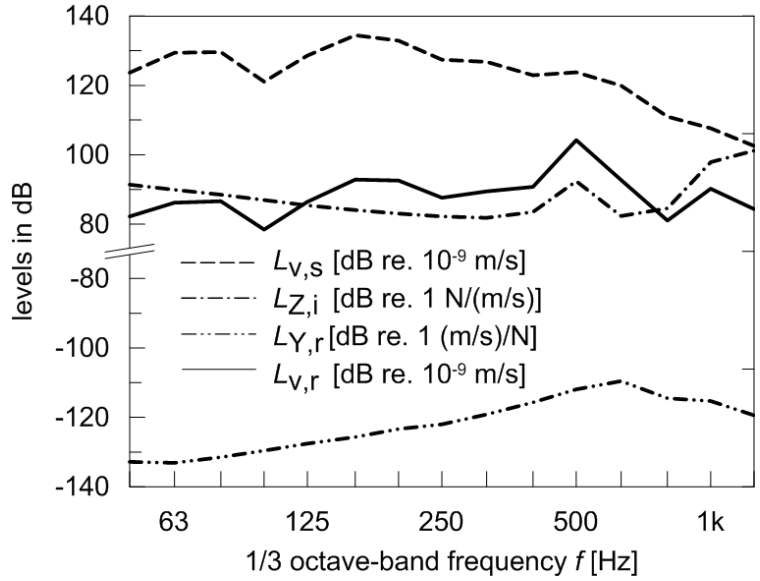

Figure 100 - Source velocity levels $L_{v,s}$, Resilient mount impedance levels L_{Z21}, Foundation mobility levels $L_{Y,r}$, Velocity levels of the foundation $L_{v,r}$

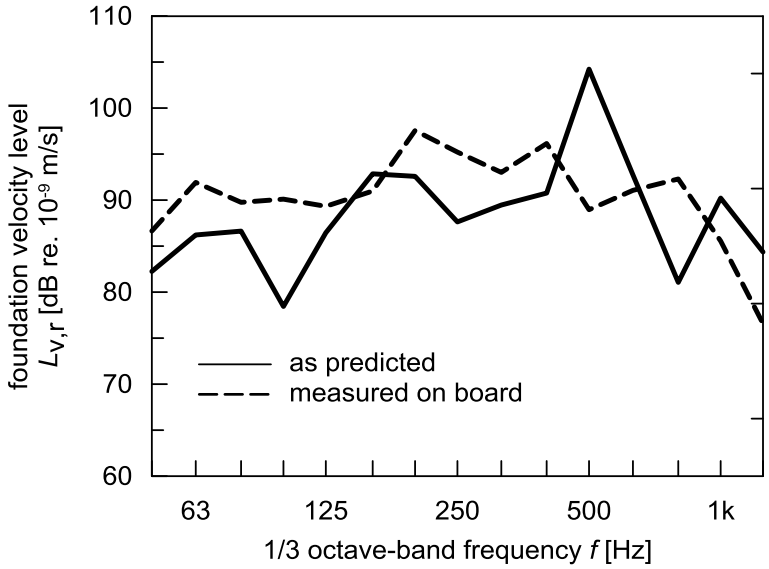

Figure 101 - Comparison of the predicted levels with the measured levels of the structure-borne noise

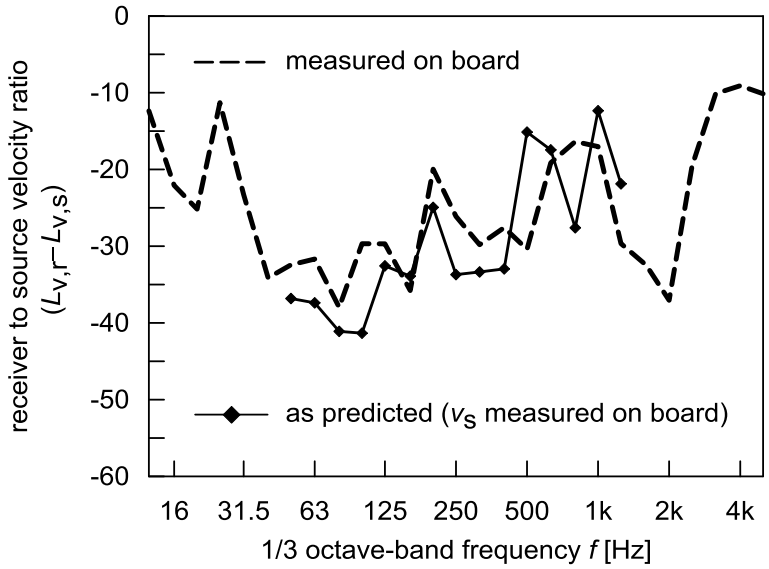

Figure 102 - Receiver to source velociy ratio

Data reported in the previous figures, from Figure 97 till Figure 102, summarize the results of measurement campaigns carried out in laboratory ($k_{2,1}$), in the shipyard (Y_r) and on board the ship during navigation (V_s and V_r). The measured structure-borne noise levels have been compared with the predicted ones in Figure 101.

In Figure 100, the different curves show the influence of the three dynamic parameters $L_{V,s}$, $L_{Z,i}$ and $L_{Y,r}$ of the 2-DOF system, to the predicted value of the structure borne noise level $L_{V,r}$. In particular, it is worth pointing out the influence of the dynamic impedance of the resilient mount on the structure-borne noise: the higher transmissibility of the resilient mount in correspondence of its inner resonance at about 500 Hz, leads to an increase of predicted the structure-borne noise in the same frequency band. On the other hand, the increase of the mobility levels of the diesel engine foundation has a secondary effect on the structure borne noise predicted.

The comparison of the structure-borne noise levels predicted with those ones measured on board ships shows that, even if the overall noise level is predicted quite well, some discrepancies are present at each frequency band. In the low frequency range the structure-borne noise levels predicted is lower than the measured ones, while at 500 Hz, in correspondence of the resonance of the resilient mount, the predicted structure-borne noise is characterized by a peak that is higher in magnitude and is shifted at higher frequency respect to that one shown in the measured structure-borne noise.

The discrepancy between the measured data and the predicted ones is due to several reasons. The different test conditions of the single parts of the system inevitably lead to a grade of inaccuracy which is difficult to quantify and which should be subject of further investigations.

With regards to the mobility levels of the diesel engine foundations $L_{Y,r}$, it should be noted that all the measured data have been acquired when the ship was under construction, the structures were placed in a dry dock and not yet completed nor joined to the ship's hull. The data for the assessment of the structure-borne noise have been acquired during sea trials, so the boundary conditions of ship structures were different. The numerical models for studying the dynamics of diesel engine foundations simulate the condition of the ship under construction. Further analyses should be carried out to deeper understand how the boundary conditions, e.g. sea water, affect the dynamics of diesel engine foundations. Moreover, the foundation mobility under a resilient element cannot be correlated to a single point as the contact between isolator and foundation extends over the small areas around each joining bolt. These areas can be close or not to a vertical support of the bed plate, and direct mobility can differ of 10 dB or more moving from one point to another, as shown in Figure 98. An average value of the direct mobility measured at the different points of the resilient element base should be used.

A factor which affects the chain of calculation of the receiver velocity level is the actual value of the load acting on the resilient mounting. Indeed, the resilient mounting dynamic transmissibility is almost non-linear with respect to both the static and the dynamic load. The values of the resonance frequencies depend on the static loads applied to the resilient element. Variations of the dynamic load

cause variations in the response vibration levels (i.e., an up-down translation of the L_T curve). On board ships, the medium speed marine diesel engines are suspended by several resilient mounts (about 30 for medium speed marine diesel engines of 19000 kW). The nominal static load applied to each resilient mount is 75 kN, that is the design static load that was applied to the resilient mount when it has been tested in the laboratory. Nevertheless, the actual static load applied to the resilient mounts, when they are installed under the diesel engines, may be different because of the unavoidable inaccuracy of the planarity of the upper plate of the foundation. This leads to a different dynamic response of the resilient mount. The dependence of $k_{2,1}$ from the static load can be managed by carrying out a set of laboratory tests at different preloads and then selecting the proper $k_{2,1}$ curve according to the actual load, that can be simply derived by measuring the static deflection of the resilient below the engine.

The underestimation of structure-borne noise levels can be also due to the use of the single-point approach. Implementing a procedure to apply the multi-point approach that takes into account the mutual interaction of the resilient mounts and the effective mobility of the diesel engine foundation (see Chapter 5) could improve the quality of the results, but this leads to some practical problems to be addressed. First of all, the actual static load of each resilient mount installed under the diesel engine has to be known. Then the forces transmitted by each resilient mount should be measured along with their phases. That measurement implies some practical problems due to the high number of measurement points and to the wide frequency range of the signals. Indeed, in the high frequency range, the background noise that always affects the measured data acquired in the engine room decreases the coherence of the transfer functions and of the phases between the signals.

Conclusions and future research

The main objective of the research activity that has been presented in this work is to define a practical procedure to be applied in the design phase of a ship in order to predict the structure-borne noise due to marine diesel engines. That procedure is based on the so-called single-point approach. The motivation of this study comes from the consideration that the prediction methods that nowadays are used in actual design processes are generally based on a large amount of empiricism and are not always sufficiently accurate.

According to the single-point approach, to predict the structure-borne noise due to the marine diesel engine, the dynamic transfer stiffness of the resilient mount the mechanical mobility of the diesel engine foundation must be known, along with the velocity levels of the source. In the research activity, special attention has been paid to the study of the dynamics of the resilient mount.

The work has been developed in several phases:

1. experimental tests for the dynamic characterization of resilient mounts;
2. numerical simulation of the dynamic transfer stiffness of resilient mounts;
3. on-board measurement and numerical simulation of the driving point mechanical mobility of diesel engine foundation;
4. prediction of the structure-borne noise according to the single-point approach.

Before developing the first phase of the work, a new test rig, which has been built at the Ship Noise and Vibration Laboratory of the University of Trieste, has been tuned and tested to verify its effectiveness in performing the experimental tests for the dynamic characterization of the isolators. The followed procedure has been presented in Chapter 0 and the outcomes of the experimental tests show the accuracy of the measures once the test rig has been properly set up.

The results of the experimental tests for the measurement of the dynamic transfer stiffness have been presented in Chapter 18. The experiments allowed identifying the frequency range in which standing waves appear inside the rubber core of the resilient mount, increasing the dynamic transfer stiffness of the isolator.

Then, two different configurations of the resilient mount have been studied, by applying or removing the fixture on the top casting that is commonly used to adjust, in height, the alignment of the suspended marine diesel engine. The results of these tests are shown in Chapter 19. The attention has been focused on the high levels of unwanted input vibrations measured at the excitation mass when the resilient mount was under test. The results of the ODS tests and of the numerical simulations have shown that those high levels of unwanted vibrations were due to a coupling between the resilient mount top casting and the excitation mass. The mechanism by which a dynamic coupling takes place between the resilient mounting and the upper mass has been deeply studied. According to the prescription for the accuracy of the laboratory tests, presented in the Standards, the outcomes obtained by the experimental tests in that frequency range should not be taken into account. Nevertheless, in this case the analyses carried out to understand the reasons of such high levels of unwanted vibrations on the excitation mass lead to understand that they were generated by the coupling of the top casting of the resilient mount with the excitation mass. The outcomes of the numerical simulations confirmed that behaviour. The main practical implication of those results is the necessity to define new standards to properly simulate, in laboratory tests, the real coupling between resilient mount and engine frame.

Then, a procedure has been defined to simulate the dynamics of the resilient mount. First of all, some runs have been carried out to achieve the Yeoh coefficients that describe the non-linear elastic behaviour of the rubber. A force-deflection curve has been used as reference to compare the outcomes of the numerical simulation and to update the FE model characteristics. Once the three coefficients have been defined a dynamic analysis has been performed to simulate the dynamic behaviour of the resilient mount in terms of dynamic transfer stiffness. The defined model simulates the non-linear behaviour of the rubber and takes into account the contact between the rubber core of the isolator and the resilient mount top and base casting. Even if such numerical model can be

properly tuned once the outcomes of experimental tests are available, it is useful to investigate an improvement of the dynamic response of the studied resilient mount and to compare different solutions obtained by an optimization procedure. The limitations of such model are due to the high computational cost to solve the simulation at each frequency step. Moreover, the outcomes of the FE analyses have to be post-processed in order to calculate the dynamic transfer stiffness and this increases the overall time spent to perform the analysis. For these reasons, the presented procedure for the numerical simulation of the resilient mount could encounter difficulties in practical applications and in its usage in the design phases. In the high frequency range, as the displacements are very small, another way to simulate the dynamics of the resilient mount could be that one proposed by Beijers [30] which has been tested only in the case of a cylindrical resilient mount and should be tested in the case of a conical one.

With regards to the simulations of the mechanical mobility of the diesel engine foundation, the following consideration can be stated. The analyses have been carried out using several models that differ in extensions, constraints and mesh fineness. The results of the analyses show that the models that do not take into account the double bottom are too stiff, and this is due to the boundary conditions. Moreover, the results of the analyses carried out on the models that take into account the dynamics of the double bottom, show that the mechanical mobility of the foundation depends on the dynamics of the double bottom. The comparison between the outcomes of the simulations of these models show that taking into account the whole double bottom of the engine room, does not improve significantly the quality of the outcomes of the analyses. Furthermore, that model increases considerably the computational cost in solving the analysis and a reduction technique should be used. Further analyses are required to improve the quality of the results. A wider usage of the correlation indexes, generally used in the dynamic analyses of structures, could improve the correlation of the numerical results with the experimental data. The quality of the numerical models could be also improved updating the physical characteristics of the model. This can be performed using the outcomes of an experimental modal analysis of the foundation. Moreover, the influence of the boundary condition of the ship structure on the dynamic response of the foundation should be deeper investigated. The experimental measurements of the mechanical mobility

foundation are carried out when the ship is under construction and so the structures are supported in the dry dock by the bilge blocks and when the ship is operating, the dynamics of the structures is affected by the surrounding water. Also the weight of auxiliaries systems and plants that are installed on board, in the engine room, can affect the dynamics of the structures and when the measurement campaign is carried out, they are usually not yet installed.

The results of the prediction of the structure-borne noise due to the marine diesel borne noise levels predicted and measured on the foundation may be quite good, even if not yet satisfactory for the purpose of comfort design.

In Figure 103, a flowchart shows the proposed procedure to predict the structure-borne noise according to the single-point approach. On the left hand side of the Figure, the experimental tests needed to update the numerical models and to apply the procedure are shown. On the right hand side of the Figure, the numerical models that are to be created to simulate the dynamics of the resilient mount and of the diesel engine foundations are presented. Once the structure-borne noise levels $L_{v,r}$ have been obtained in the audio-frequency range, they are compared with the required structure-borne noise levels $L_{v,r(lim)}$. If the former are higher than the required structure-borne noise levels, an improvement of the resilient mounts and of the diesel engine foundation can be performed and verified using the existing numerical models. The procedure ends once the calculated structure-borne noise levels do not succeed the required structure-borne noise levels.

The sources of uncertainty are related to the method itself, based on a series of independent measurements of data which are treated as uncoupled, and to the model used to describe the vibration path from source to receiver. This implies that two lines of investigation should be undertaken. The first is to enhance the model describing the vibration path from engine to ship structure, possibly by taking into consideration a certain level of coupling between the resilient mountings. The second is to reduce the uncertainties in the measurement campaigns, by investigating on the effects of the assumed hypotheses, by performing a sensitivity analysis on the parameters which affect the data obtained

in any measurement stage, and by deeply analysing the foundation dynamics through coupled experimental and numerical methods.

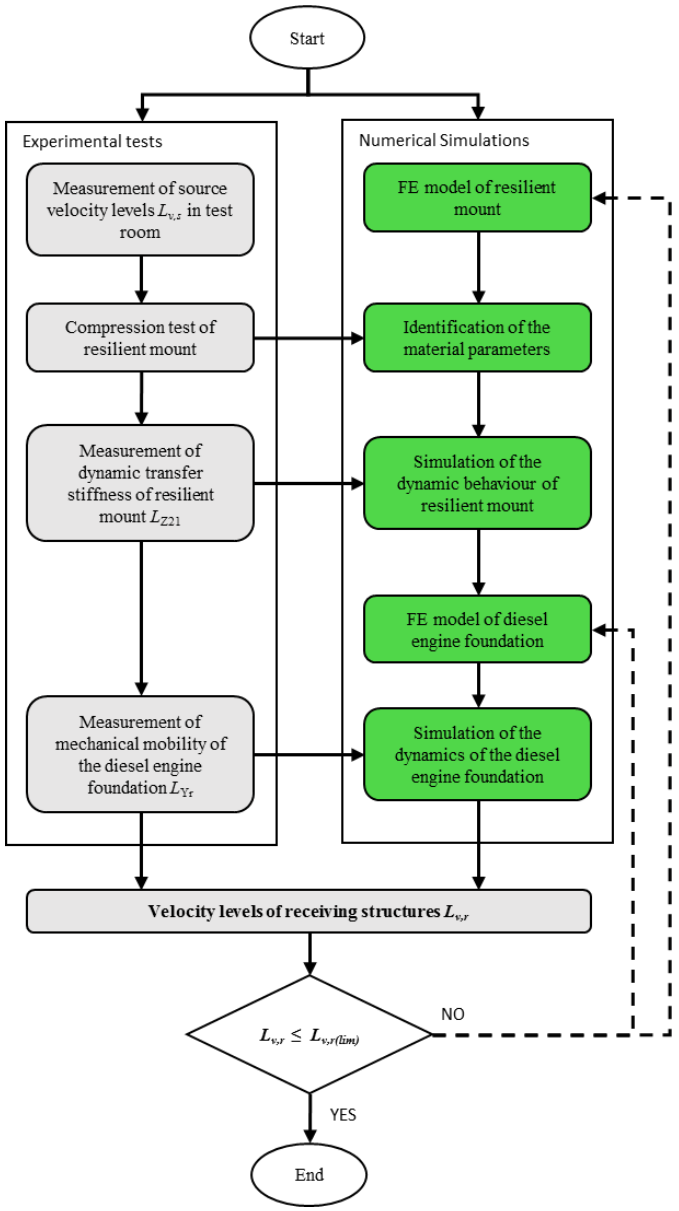

Figure 103 - Procedure for the prediction of the structure-borne noise generated by resiliently mounted diesel engines, according to the single-point approach

Performing an experimental campaign that takes into account the coupling between the resilient mountings implies a series of practical problems. Indeed, the coupling of the mounts can be studied measuring the forces transmitted through each resilient mount in terms of amplitude and relative phases. This implies the usage of very sophisticated load cells that should withstand the high static load and, at the same time, that measure the dynamic forces which, in the high frequency range, are usually quite small. Furthermore, from a practical point of view, the measurement of the signal phases is affected, in the high frequency range, by high levels of background noise that decrease the coherence between the measured signals.

Once a procedure that take into account the coupling between the resilient mounts could be practically applied to the case of a medium speed diesel engines, resilient mountings and foundation impedance could be properly designed in order to come to the desired level of the structure-borne noise on board ships.

This research activity has led to some results which have practical implication and can be useful to researchers and designers. The attention has been focused particularly on the study of the dynamic response of resilient mounts. The outlined procedure to tune the test rig can be easily applied to other test rigs for the dynamic characterization of isolators in the audio frequency range. The experimental study performed to characterize a resilient mount highlights that special attention should be paid to the coupling between the resilient mount top casting and the excitation mass in order to do not affect the outcomes of the experiments. The procedure to simulate the dynamics of resilient mounts can be used to verify the effectiveness of improved solutions of the isolator under investigation. Indeed, the numerical model can be used to identify some improved solutions that can then be tested in laboratory to verify the effectiveness of the improved isolator. This avoids performing a large number of experimental tests selecting, in the design phase of an isolator, the best solutions to test. The numerical procedure presented to study the mechanical mobility of engine foundations gives some useful indication to define a proper numerical model. Finally, the application to a case study of the procedure to predict the structure-borne noise according to the single-point approach, gives some useful information to better understand pros and cons of such simplified approach.

Bibliography

[1] R. A. Fulford e B. M. Gibbs, «Structure-borne sound power and source characterization in multi-point-connected systems, Part 1: Case studies for assumed force distributions,» *Journal of Sound and Vibration,* vol. 204, n. 4, pp. 659-677, 1997.

[2] J. W. Verheij, *Multi-path sound transfer from resiliently mounted shipboard machinery,* Delft: Technisch Physische Dienst TNO-TH, PhD Thesis, 1982.

[3] L. Cremer, M. Heckl e B. A. T. Petersson, Structure-Borne Sound, Structural Vibrations and Sound Radiation, Berlin: Springer, 2005.

[4] F. Fahy, Foundations of Engineering Acoustics, London: Academic Press, 2001.

[5] C. W. de Silva, Vibration, Fundamentals and Practice, New York: Taylor & Francis Group, 2007.

[6] R. W. Fischer, C. B. Burroughs e L. D. Nelson, Design Guide for Shipboard Airborne Noise Control, New York: SNAME, 1983.

[7] R. A. Fulford e B. M. Gibbs, «Structure-borne sound power and source characterization in multi-point-connected systems, Part 2: About mobility functions and three velocities,» *Sound and Vibration,* vol. 220, n. 2, pp. 203-224, 1999.

[8] R. A. Fulford e B. M. Gibbs, «Structure-borne sound power and source characterization in multi-point-connected systems, Part 3: Force ratio estimates,» *Journal of Sound and Vibration,* vol. 225, n. 2, pp. 239-282,

1999.

[9] S. Mathiowetz e H. A. Bonhoff, «Interface mobilities for characterization of structure-borne sound sources resiliently mounted via multiple contact points,» *Journal of Sound and Vibration,* vol. 332, pp. 5789-5803, 2013.

[10] B. A. Petersson, «Approaches for structure-borne sound source characterization,» in *16th International Congress on Sound and Vibration, ICSV 2009*, Krakow, 2009.

[11] M. Ohlirich, «Predicting transmission of structure-borne sound power from machines by including terminal cross-coupling,» *Journal of Sound and Vibration,* vol. 330, n. 21, pp. 5058-5076, 2011.

[12] B. A. Petersson e B. M. Gibbs, «Towards a structure-borne sound source characterization,» *Applied Acoustics,* vol. 61, n. 3, pp. 325-343, 2000.

[13] A. Elliot, *Characterization of Structure-borne sound sources in situ,* Salford: University of Salford, PhD Thesis, 2009.

[14] A. Nilsson e L. Kari, «Resilient Mounting of Engines,» in *International Commission on Acoustics, ICA*, Seattle, 1998.

[15] J. D. Dickens, «Dynamic model of vibration isolator under static load,» *Journal of Sound and Vibration,* vol. 236, n. 2, pp. 323-337, 2000.

[16] L. Kari, «The audible stiffness of preloaded vibration isolators,» in *6th International Conference on Sound and Vibration*, Copenhagen, 1999.

[17] L. Kari, «On the waveguide modelling of dynamic stiffness of cylindrical vibration isolators. Part I: the model, solution and experimental comparison,» *Journal of Sound and Vibration,* vol. 244, n. 2, pp. 211-233, 2001.

[18] C. A. J. Beijers, *A modelling approach to hybrid isolation of Structure-*

Borne Sound, Enschede: University of Twente, PhD Thesis, 2005.

[19] B. Petersson e J. Plunt, «On effective mobilities in the prediction of structure-borne sound transmission between a source structure and a receiving structure, Part 1: Theoretical background and basic experimental studies,» *Journal of Sound and Vibration,* vol. 82, n. 4, pp. 517-529, 1981.

[20] B. Petersson e J. Plunt, «On effective mobilities in the prediction of structure-borne sound transmission between a source structure and a receiving structure, Part 2: Procedures for the estimation of mobilities,» *Journal of Sound and Vibration,* vol. 82, n. 4, pp. 531-540, 1982.

[21] T. R. Lin, J. Pan, P. J. O'Shea e C. K. Mechefske, «A study of vibration and vibration control of ship structures,» *Marine Structures,* vol. 22, n. 4, pp. 730-743, 2009.

[22] D. J. Ewins, Modal Testing: Theory, Practice and Application, Baldock: Research Studies Press LTD, 2000.

[23] J. D. Dickens e C. J. Norwood, «Universal method to measure dynamic performance of vibration isolatores under static load,» *Journal of Sound and Vibration,* vol. 244, n. 4, pp. 685-696, 2001.

[24] T. Ten Wolde, J. W. Verheij e H. F. Steenhoek, «Reciprocity method for the measurement of mechano-acoustical transfer functions.,» *Journal of Sound and Vibration,* vol. 42, n. 1, pp. 49-55, 1975.

[25] L. Kari, «Dynamic transfer stiffness measurements of vibration isolators in audible frequency range,» *Noise Control Engineering Journal,* vol. 49, n. 2, pp. 88-102, 2001.

[26] M. Sjöberg e L. Kari, «Nonlinear isolator dynamics at finite deformations: an effective hyperelastic, fractional derivative, generalized friction model,» *Nonlinear Dynamics,* vol. 33, n. 3, pp. 323-336, 2003.

[27] M. Sjöberg, *On Dynamic Properties of Rubber Isolators*, Stockholm, Sweden : KTH, Dept. of Mechanical Engineerign, The Marcus Wallenberg Laboratory (PhD Thesis), 2002.

[28] J. D. Dickens e C. J. Norwood, «Design of a test facility for vibration isolator characterization,» *Acoustics Australia*, vol. 25, n. 1, pp. 23-28, 1997.

[29] C. A. J. Beijers, B. Noordman e A. de Boer, «Numerical modelling of rubber isolators: identification of material parameters,» in *11th International Congresso on Sound and Vibration ICSV 2004*, St. Petersburg, Russia, 2004.

[30] C. A. Beijers e A. de Boer, «Numerical modelling of rubber isolators,» in *10th International Congress on Sound and Vibration ICSV 2003*, Stockholm, Sweden, 2003.

[31] R. A. Ibrahim, «Recent advances in nonlinear passive vibration isolators,» *Journal of Sound and Vibration*, vol. 314, n. 1, pp. 371-452, 2008.

[32] E. Rizzuto, «Viscoelastic materials for noise reduction on board,» in *9th International Congress of the Maritime Association of the Mediterranean (IMAM)*, Ischia, Italy, 2000.

[33] E. Rizzuto e A. Ferrari, «Characterization of anti-noise treatments for cabin floors,» in *International Maritime Research and Transportation (ICMRT)*, Ischia, Italy, 2005.

[34] M. Biot, D. Boote, E. Brocco, A. Clericuzio, L. Moro, P. N. Mendoza Vassallo e T. Pais, «Cutting off deck vibration with floating floors: problem definition and solution strategy,» in *6th Congresso Sea-MED, Sicurezza e Innovazione nella Nautica*, Messina, Italy, 2014.

[35] C. Höller, Indirect methods of obtaining activity and mobility of structure-borne sound sources, Liverpool: University of Liverpool, (PhD Thesis), 2013.

[36] F. Fahy e J. Walker, Advanced applications in acoustics, noise and vibration, London: CRC Press, 2004.

[37] ISO 9611:1996 Acoustics - Characterization of sources of structure-borne sound with respect to sound radiation from connected structures - Measurement of velocity at the contact points of machinery when resiliently mounted, Geneve.

[38] C. T. Molloy, «Use fo four-pole parameters in vibration calculations,» *The Journal of the Acoustical Society of America,* vol. 41, n. 5, pp. 1171-1179, 1967.

[39] J. C. Snowdon, «Mechanical four-pole parameters and their application,» *Journal of Sound and Vibration,* vol. 15, n. 3, pp. 307-323, 1971.

[40] T. Ten Wolde, Reciprocity experiments on the transmission of sound in ships, Delft: Technical University of Delft, 1973.

[41] ISO 10846-1:2008 Acoustics and vibration - Laboratory measurement of vibro-acoustic transfer properties of resilient elements - Part 1: Principles and guidelines, Geneve.

[42] A. T. Moorhouse, «On the characteristic power of structure-borne sound sources,» *Journal of Sound and Vibration,* vol. 248, n. 3, pp. 441-459, 2001.

[43] J. M. Mondot e B. Petersson, «Characterization of structure-borne noise sources: The source descriptor adn the coupling function,» *Journal of Sound and Vibration,* vol. 28, n. 1, pp. 5-14, 1987.

[44] B. Petersson e B. M. Gibbs, «Use of source descriptor concept in studies of multi-point and multi-directional vibrational sources,» *Journal of Sound and Vibration,* vol. 168, pp. 157-176, 1991.

[45] ISO 10846-2:2008 Acoustics and vibration - Laboratory measurement of vibro-acoustic transfer properties of resilient elements - Part 2: Direct

method for determination of the dynamic stiffness of resilient supports for translatory motion, Geneve.

[46] ISO 10846-3:2002 Acoustics and vibration - Laboratory measurement of vibro-acoustic transfer properties of resilient elements - Part 3: Indirect method for determination of the dynamic stiffness of resilient supports for translatory motion, Geneve.

[47] ISO 10846-4:2003 Acoustics and vibration - Laboratory measurement of vibro-acoustic transfer properties of resilient elements - Part 4: Dynamic stiffness of elements other than resilient supports for translatory motion, Geneve.

[48] ISO 10846-5:2008 Acoustics and vibration - Laboratory measurement of vibro-acoustic transfer properties of resilient elements - Part 5: Driving point method for determination of the low-frequency transfer stiffness of resilient supports for translatory, Geneve.

[49] M. Biot e L. Moro, «Experimental study of resilient mounting,» in *11th International Marine Design Conference, IMDC 2012*, Glasgow, UK, 2012.

[50] P. Hynnä, «Mechanical Mobility Technique,» VTT Techincal Research Centre of Finland, Espoo, 2002.

[51] ISO 7626-1:2011 Mechanical vibration and shock - Experimental determination of mechanical mobility - Part 1: Basic terms and definitions, and transducer specifications, Geneve.

[52] ISO 7626-2:1990 Vibration and shock - Experimental determination of mechanical mobility - Part 2: Measurements using single-point translation excitation with an attached vibration exciter, Geneve.

[53] ISO 7626-5:1994 Vibration and shock - Experimental determination of mechanical mobility - Part 5: Measurements Measurements using impact excitation with an exciter which is not attached to the structure, Geneve.

[54] ISO 2041: 2009 Mechanical vibration, shock and condition monitoring - Vocabulary, Geneve.

[55] S. Aatola , «Measurements of vibrational power transmission from ship main engine,» VTT Tecnical Research center of Finland, Espoo, 2002.

[56] M. Ohlrich, «In-situ estimation of structural power transmission from machinery source installations,» in *Proceedings of the Sixth International Congress on Sound and Vibration*, Auburn, 1999.

[57] J. Harris e A. Stevenson, «On the role of nonlinearity in the dynamic behaviour of rubber components,» *Rubber Chemistry and Technology*, vol. 59, n. 5, pp. 740-764, 1986.

[58] J. C. Snowdon, «Vibration isolation: use and characterization,» *Journal of the Acoustical Society of America*, vol. 66, n. 5, pp. 1245-1274, 1979.

[59] J. D. Ferry, Viscoelastic Properties of Polymers, New York: John Wiley and Sons, 1980.

[60] M. L. Williams, R. F. Landel e J. D. Ferry, «The Temperature Dependence of Relaxation Mechanisms in Amorphous Polymers and Other Glass-forming Liquids,» *Journal of American Chemical Society*, vol. 77, n. 14, p. 3701–3707, 1955.

[61] J. D. Dickens, «Phase velocity of rubber element in vibration isolator under static load,» *Journal of Sound and Vibration*, vol. 234, n. 1, pp. 21-42, 2000.

[62] S. Kim e R. Singh, «Vibration transmission through an isolator modelled by continuous system theory,» *Journal of Sound and Vibration*, vol. 248, n. 5, p. 925–953, 2001.

[63] L. Kari, «Stiffness scaling laws and vibration isolators,» *Applied Acoustics*, vol. 63, p. 583–594, 2002.

[64] L. Kari, «On the dynamic stiffness of preloaded vibration isolators in the audible frequency range: Modeling and experiments,» *Journal of the Acoustical Society of America*, vol. 113, n. 4, pp. 199-1921, 2003.

[65] T. R. Lin, J. Pan, P. J. O'Shea e C. K. Mechefske, «A study fo vibration and vibration control of ship structures,» *Marine Structures*, vol. 22, n. 4, pp. 730-743, 2009.

[66] M. N. Norwood e R. S. Dow, «Dynamic Analysis of Ship Structures,» *Ship and Offshore Structures Journal*, vol. 8, pp. 270-288, 2013.

[67] M. Biot, D. Boote, E. Brocco, P. N. Mendoza Vassallo, L. Moro e T. Pais, «Validation of a Design Method for the Simulation of the Mechanical Mobility of Marine Diesel Engine Seatings,» in *18th International Conference Transport Means*, Klaipeda, Lithuania, 2014.

[68] M. Corporation, *MSC.Nastran 2013.1: Dynamic Analysis User's Guide*, Newport Beach, CA, U.S.A.: MSC.Software Corporation, 2013.

[69] L. Moro, M. Biot, N. Mantini e C. Pestelli, «Solutions to improve accuracy in experimental measurement of the dynamic response of resilient mountings for marine diesel engines,» in *4th International Conference on Marine Structures, MARSTRUCT 2013*, Espoo, Finland, 2013.

[70] O. H. Yeoh, «Some forms of strain energy function for rubber,» *Rubber Chemistry and Technology*, vol. 66, n. 5, pp. 754-771, 1993.

[71] L. Moro, H. Le Sourne, E. Brocco, P. . N. Mendoza Vassallo e M. Biot, «Numerical simulation of resilient mount for marine diesel engines,» in *5th International Conference on Marine Structures, MARSTRUCT 2015*, Southampton, 2015.

[72] N. Mantini, *Simulazioni numeriche delle prove sperimentali per la caratterizzazione dei supporti resilienti per motori navali*, Master Degree Thesis, Trieste: University of Trieste, 2011.

[73] L. Moro e M. Biot, «Laboratory tests pave the way for the knowledge of dynamic response of resilient mountings on board ships,» in *12th International Symposium on Practical Design of Ships and Other Floating Structures, PRADS 2013*, Changwon, South Korea, 2013.

[74] M. Biot, D. Boote, E. Borcco, L. Moro e T. Pais, «Numerical and experimental analysis of the dynamic behavior of the engine foundation,» in *The 25th International Ocean and Polar Engineering Conference ISOPE2015*, Hawaii, USA, 2015.

[75] T. Rosolen, *Studio della dinamica delle fondazioni dei motori principali di una nave da crociera*, Master Degree Thesis, Trieste: University of Trieste, 2011.

[76] M. Biot, L. Moro e P. N. Mendoza Vassallo, «Prediction of the structure-borne noise due to marine diesel engines on board cruise ships,» in *21st International Congress on Sound and Vibration, ICSV 21*, Beijing, China, 2014.